Analyst

Attenuated total reflection Fourier-transform infrared spectroscopy for the prediction of hormone concentrations in plants

Journal:	*Analyst*
Manuscript ID	AN-ART-10-2023-001817.R4
Article Type:	Paper
Date Submitted by the Author:	n/a
Complete List of Authors:	Holden, Claire; Lancaster University Faculty of Science and Technology McAinsh, Martin; Lancaster University, Lancaster Environment Centre Taylor, Jane; Lancaster University Faculty of Science and Technology Beckett, Paul; Lancaster University Faculty of Science and Technology Albacele, Alfonso; Lancaster University Faculty of Science and Technology Martinez-Andujar, Cristina; Lancaster University Faculty of Science and Technology de Morais, Camilo; UFRN, Martin, Francis; Biocel UK Ltd, Biocel analytics; Blackpool Victoria Hospital, Cellular Pathology

Analyst

Guidelines for Referees

Thank you very much for agreeing to review this manuscript for *Analyst*.

Analyst publishes analytical and bioanalytical research that reports premier fundamental discoveries and inventions, and the applications of those discoveries, unconfined by traditional discipline barriers.

The following manuscript has been submitted for consideration as a

FULL PAPER

Original scientific work that has not been published previously. Full papers must represent a significant development in the particular field of analysis and are judged according to originality, quality of scientific content and contribution to existing knowledge. Although there is no page limit for full papers, appropriateness of length to content of new science will be taken into consideration. Further information on article types can be found on our website.

Please consider these standards when making your recommendation for publication in *Analyst*:

- Use the **journal scope and expectations** to assess the manuscript's suitability for publication in *Analyst*
- **Comment on** the originality, importance, impact and reliability of the science, with references as appropriate. Your comments should both help the Editor to make a decision on the article and the authors to improve it.
- English language and grammatical errors do not need to be discussed in detail, except where it impedes scientific understanding.
- All articles submitted to *Analyst* must meet the significant novelty criteria; routine and incremental work – however competently researched and reported – should not be recommended for publication.

Best regards,

Professor Norman Dovichi
Editor-in-Chief
University of Notre Dame, USA

Rebecca Garton
Executive Editor
Royal Society of Chemistry

Contact us

Please visit our reviewer hub for further details of our processes, policies and reviewer responsibilities as well as guidance on how to review, or click the links below.

What to do when you review

Reviewer responsibilities

Process & policies

Spectroscopy-based environmental metabolomics

Attenuated total reflection Fourier-transform infrared spectroscopy for the prediction of hormone concentrations in plants

Claire A Holden[1], Martin McAinsh[1], Jane E Taylor[1], Paul Beckett[2], Alfonso Albacete[3,4], Cristina Martínez-Andújar[4], Camilo L. M. Morais[5,6], Francis L Martin[7,8]*

[1] Lancaster Environment Centre, Lancaster University, UK

[2] Phlorum Ltd, UK

[3] Institute for Agro-Environmental Research and Development of Murcia (IMIDA), Department of Plant Production and Agrotechnology, C/ Mayor s/n, E-30150 La Alberca, Murcia, Spain

[4] CEBAS-CSIC. Department of Plant Nutrition. Campus Universitario de Espinardo, E-30100 Murcia, Spain

[5] Center for Education, Science and Technology of the Inhamuns Region, State University of Ceará, Tauá 63660-000, Brazil

[6] Graduate Program in Chemistry, Institute of Chemistry, Federal University of Rio Grande do Norte, Natal 59072-970, Brazil

[7] Department of Cellular Pathology, Blackpool Teaching Hospitals NHS Foundation Trust, Whinney Heys Road, Blackpool FY3 8NR, UK

[8] Biocel UK Ltd., Hull HU10 6TS, UK

***Corresponding author:** Francis L Martin; Email: francis.martin2@nhs.net

Spectroscopy-based environmental metabolomics

ToC graphic

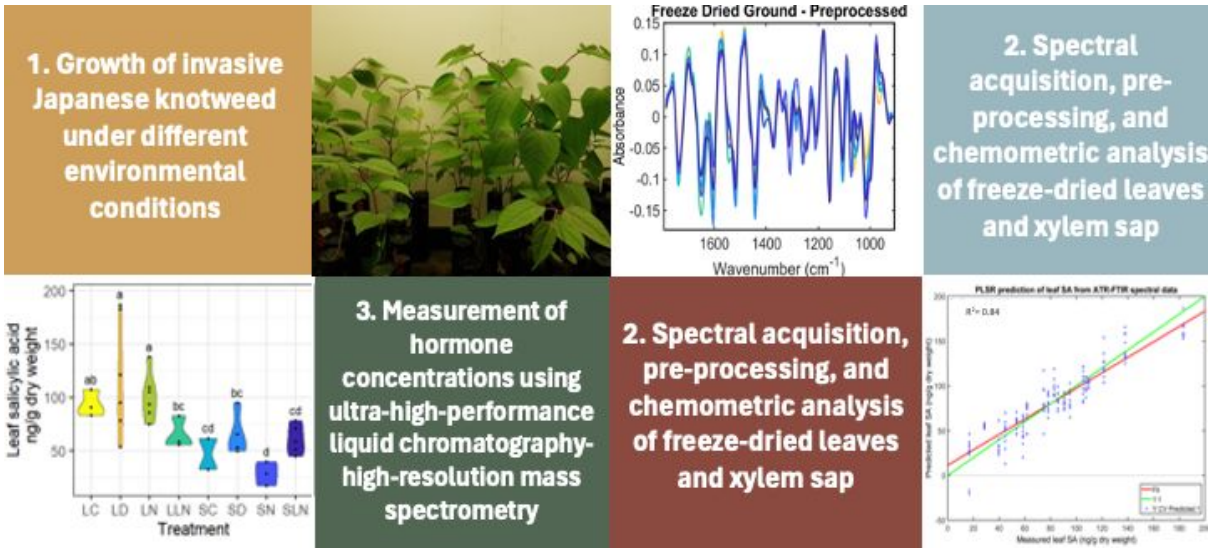

Analysis with ATR-FTIR spectroscopy combined with chemometrics methods facilitates determination of hormone concentrations in Japanese knotweed samples under different environmental conditions.

Abstract

Plant hormones are important in the control of physiological and developmental processes including seed germination, senescence, flowering, stomatal aperture, and ultimately the overall growth and yield of plants. Many currently available methods to quantify such growth regulators quickly and accurately require extensive sample purification using complex analytic techniques. Herein we used ultra-performance liquid chromatography-high-resolution mass spectrometry (UHPLC-HRMS) to create and validate the prediction of hormone concentrations made using attenuated total reflection Fourier-transform infrared (ATR-FTIR) spectral profiles of both freeze-dried ground leaf tissue and extracted xylem sap of Japanese knotweed (*Reynoutria japonica*) plants grown under different environmental conditions. In addition to these predictions made with partial least squares regression, further analysis of spectral data was performed using chemometric techniques, including principal component analysis, linear discriminant analysis, and support vector machines (SVM). Plants grown in different environments had sufficiently different biochemical profiles, including plant hormonal compounds, to allow successful differentiation by ATR-FTIR spectroscopy coupled with SVM. ATR-FTIR spectral biomarkers highlighted a range of biomolecules responsible for the differing spectral signatures between growth environments, such as triacylglycerol, proteins and amino acids, tannins, pectin, polysaccharides such as starch and cellulose, DNA and RNA. Using partial least squares regression, we show the potential for accurate prediction of plant hormone concentrations from ATR-FTIR spectral profiles, calibrated with hormonal data quantified by UHPLC-HRMS. The application of ATR-FTIR spectroscopy and chemometrics offers accurate prediction of hormone concentrations in plant samples, with advantages over existing approaches.

Introduction

As sessile organisms, plants rely on signalling molecules such as plant hormones to enable them to react appropriately to their environment; they contribute to a plastic adaptive response, regulating plant growth and stress tolerance [1], and plants grown under different environmental conditions show significant differences in hormone profiles [2,3]. Plant hormones include: ethylene, auxin, gibberellins (GAs), cytokinins (CKs), abscisic acid (ABA), salicylic acid (SA), strigolactones (SLs), brassinosteroids (BRs) and jasmonic acid (JA) [1,3]. Plant hormone identification is challenging due to their low concentrations, ranging stabilities and similar core structures, including isomers with the same MS fragmentation patterns (e.g. cis- and trans-zeatin, topolin isomers, brassinolide and 24-epibrassinolide [24-epiBL], and castasterone and 24-epicastasterone; Šimura *et al.*, 2018). Current methods for plant hormone analysis include: gas chromatography-mass spectrometry (GC-MS), capillary electrophoresis-mass spectroscopy (CE-MS) [5], enzyme-linked immune sorbent assay (ELISA) [6], ultra-performance liquid chromatography-mass spectrometry (UPLC-MS) [7], high performance liquid chromatography-mass spectrometry (HPLC-MS) [8] and liquid chromatography-ultraviolet detection (LC-UV) [9]. Liquid chromatography is a versatile method that allows the separation of compounds of a wide range of polarity, but these classical chromatographic techniques require destruction of the plant and lengthy sample preparation. More recently the research focus has shifted towards the development of non-destructive spectroscopic techniques for plant hormone detection, such as Raman spectroscopy [10,11] and desorption electrospray ionisation mass spectrometry imaging (DESI-MSI)[12].

Plant hormones control a range of complex physiological and developmental processes including seed germination, senescence, flowering, and stomatal control, and affect overall plant growth and crop yield [1]. Antagonistic hormonal crosstalk also regulates numerous

factors influencing the success of invasive alien species (IAS), for example, the trade-off between growth and defence [13], adaptive transgenerational plasticity [14], and the biosynthesis of allelopathic chemicals [15]. The importance of hormonal regulation in plant invasions has been demonstrated in the differential biomass allocation [16] and defence responses [17] of invasive and native plants, and in locally adaptive chromosomal inversion in invasive plants [18]. Additionally, many herbicides used for the control of IAS are plant hormone analogues or interfere with hormonal signalling and synthesis pathways [19]. IAS have significant negative socio-economic [20,21] and environmental [22] impacts and therefore it is critical to gain an increased understanding of the factors, including the role of plant hormones, that enable the invasiveness and superior growth performance of these species [23–26].

Japanese knotweed (*Reynoutria japonica*) is an IAS found across a broad geographic range, colonising diverse habitats including riparian wetlands, urban transport courses, and coastal areas [27,28]. It is very tolerant to abiotic stress, occupying extreme environments such as salt marshes [29] and metal-polluted soil [30,31]. Although its habitats are diverse, Japanese knotweed exhibits minimal genetic variation in Central Europe [27], Norway [32] and the USA [28], and exists as a female clone in the United Kingdom from a single introduction [33,34]. The ecological adaptability of Japanese knotweed as an invasive weed renders this species an ideal model for investigating the contribution of plant hormones to IAS invasiveness through a concatenated approach combining ultra-performance liquid chromatography-high resolution mass spectrometry (UHPLC-HRMS) and attenuated total reflection Fourier-transform infrared (ATR-FTIR) spectral data.

In this study we used UHPLC-HRMS to quantitatively measure the concentrations of a set of plant hormones at nanogram per millilitre concentrations: the active CKs *trans*-Zeatin (t-Z), *trans*-zeatin riboside (tZR) and isopentyl-adenine (iP), the active GAs gibberellin A1 (GA_1), gibberellin A4 (GA_4), gibberellin A3 (GA_3), the active auxin indole-3-acetic acid (IAA),

ABA, JA, SA, and the ethylene precursor 1-amino-cyclopropane-1-carboxylic acid (ACC); and compared these measured concentrations to those predicted from ATR-FTIR spectral profiles of both xylem sap and freeze-dried ground leaves. ATR-FTIR spectroscopy employs infrared (IR) light to alter the molecular vibrations of a sample, providing information on the compounds within. It is a rapid analytical technique well-suited to environmental monitoring with the advantages of a high degree of specificity and sensitivity, minimal sample preparation, and portable enough for use in the field. It can be used non-destructively on whole plant tissues, even *in planta* [35,36]. We used chemometric algorithms to allow further information to be gained from the absorbance profiles, such as molecular biomarkers associated with the plants' environments. Chemometric techniques used included principal component analysis (PCA), PCA in combination with linear discriminant analysis (LDA), support vector machines (SVMs), and partial least squares regression (PLSR) [37–39]. These highlighted a range of biomolecules responsible for the differing IR spectral signatures between growth environments, such as triacylglycerol, proteins and amino acids, tannins, pectin, polysaccharides such as starch and cellulose, deoxyribonucleic acid (DNA) and ribonucleic acid (RNA) [40]. PLSR comparison of the ATR-FTIR spectral data with the quantitative data from UHPLC– HRMS analysis allowed the effect of each hormone on the spectral absorbances to be viewed in isolation. Key wavenumbers within the mid-infrared fingerprint region were identified for prediction of plant hormone concentrations using ATR-FTIR spectroscopy; predominantly in the region of 1200-1000 cm^{-1} for leaf samples and 1600-1500 cm^{-1} for xylem sap samples. In leaf samples these often related to polysaccharide molecules, whilst in xylem compounds these key wavenumbers were more commonly associated with nucleic acids and bases. Predictive models were built to consider the concentrations of each hormone in turn and also to detect concentrations of several different hormones at once.

Materials and Methods

Plant growth

Japanese knotweed readily reproduces asexually from small fragments of an underground storage organ called a rhizome, which has a woody root-like structure. Rhizomes were collected from a site on the River Wyre, Google map reference 53.94977780, -2.75541670, with landowner permission from Lancashire County Council. Ninety fragments of rhizome (10-50 g, volume 2-58 cm^3) were planted in fertilized organic loam (John Innes No. 1, J. Arthur Bowers, UK) in cylindrical pots designed to tightly fit in a Scholander-type pressure chamber (Soil Moisture Equipment Corp., Santa Barbara, CA, USA) measuring 6.5 cm in diameter and 23 cm in length with a volume of 763.2 cm^3, and featured a stainless-steel mesh (0.7 mm aperture) at the base to assist drainage. Pots were placed in one of two climate-controlled cabinets (Microclima 1750, Snijders Scientific BV, Netherlands) at 80% humidity, 16 h of photoperiod, and 19/11°C day/night temperature where the treatments were applied and plants were grown for a total of fifty days before harvesting. The long photoperiod and temperature range were selected to simulate an average British Summer in the areas where Japanese knotweed usually colonises, using a comparison of temperature maps from the Met Office [41] and a distribution map of Japanese knotweed in the British Isles [42].

Treatments

Rhizome fragments were divided into eight treatment groups to give an even split of rhizome masses in each group. The treatments applied were: Light Control ‘LC’, Light Drought ‘LD’, Light Nitrogen ‘LN’, Light Low Nutrient ‘LLN’, Shade Control ‘SC’, Shade Drought ‘SD’, Shade Nitrogen ‘SN’ and Shade Low Nutrient ‘SLN’. Four groups were placed in each of two growth cabinets. In both cabinets, the light emitted from the two high-pressure sodium lamps (SON-T 400 W, Philips Lighting, Eindhoven, The Netherlands) was reduced using a LEE 209 filter (LEE Filters Worldwide, Andover, Hampshire, UK). In one cabinet, a matrix

of far-red LEDs (EPILEDS, 740-745 nm) distributed in five rows 30 cm apart was used to decrease the red: far-red ratio (R:FR) to simulate shading. Wavelengths emitted were measured using an UPRtek (Taiwan) PG100N light spectrometer. The resultant combined light conditions (see Table S1†) resulted in a 'light' treatment with a R:FR of 5.6 and a 'shade' treatment with a R:FR of 0.4 (see Figure S1† for the spectral profile). Plants were shuffled weekly within each cabinet to minimise positional effects from the LED matrix pattern. The R:FR of natural sunlight during the day is approximately 1.15 [43] and the R:FR of 0.4 in the shade treatment was chosen to replicate that found within vegetative canopies such as sugar beet, deciduous woodland, coniferous woodland and tropical rainforest [43]. In both cases, the photosynthetic photon flux density (PPFD) was between 124.7 and 189.8 $\mu mol \cdot m^{-2} \cdot s^{-1}$ which is typical of growth cabinet studies [44–47].

Plants were provided with water (75 mL/pot / 48 h), apart from LD and SD in which water was withheld for 7 days prior to harvest. Once a week, four groups (LC, LD, SC, SD) were watered with 75 mL Hoagland solution to provide both nitrogen and micronutrients, see Table S2† for details. LN and SN were fed with the commonly used agricultural dose of 50 $kg\ ha^{-1}\ year^{-1}$ [48]; this was scaled down for a pot diameter of 6.2 cm and applied across a split-dose at 21 and 23 days to prevent leaching. Groups LLN and SLN were provided only with water and received no additional nitrogen or micronutrients.

Harvest

Two leaves were excised from each plant for the analysis 4-8 h into the photoperiod in order to fall within a stable period of the plants' circadian rhythm. The youngest leaf from the top of plants was placed in liquid nitrogen, freeze-dried, and finely ground for hormone analysis by U-HPLC-HRMS, and the second leaf down was treated similarly for analysis by ATR-FTIR spectroscopy. Following this, the plant was de-topped and the whole pot inserted into a Scholander-type pressure chamber (Soil Moisture Equipment Corp., Santa Barbara, CA,

USA) with the stem protruding for xylem sap collection. The pressure was matched to the flow rate by increasing the pressure gradually above the balance pressure. For each trial pressure, the flow rate was calculated by weighing the sap collected for twenty seconds, until the flow rate matched that calculated by mass loss following the method previously described in [49]. This was necessary as it has been shown that ABA concentration are influenced by sap flow rate [49]. Sap was collected in Eppendorf vials, immediately frozen in liquid nitrogen and stored at −80°C for hormone determination, and ATR-FTIR spectral analysis.

Plant hormones

Plant hormones were quantified from frozen xylem sap and freeze-dried ground leaf material using UHPLC–HRMS as described previously with some modifications [50,51]. Freeze-dried ground leaf samples were prepared with several extraction steps and sonication before analysis, whilst only the filtration and centrifugation steps were necessary for the xylem sap samples. In the first extraction up to 250 mg of raw material was mixed with methanol (1.25 mL, 80%) and an internal-standards mix composed of deuterium labelled hormones ($[^2H_5]$tZ, $[_2H^5]$tZR, $[^2H_6]$iP, $[^2H_2]GA_1$, $[^2H_2]GA_3$, $[^2H_2]GA_4$, $[^2H_5]$IAA, $[^2H_6]$ABA, $[^2H_4]$SA, $[^2H_6]$JA, $[^2H_4]$ACC, Olchemim Ltd, Olomouc, Czech Republic) at a concentration of 5 μg mL^{-1} in 80% methanol. Samples were vortexed, incubated for 30 min at 4°C, and centrifuged (20000 g, 4°C, 15 min). Supernatants were passed through Chromafix C18 columns (MachereyNagel, Düren/Germany) previously pre-equilibrated with 80% methanol and filtrates were collected on ice. Extraction was repeated with 1.25 mL 80% methanol; second extracts were passed through the same columns. The combined extracts were collected and concentrated to complete dryness using the Integrated SpeedVac® Concentrator System AES1000 (Savant Instruments Inc., Holbrook/USA). The residues were resolved in 500 or 1000 μL 20% methanol, sonicated for 8 min using a ultrasonic bath, passed through 0.2-μm syringe filters (Chromafil PES-20/25) and placed in HPLC vials for analysis, and optionally

stored at –80°C. Phytohormone analyses were performed using a UHPLC–HRMS system consisting of a Thermo ACCELA pump (Thermo Scientific, Waltham/USA) coupled to a tempered HTC-PAL autosampler (CTC Analytics, Zwingen/Switzerland), and connected to a Thermo Exactive Spectrometer (Thermo Scientific) with a heated electrospray ionization (HESI) interface. Due to the high resolution of the Orbitrap, we recorded the total ion chromatogram of the samples and did not fragment the molecules. A typical chromatogram for SA is shown in Figure S2†. The analysis was performed in the negative mode $[M-H]^-$ (Table S3†), and the instrument settings included: sheath gas flow rate = 35 $ml \cdot min^{-1}$, auxiliary gas flow rate = 10 $ml \cdot min^{-1}$, spray voltage = 2.5 kV, capillary temperature = 275ºC, capillary voltage = -40 V, tube lens voltage = -110 V, skimmer voltage = -20 V. Mass spectra were obtained using the Xcalibur software version 2.2 (ThermoFisher Scientific, Waltham, MA, USA). For quantification of the plant hormones, calibration curves were constructed for each analysed component (1, 10, 50, and 100 µg l^{-1}) and corrected for 10 µg l^{-1} deuterated internal standards. Recovery percentages ranged between 92 and 95%.

ATR-FTIR spectral acquisition

Freeze-dried ground leaves and xylem sap were analysed using a Tensor 27 FTIR spectrometer with a Helios ATR attachment (Bruker Optics Ltd, Coventry, UK). The sampling area, defined by the Internal Reflection Element (IRE), which was a diamond crystal, was 250 µm x 250 µm. Spectral resolution was 8 cm^{-1} with 2 times zero-filling, giving a data-spacing of 4 cm^{-1} over the range 4000 to 400 cm^{-1}; 32 co-additions and a mirror velocity of 2.2 kHz were used for optimum signal to noise ratio. To minimise bias, ten spectra were taken for each sample. Each sample was placed on a slide with the side to be analysed facing upwards, placed on a moving platform, and then raised to ensure a consistent contact with the diamond crystal. For xylem sap samples, 30 mL of xylem sap was placed on a tin foil-covered slide and allowed to dry before analysis. For freeze-dried ground leaves a

small amount of powder was transferred to each slide using a spatula. A total of 410 spectra were taken for xylem sap and 330 spectra were taken of freeze-dried ground leaf tissue.

Data analysis

The 'mergetool' function of an in-house developed MATLAB (Mathworks, Natick, USA) toolbox called IRootLab [52,53] was used to convert all spectral information from OPUS format to suitable files (.txt). Following this, it was necessary to pre-process the acquired spectra to improve the signal-to-noise ratio. Pre-processing corrects problems associated with random or systematic artefacts during spectral acquisition and is an essential step of all spectroscopic experiments. Pre-processing and computational analysis of the data were performed using a combination of IRootLab toolbox [52,53] and the PLS Toolbox version 7.9.3 (Eigenvector Research, Inc., Manson, USA). The pre-processing steps applied to all spectra were firstly the selection of the spectral biochemical fingerprint region (1800-900 cm^{-1}), followed by Savitzky–Golay (SG) second differentiation (nine smoothing points) and vector normalisation. All data were mean centred before multivariate analysis, where multiple dependant variables are observed simultaneously to determine a pattern.

Four machine learning techniques were used in this study: an unsupervised dimensionality reduction method, two supervised classification methods and one regression. The unsupervised method principal component analysis (PCA) simplifies complex multivariate datasets, allowing them to be presented intuitively and enabling pattern recognition. Two supervised chemometric techniques, principal component analysis with linear discriminant analysis (PCA-LDA) and support vector machines (SVM), were used for the classification of groups [37,38]. PCA-LDA was also used for the determination of biomarkers. Most importantly, hormone prediction was achieved using a multivariate analysis technique called PLSR of both ATR-FTIR spectral data and real hormone data as measured by UHPLC-HRMS [39]. Regression by PLSR was performed with the same pre-processed data without vector

normalization. Multivariate analysis techniques allow multiple variables to be compared at the same time enabling spectral absorbance values across a range of wavelengths to be simultaneously correlated against concentrations of multiple hormones for numerous samples. Observing all these data at once allows patterns to be seen and enables predictions to be made. To form these models, an X-block of ATR-FTIR spectral absorbance data for plants was analysed by PLSR against a Y-block of hormone concentrations for the corresponding plants as measured using UHPLC-HRMS. Environments were analysed separately, allowing a model to be created for each of them. The PLSR models were validated by Monte-Carlo cross-validation, where 20% of the spectral data is randomly left-out for validation and the remaining 80% is used for training the model in an exhaustive process to ensure model consistency and validation reliability. In this study, Monte-Carlo cross-validation was performed with 1000 iteration cycles. The number of principal components for PCA-LDA was set at 10, to ensure more than 95% of the original data explained variance was contemplated. PLSR models were built varying the number of latent variables according to the smallest root-mean-squared error (RMSE) of cross-validation. Once made, these models can be applied to new ATR-FTIR spectral data in the absence of UHPLC-HRMS data to predict plant hormone concentrations.

Results

ATR-FTIR spectral analysis classifies plants from different environments via spectral differences

The sensitive nature of IR spectroscopy allowed indications of plant responses to environment to be observed visually as differences between spectral profiles. The pre-processed fingerprint spectra exhibit distinguishable differences between spectra of different treatment groups, for both xylem sap and freeze-dried ground samples, at 950, 1050, 1150, 1250, 1325, 1400, 1525, 1575 and 1610 cm^{-1} (Figure S3b†) and 950, 1050, 1275, 1400, 1525

and 1610 cm^{-1} (Figure S3d†), respectively. Three chemometric techniques (PCA, PCA-LDA and SVM) were used to extract further information from the spectral absorbance profiles of xylem sap (Figures 1a-d) and freeze-dried ground leaves (Figures 2a-d). The unsupervised technique, PCA, showed poor separation between treatment groups in xylem sap samples (Figure 1a). However, addition of the supervised classifier LDA created biologically meaningful separation along the linear discriminant 1 (LD1) axis. Xylem sap samples in the low nutrient categories (LLN and SLN) fall to the right of the other samples with the same lighting regine (LC, LD, LN and SC, SD and SN respectively) along the LD1 axis (Figure 1b). In leaf samples, the separation along the LD1 axis relates to light regime (Figure 2b), with 'light' to the left and 'shade' to the right. For the xylem sap samples, the left-hand side of the PCA-LDA scatter graph contains both control and drought plant samples (LC and LD) which were watered with Hoagland solution, the central portion contains clusters of nitrogen fed and low nutrient shaded plants (SN and SLN), and the right-hand side contains the light samples of the nitrogen and low nutrient categories (LN and LLN). The pattern observed in Figure 2a is distinctive due to the homogenisation introduced by the grinding process; PCA of freeze-dried ground leaves separated spectra from individual samples into clusters. PCA-LDA of freeze-dried leaf samples (Figure 2b) resulted in a separation along the axis LD1; LD to the left, LC, LN and LLN in the central portion, and all shaded groups to the right (SC, SD, SN and SLN). The stronger chemometric technique, SVM, achieved the best classification results for both sample types. Analysis of spectra from xylem sap samples using SVM achieved 99.0% accuracy, 98.2% sensitivity, and 99.8% specificity (Figures 1c-d). However, application of SVM to spectra of freeze-dried ground leaves attained even better separation with 99.8% accuracy, 99.6% sensitivity and 100.0% specificity (Figures 2c-d). For SVM model parameters, cost, gamma and number of support vectors, see Table S4†.

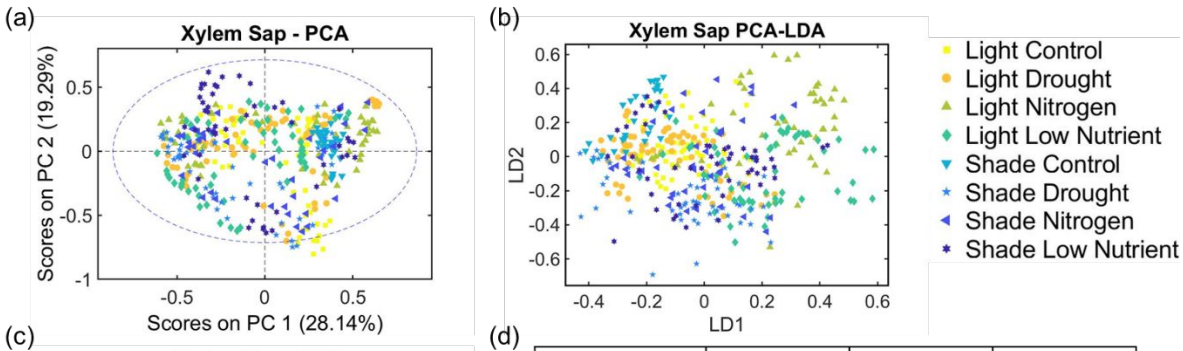

(d)

Xylem Sap - SVM	% Accuracy	% Sensitivity	% Specificity
Light Control	99.9	100	99.7
Light Drought	99.9	100	99.7
Light Nitrogen	99.6	100	99.2
Light Low Nitrogen	99.0	98.3	99.7
Shade Control	100	100	100
Shade Drought	96.0	92.0	100
Shade Nitrogen	97.4	95.0	99.7
Shade Low Nitrogen	100	100	100

Figure 1: (a) PCA scores plot showing poor separation between classes, **(b)** PCA-LDA scatter plot showing some separation by nutrient levels, **(c)** SVM sample/measured plot showing correct classification (Y-axis) of spectra from samples of different treatment categories (X-axis) and **(d)** SVM results for ATR-FTIR spectra taken of xylem sap samples showing excellent classification, grouped by treatments; Light Control (LC), Light Drought (LD), Light Nitrogen (LN), Light Low Nitrogen (LLN), Shade Control (SC), Shade Drought (SD), Shade Nitrogen (SN) and Shade Low Nitrogen (SLN).

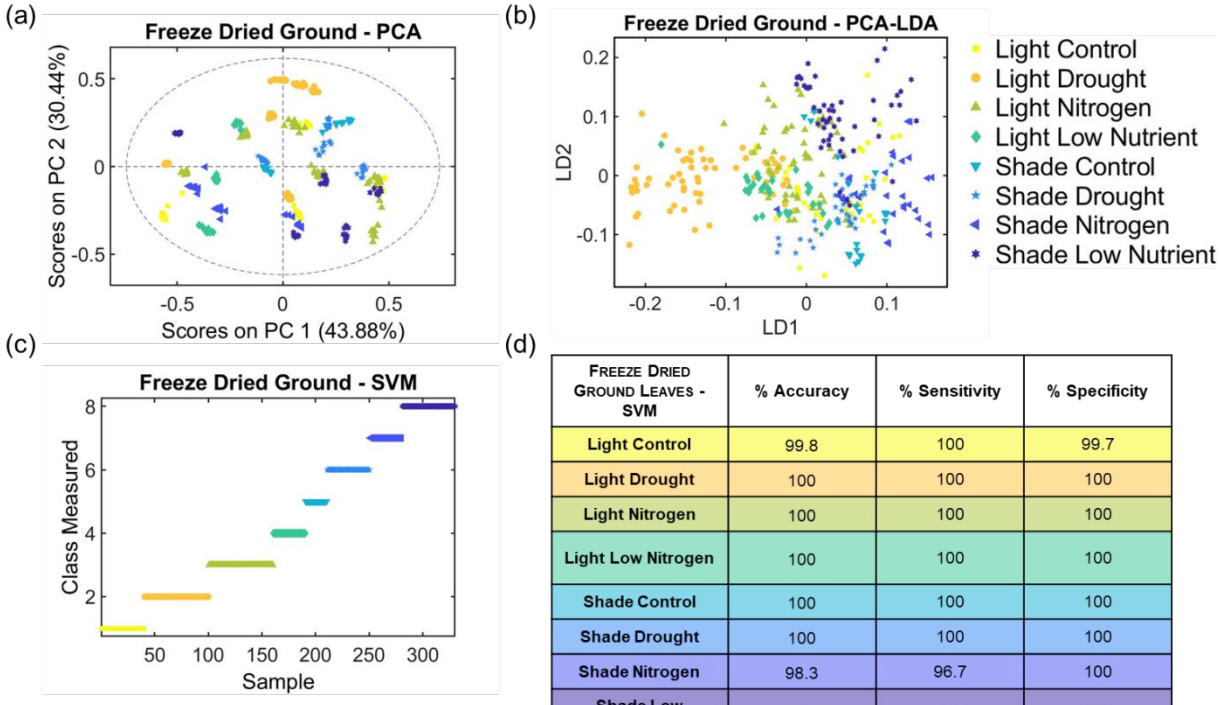

(d)

Freeze Dried Ground Leaves - SVM	% Accuracy	% Sensitivity	% Specificity
Light Control	99.8	100	99.7
Light Drought	100	100	100
Light Nitrogen	100	100	100
Light Low Nitrogen	100	100	100
Shade Control	100	100	100
Shade Drought	100	100	100
Shade Nitrogen	98.3	96.7	100
Shade Low Nitrogen	100	100	100

Figure 2: (a) PCA scores plot in which each cluster is formed from separate samples due to the homogenisation introduced by the grinding process, **(b)** PCA-LDA scatter plot showing some separation by light levels, **(c)** SVM sample/measured plot showing correct classification (Y-axis) of spectra from samples of different treatment categories (X-axis) and **(d)** SVM results for ATR-FTIR spectra taken of freeze-dried ground leaves samples showing excellent classification, grouped by treatments; Light Control (LC), Light Drought (LD), Light Nitrogen (LN), Light Low Nitrogen (LLN), Shade Control (SC), Shade Drought (SD), Shade Nitrogen (SN) and Shade Low Nitrogen (SLN).

ATR-FTIR spectral analysis identifies biomolecular differences between treatments

ATR-FTIR spectroscopy can detect changes in concentration or molecular structure of compounds. Significant biomolecular differences can be deciphered by examination of the key wavenumbers, which differentiate spectral profiles of different treatment groups from one another. These wavenumbers are called loadings (Figure S4†) and their tentative molecular assignments have been found through examination of the literature for both xylem sap and leaf sample types for biomarker information and references (see Table S5†). The peaks which differentiate treatment groups in xylem sap samples were related to a range of biomolecules such as triacylglycerol, proteins, glutamate, cellulose, tannins, starch, and RNA [54–62]. For freeze-dried ground leaves, the differences were found in much the same compounds: triacylglycerol, proteins and amino acids, pectin, polysaccharides such as starch and cellulose, and DNA [55,56,59,63–65].

UHPLC– HRMS hormone analysis indicates that hormone concentrations are impacted by applied treatments

Plants respond to their environment via signalling molecules such as hormones, to enable a plastic response. This is reflected in the concentrations of plant hormones measured by UHPLC-HRMS (ACC, tZ, iP, SA, ABA, JA, GA_1, GA_4, GA_3, tZR, and IAA) which were different between plants belonging to different treatment groups (see Figure 3a and c; Figures S5† and S6†). Figure 3a shows separation of LD and SD plants along PC1 based on xylem sap hormone concentrations accounting for 65.07% of the variance. This is primarily due to

increased ABA and tZ (see Figure 3b, PC1 loadings in blue). The separation along PC2 for xylem sap samples is due to the antagonistic relationship between JA and ABA (Figure 3b, PC2 loadings in green), which is variable within treatment categories (Figure 3a). Figure 3c also shows a separation along PC1 of droughted samples based on the hormone concentrations of freeze-dried ground leaves, accounting for 46.32% of the sample variance. High leaf ABA and low leaf ACC, JA and tZ concentrations were primary responsible for separation along axis PC1 (Figure 3d, PC1 loadings in blue). The PC2 axis of Figure 3c shows some separation by lighting treatment, however this separation was of lesser importance and only explained 38.23% of the variance. The green line in Figure 3d indicates that ABA, JA, tZ, and SA were all higher in LC and LD samples to create this separation along axis PC2, whilst ACC was lower. JA concentrations in plants with a low red: far-red ratio were lower.

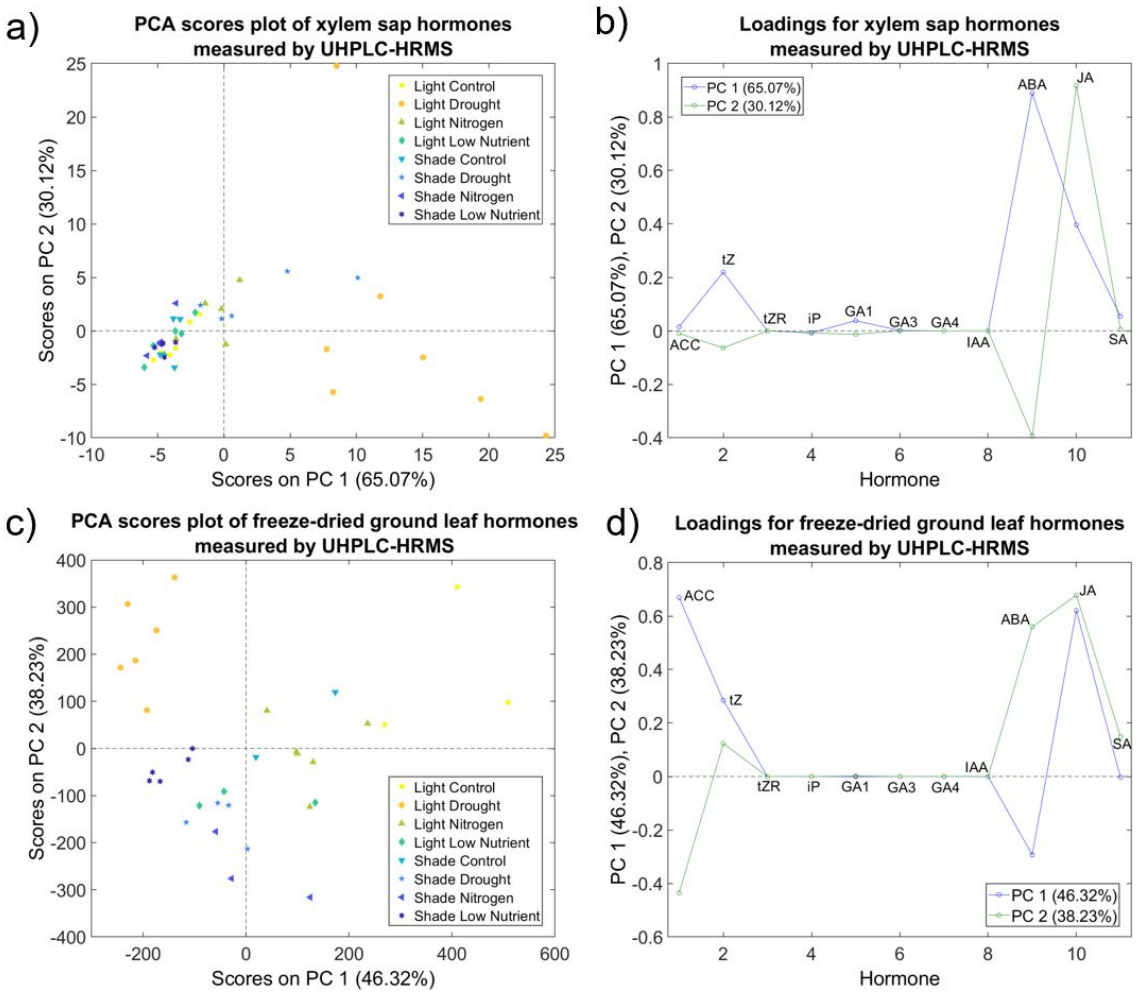

Figure 3: UHPLC-HRMS measurements of plant hormone concentrations analysed by PCA: a) xylem sap PCA scores showing separation of droughted plants along the PC1 axis, b) xylem sap loadings highlighting the importance of ABA in droughted samples, c) freeze-dried ground leaf scores showing separation by drought along PC1 and red: far red ratio along PC2, d) freeze-dried ground leaf loadings indicating that droughted plants exhibited high ABA and low ACC, JA and tZ concentrations whilst plants with a high red: far-red ratio had high ABA, JA, tZ, and SA but low ACC concentrations.

In xylem sap samples (Figure S5†), ABA concentration was highest in the drought categories; LD and SD, at ~17 and ~7 ng·ml^{-1} of sap ABA respectively, whilst the other categories ranged between ~1 and 3 ng·ml^{-1} sap. Leaf ABA concentrations (Figure S6†) were approximately quadruple in LD than those of the other categories. Shade plants had notably lower xylem SA concentrations, in the range of 0.7-1.1 ng·ml^{-1} sap compared with 1.6-4.5 ng·ml^{-1} sap for 'light' plants. Leaf tZ was 4.5-fold higher in LC plants than in those of SLN.

Leaf JA concentration was significantly higher in the light control group LC (~710 $ng \cdot g^{-1}$ dry weight) compared to all other groups (ranging 170-420 $ng \cdot g^{-1}$ dry weight), except the shade control group SC (~460 $ng \cdot g^{-1}$ dry weight). LC had the highest iP concentrations at 0.25 $ng \cdot g^{-1}$ dry weight, significantly higher compared to groups LD, LN, SD, SN (ranging 0.03-0.6 $ng \cdot g^{-1}$ dry weight), with the other groups falling in between.

Combined ATR-FTIR UHPLC-HRMS analysis identifies key spectral wavenumber for hormone prediction via ATR-FTIR spectroscopy

Whilst the plant hormone concentrations quantified by using UHPLC-HRMS served to confirm that the applied treatments were effective at inducing a phenotypic response, importantly the UHPLC-HRMS data enabled the generation of predictive models for hormone concentrations using ATR-FTIR spectral data by means of a multivariate analysis technique called partial least squares regression. PLSR allows simultaneous comparison of multivariate datasets, in this case, the spectral absorbance values for either freeze-dried ground leaf tissue or from xylem sap compared with the plant hormone values obtained by HPLC-HRMS. Using PLSR, the extracted plant hormone concentrations measured by UHPLC-HRMS were accurately predicted from ATR-FTIR spectral profiles of the same sample material.

Spectroscopy-based environmental metabolomics

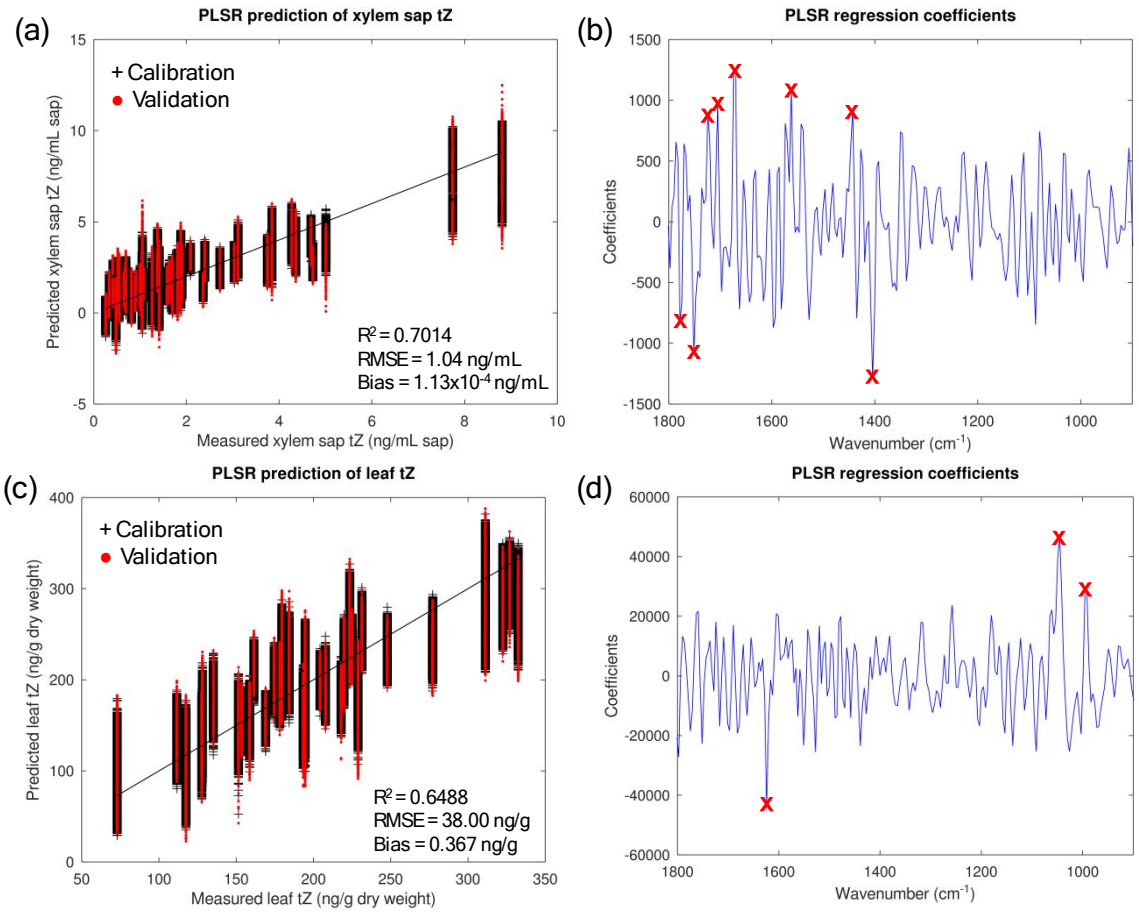

Figure 4: PLS regression and regression coefficients of *trans*-Zeatin concentrations as measured using UHPLC-HRMS against predicted values using ATR-FTIR spectra of a) xylem sap (ng mL^{-1}), and c) freeze-dried ground leaves (in ng·g^{-1} dry weight) grown under all treatment conditions. In panels a) and c), the black line shows the ideal prediction gradient of one, which would be 100% accurate. The black and red scatters points represent the calibration and validation samples during the Monte-Carlo cross-validation with 1000 iterations. The R^2, root mean square error (RMSE) and bias are reported for the validation samples of xylem sap (a) and freeze-dried ground leaves (c). These models were created using spectral data from all treatment categories for individual hormones. The model in panels a) and c) were constructed using 10 latent variables. Panels b) and d) show the regression coefficients which indicates some of the most important wavenumbers (marked with a red X) involved in making this prediction for xylem sap and freeze-dried leaves, respectively.

The graphs in Figure 4 show the PLS regressions and regression coefficients of tZ hormone concentrations as measured using UHPLC-HRMS against predicted concentrations using ATR-FTIR spectra of either xylem sap or freeze-dried ground leaves from all treatment categories as an example of the predictive models generated using this approach (see Figure S7† and S9† for of the predictive models for the other hormones). For the regressions in

Figure 4a and Figure 4c, the black lines show the ideal prediction gradient of one, which would be 100% accurate. Leaf samples achieved a more accurate prediction of R^2s= 0.649 ($[^2H_5]$tZ) to 0.848 ($[^2H_6]$ABA) compared with 0.529 ($[^2H_4]$SA) to 0.820 ($[^2H_2]GA_1$) for xylem sap samples (see Figures S7 and S9†). The PLSR models in Figures 4, S7† and S9† use hormonal data measured by UHPLC-HRMS to train them on the correlation between different hormone concentrations and the corresponding differences in ATR-FTIR spectral profiles. For each hormone, and each sample type, different spectral wavenumbers are important in making this prediction. These key wavenumbers can be identified by the PLS regression coefficients, which are presented in Figures S8† and S10† for each hormone and sample type. The regression coefficients with higher weights (either positive or negative) represent key wavenumbers, since they are more correlated with the increase or decrease of hormone concentration. These were detected mostly in the regions around 1000, 1400-1600 and 1750 cm^{-1} (ABA); 1000-1100 and 1600-1650 cm^{-1} (tZ); 1000-1100, 1300 and 1500-1700 cm^{-1} (SA); 1000-1100 cm^{-1} (JA); 1000-1000 cm^{-1} and 1600-1800 cm^{-1} (ACC) for prediction of leaf hormone concentration; and, around 1000-1100 and 1500-1800 cm^{-1} (ABA); 1400, 1600-1800 cm^{-1} (tZ); 1300-1450 and 1700-1800 cm^{-1} (SA); 1100, 1400 and 1600-1700 cm^{-1} (JA); 1000-1200 and 1700-1800 cm^{-1} (GA1) for xylem sap hormone concentration.

Combined ATR-FTIR UHPLC-HRMS analysis gives a high correlation between predicted and measured hormone concentrations

Analysis of data from each treatment separately allowed the generation of treatment-specific models. Table 1 shows the validation R^2 and root mean square error (RMSE) values for predicted against measured hormone concentrations from xylem sap, with each row being a separate treatment. The R^2 values for the predictions from xylem sap samples ranged between 0.831 (iP for light control) to 0.940 (GA1 for light nitrogen), and the RMSE values ranged from 0.0004 ng/mL sap (GA4 for light control) to 2.655 ng/mL sap (ABA for light drought)

(Table 1). Likewise, the validation R^2 and RMSE values for predicted against measured hormone concentrations from freeze-dried ground leaves are shown in Table 2. The R^2 values varied between 0.811 (ABA for shade control) to 0.957 (JA for shade low nutrient), and the RMSE values ranged from 1.692 ng/g dry weight (ABA for shade nitrogen) to 60.244 ng/g dry weight (JA for light control) (Table 2). In xylem sap samples, light nitrogen achieved the best correlations for hormones iP (R^2 = 0.934), GA1 (R^2 = 0.940) and GA3 (R^2 = 0.889); shade low nutrient for hormones ABA (R^2 = 0.933) and JA (R^2 = 0.935); light drought for hormone tZ (R^2 = 0.904); shade nitrogen for hormone IAA (R^2 = 0.892); shade drought for hormone SA (R^2 = 0.926); and, light control for GA1 (R^2 = 0.924), being the only treatment associated with GA1 hormone. In freeze-dried ground leaves, the best correlations were: shade low nutrient for hormones ACC (R^2 = 0.948) and JA (R^2 = 0.957); shade drought for hormone tZ (R^2 = 0.932); shade nitrogen for hormone ABA (R^2 = 0.950); and, light drought for hormone SA (R^2 = 0.952). These models therefore provide a valuable resource that can be saved and applied to new spectral data obtained from plants grown under similar conditions thereby allowing the hormone concentrations to be accurately predicted without the requirement for exhaustive UHPLC– HRMS analysis.

Table 1: R^2 and root-mean square error (RMSE) values for predicted against measured hormone concentrations from partial least squares regression for xylem sap ATR-FTIR spectral data against UHPLC-HRMS-measured hormone concentrations. Hormones with zero values for multiple plants were excluded from the model and are designated as NA. The treatments with best R^2 results for each hormone are shaded in gray. The number of latent variables to construct the PLSR regression models are shown in Table S6†.

Xylem Sap RMSE (ng/mL sap)	**tz**	**iP**	**GA1**	**GA3**	**GA4**	**IAA**	**ABA**	**JA**	**SA**
Light Control	0.294	0.347	0.042	NA	0.0004	0.006	0.190	0.589	0.323
Light Drought	0.741	0.008	0.116	0.034	NA	NA	2.655	2.570	0.482
Light Nitrogen	0.384	0.001	0.001	0.010	NA	NA	0.326	0.817	0.737
Light Low Nutrient	0.205	0.002	0.001	NA	NA	NA	0.189	0.708	0.222
Shade Control	0.031	0.060	0.014	0.006	NA	NA	0.295	0.671	0.138
Shade Drought	0.318	NA	0.044	0.009	NA	NA	0.939	0.870	0.043
Shade Nitrogen	0.051	0.002	0.008	0.001	NA	0.007	0.084	0.534	0.086
Shade Low Nutrient	0.088	NA	0.020	NA	NA	NA	0.112	0.143	0.086
Xylem Sap R^2	**tz**	**iP**	**GA1**	**GA3**	**GA4**	**IAA**	**ABA**	**JA**	**SA**

Light Control	0.876	0.831	0.881	NA	0.924	0.865	0.856	0.905	0.888
Light Drought	0.904	0.887	0.914	0.862	NA	NA	0.894	0.897	0.863
Light Nitrogen	0.891	0.934	0.940	0.889	NA	NA	0.902	0.886	0.884
Light Low Nutrient	0.872	0.881	0.888	NA	NA	NA	0.865	0.875	0.907
Shade Control	0.896	0.891	0.918	0.880	NA	NA	0.881	0.884	0.902
Shade Drought	0.886	NA	0.889	0.884	NA	NA	0.914	0.932	0.926
Shade Nitrogen	0.900	0.902	0.876	0.884	NA	0.892	0.862	0.928	0.867
Shade Low Nutrient	0.903	NA	0.910	NA	NA	NA	0.933	0.935	0.882

Table 2: R^2 and root-mean square error (RMSE) values for predicted against measured hormone concentrations from partial least squares regression for freeze-dried ground (FDG) leaves ATR-FTIR spectral data against UHPLC-HRMS-measured hormone concentrations. The treatments with best R^2 results for each hormone are shaded in gray. The number of latent variables to construct the PLSR regression models are shown in Table S6†.

FDG Leaves RMSE (ng/g dry weight)	**ACC**	**tz**	**ABA**	**JA**	**SA**
Light Control	52.465	18.024	6.864	60.244	11.221
Light Drought	10.090	12.066	24.915	19.672	11.330
Light Nitrogen	27.340	11.509	6.686	19.963	5.345
Light Low Nutrient	25.134	7.362	6.981	11.333	2.982
Shade Control	7.344	17.257	6.601	29.534	4.753
Shade Drought	14.084	9.137	5.466	9.035	4.121
Shade Nitrogen	32.843	9.663	1.692	5.879	2.691
Shade Low Nutrient	3.852	10.446	2.218	7.824	3.650
FDG Leaves R^2	**ACC**	**tz**	**ABA**	**JA**	**SA**
Light Control	0.904	0.873	0.916	0.901	0.900
Light Drought	0.883	0.909	0.914	0.894	0.952
Light Nitrogen	0.909	0.902	0.902	0.925	0.926
Light Low Nutrient	0.921	0.906	0.887	0.953	0.909
Shade Control	0.840	0.829	0.811	0.855	0.860
Shade Drought	0.876	0.932	0.925	0.917	0.942
Shade Nitrogen	0.892	0.863	0.950	0.954	0.907
Shade Low Nutrient	0.948	0.900	0.933	0.957	0.918

Discussion

Differences in ATR-FTIR spectral profiles are highlighted through chemometrics

Japanese knotweed and other invasive species with low genetic variation exhibit a plastic response to their environment which is thought to contribute to their invasion success [23,66,67]. This phenotypic plasticity was reflected in the present study in the differences found between spectral profiles between treatment groups. This is consistent with the results of studies in

which ATR-FTIR spectroscopy has been successful in differentiating plants' nutrient status and plants from different growing environments [68–71]. The environmentally induced phenotypic changes were successfully captured by the ATR-FTIR spectral profiles, which were visibly different (see Figure S3†). Figures 1 and 2 demonstrate the power of chemometrics to emphasise these differences. SVM was the most successful technique applied and had marginally more success in the freeze-dried ground samples, likely due to the homogenisation of the samples during the grinding process leading to more predictable results. The higher separation of spectra from freeze-dried ground leaves (Figure 2a) by PCA than that of xylem sap spectra (Figure 1a) could be due to the averaging effect of leaf growth over time, adapted to each environment, compared with the nature of the xylem-sap samples which capture a moment in time and could be influenced by compounds related to development stage. Leaf samples reflect a balance between synthesis and metabolism and the import and export of compounds, whilst xylem sap samples reflect instantaneous transport. The sample type more closely correlated to the physiological response therefore depends on the analyte of interest.

Hormone profiles reflect plant response to environment

It is well established that plant stresses such as drought, nutrient deficiency and shading can have a marked impact on the concentrations of plant hormones [1,3]. Our measurement of plant hormones with the highly specific technique, UHPLC-HRMS, from xylem sap (Figure S5†) and leaves (Figure S6†) are consistent with this. The applied treatments (LC, LD, LN, LLN, SC, SD, SN and SLN) were sufficiently different to alter the hormone profiles in the plants, reflecting adaptations to each environment [72]. Importantly, such a range of hormone concentrations was essential prerequisite to create good datasets for regression analysis.

Hormonal biomarkers identified for mid-infrared spectroscopy

The process from chemometric biomarker identification to physical biomolecular extraction is a developing area of spectroscopy with ongoing research to optimise concentration quantification [73,74], molecular definition databases [59] and new applications [35,36,69,71,75]. It was therefore crucial that predictions for expected hormone profiles from spectroscopic data were made and verified against actual hormone concentrations quantified by mass spectrometry. PLSR comparison of the ATR-FTIR spectral data with the quantitative data from UHPLC–HRMS analysis allowed the effect of each hormone on the spectral absorbances to be viewed in isolation. The regression coefficients in Figure 4 aid to point to key spectral wavenumbers used in the model creation for tZ concentration prediction. These suggest that the most important regions for prediction of hormone concentrations using ATR-FTIR spectral profiles are around 1000-1100 and 1620 cm^{-1} for leaf samples; and, around 1400-1450, 1580 and 1650-1780 cm^{-1} for xylem sap samples.

Three tentative wavenumbers used to predict ABA hormone concentration in leaf samples, 1612, 1566 and 1323 cm^{-1} are often attributed to the Amide I [57], Amide II bands of proteins (N-H bending and C-N stretching) [63] and Amide III, respectively [62]. As ABA does not contain nitrogen within its structure this suggests that ABA-associated biochemical changes in other compounds within the leaves could be acting as proxy indicators for the estimation of ABA concentration. Similarly, 1516 cm^{-1} is also tentatively associated with Amide II vibrations of proteins and appears to be one of the key indicators for prediction of tZ, JA and SA concentrations in leaves [59]. The Amide III-associated [62] peak identified at 1323 cm^{-1} was also used to tentatively predict leaf SA concentrations. Two phosphorus-associated peaks that were suggested were used for the prediction of leaf ABA concentration: 1211 cm^{-1}, which is tentatively associated with PO^{2-} asymmetric stretching (Phosphate I); and, 1065 cm^{-1} linked to C–O stretching of the phosphodiester and the ribose of bases [59]. As ABA also does not

contain phosphorus, this supports the hypothesis that compounds other than ABA contribute to a 'spectral signature' for ABA-associated biochemical changes and suggest the use of associated compounds as a proxy, would be useful to gain an overall picture of plant health in agricultural and ecological settings.

In contrast, leaf SA concentrations were predicted using two peaks which could be tentatively associated with the structure of SA: 1582 cm^{-1}, which is linked to the ring C–C stretch of phenyl; and, 1339 cm^{-1} is associated with in-plane C–O stretching vibration combined with the ring stretch of phenyl [59]. As a consequence, 1339 cm^{-1} was used for prediction of leaf ABA and SA, as well as xylem ABA, tZ and SA. Other tentative wavenumbers relating to Amides I and II (1663, 1547, 1570, 1555 cm^{-1}) also appeared important for the prediction of hormone concentrations [55,56,59,76].

When plants are under stress, signalling cascades including hormones and reactive oxygen species (ROS) induce biochemical changes [77]. As an important regulator in response to drought-induced stress, ABA induces ROS accumulation to facilitate stomatal closure [78], whilst SA, which is part of the innate immune response [79], ameliorates oxidative damage through regulation of redox signalling and the antioxidant defence system [80]. To prevent oxidative damage, excess ROS may be absorbed and quenched by phenolic compounds, which have antioxidant properties [81]. This coordinated biochemical response perhaps explains why the possible biomarker at 1512 cm^{-1}, which is tentatively associated with ν(C-C) aromatic (conjugated with C=C phenolic compounds [82] appears to allow the prediction of xylem sap ABA and SA concentrations. Another peak 1177 cm^{-1}, could be associated with the C–O stretch vibration of tannins [61], and is possibly a predictor of xylem JA concentrations.

Polysaccharides are another class of compounds commonly used for the prediction of hormone concentrations, particularly within leaf samples. The peak at 1038 cm^{-1} is tentatively associated with the polysaccharide galactan [83]; this appears to be important in the prediction of leaf SA concentrations. Leaf tZ and leaf JA concentrations appear to be predicted using a peak at 1130 cm^{-1}, which has previously been tentatively attributed to the stretching vibrations [ν(CO)] of the COC glycosidic linkage of polysaccharides [84]. Pectin is potentially associated with a peak at 1443 cm^{-1} [64]; this was hypothesised as useful in the prediction of leaf tZ, SA, JA and ACC concentrations. In addition, a possible peak at 972 cm^{-1} (specifically from the OCH_3 group of polysaccharides such as pectin) [59] has potential to be used in the prediction of leaf ABA, tZ, JA and ACC . This association with leaf JA could be linked to jasmonate-mediated accumulation of leaf-soluble sugars in response to far-red light [85]. A potential peak at 1636 cm^{-1} can be tentatively linked to C=O stretching of carbonyl group, typical of saccharide absorption [59]; this appears to be important in prediction of xylem JA and leaf SA concentrations. Leaf ABA levels appeared to be predicted using a peak at 1049 cm^{-1}, which is associated with cellulose [58]. A potential peak biomarker at 1732 cm^{-1} has been associated with both hemicellulose [83]; this appeared to be a predictor of leaf ABA concentrations. As a key hormone in the drought-induced response, it is perhaps unsurprising that ABA might be estimated using hemicellulose because the leaves of drought-treated plants are known to exhibit a higher content of hemicellulosic polysaccharides [86]. A potential peak biomarker at 1732 cm^{-1} has also been associated with lipid fatty acid esters [83], which is the more probable molecular assignment in its use for estimation of xylem JA concentrations because the fatty acid, linolenic acid, is an important precursor of JA synthesis [87]. Whilst an isolated and controlled peak assignment that could be unambiguously correlated with endpoint effect would be the ideal, in the complex cellular environment this is unlikely to be attainable. In this complex scenario, there will inevitably be a large number of differing peaks

with some more obvious than others. However, we would argue that these shed new insights into mechanism and have the potential to be further investigated.

Whilst leaf hormone concentrations appear to be strongly associated with sugar compounds, in xylem sap samples nucleic acids and bases generally appear to be more relevant indicators of hormone concentration. ABA, tZ and SA concentrations in xylem sap appear to be predicted using a possible peak at 1690 cm^{-1}, which is associated with nucleic acids due to the base carbonyl (C=O) stretching and ring breathing mode [59]. Similar to 1065 cm^{-1}, the peak at 991 cm^{-1} is also associated with C–O stretching of the phosphodiester and the ribose of bases [59]. This peak appeared to be important in xylem sap samples for the prediction of ABA, tZ, SA, and GA1 concentrations. A possible peak at 1713 cm^{-1}, associated with the C=O of the base thymine [59], was identified as important in prediction of tZ and SA concentrations in xylem sap samples. Another possible peak at 1690 cm^{-1}, linked to nucleic acids due to the base carbonyl (C=O) stretching and ring breathing mode [59], appeared to be useful in prediction of xylem sap concentrations of ABA, tZ and SA. A possible peak at 1574 cm^{-1} relating to the C=N of adenine [59], was identified as important in the prediction of xylem GA1 concentrations. Finally, a possible peak at 1531 cm^{-1}, associated previously with modified guanine [59], was used in the prediction of xylem tZ and SA. Again, these peak assignments are tentative but lend novel insights into this changing cellular environment.

ATR-FTIR spectral profiles allow prediction of hormone concentrations

The ATR-FTIR spectrum is information rich and provides an integrated holistic picture of the entire cellular biochemistry [40]. In response to the growth environment, biomolecules unrelated, related and influenced by hormonal activity will be altered, presumably in a dose-related fashion. Chemometrics provides a method to extract this chemical information from spectral absorbances, considering the ratios of different biochemical entities and potentially allowing us to find the "needle in a haystack" of individual hormones in their natural state.

PLSR models have previously been applied to the infrared and Raman spectroscopic absorbances of plant-derived samples to quantify individual components within molecular mixtures [10,11,88–90].

Here we have presented a demonstration of PLSR for the accurate prediction of plant hormone concentrations from ATR-FTIR spectral profiles. The accuracy of PLSR prediction of tZ concentrations was higher for xylem sap (Figure 4a, R^2=0.701) compared with leaf samples (Figure 4c, R^2=0.649). To improve the regression, for example, it would be necessary to narrow down the regression to specicic treatment-hormone models. For example, to create an ABA specific model, application of a wide range of drought severities would be ideal, because ABA is the main regulator of the drought stress response [78] and appears as a key hormone for separation of droughted plants in Figure 3, however this would not be the optimal calibration dataset for another hormone. The PCA loadings based on hormonal data alone (Figures 3b and 3d) show that in both leaf and xylem samples, tZ is a key loading for separation along the axis PC1 in Figures 3a and 3b. Whilst leaf samples in Figure 3b show a good distribution along PCA1, indicating a variety of leaf tZ levels, xylem samples Figure 3a show overlapping clusters. This overlap indicates similarity of xylem sap hormones concentrations across treatment categories, which explains why the xylem sap models have poorer predictive levels than those based on leaf samples.

This trend was also consistent when models were created by treatment categories, in which the hormone predictions based on xylem sap samples (Table 1) did not achieve as high a level of accuracy as those based on freeze-dried ground leaves (Table 2); the high R^2 values achieved in Table 2 indicate an excellent level of prediction from leaf samples. This effect could also be attributed to the fact that these are liquid samples that were injected directly into the HPLC-MS system without any previous extraction, and the higher variability between xylem sap samples (Figure S5†). Refinements to the technique used for collecting

xylem sap [91] and concentrating the samples prior to analysis with UHPLC-HRMS could improve the accuracy of xylem sap hormone quantification. Importantly, Tables 1 and 2 show that it is possible to identify different hormones at the same time to a high accuracy, as these models predicted all hormones in a row simultaneously.

Conclusions

In this study we present a method to predict hormone concentrations using ATR-FTIR spectroscopic measurements and chemometrics, calibrated by UHPLC-HRMS. Once made, the models generated can be applied to new ATR-FTIR spectral data in the absence of UHPLC-HRMS data to predict plant hormone concentrations. As plant hormone concentrations are a key physiological interface for modulation of plant responses in relation to examined processes, the ability to predict them rapidly and non-destructively from spectral data makes it a valuable tool for efficient physiological phenotyping. This methodology has potential for application across a range of species as key plant hormones are conserved [2,92]. ATR-FTIR spectroscopy is a rapid and non-destructive tool, which although demonstrated here using sample preparation, can also be used *in planta* [68]. Consequently, this method could be used in the field to monitor plant hormones and other key signalling molecules produced upon the perception of environmental stress. Biomolecular indications of stress can allow for intervention before the occurrence of phenotypic change, thereby reducing waste, increasing crop yield, and maintaining quality. As can be seen from the variation in R^2 values (Tables 1 and 2) however the accuracy of prediction varies between leaf and xylem sap and between different hormones and environments, suggesting the choice of tissue and growth environment is important when creating models, and would be improved through calibration data.

Authors' Contributions

CAH conceived, planned, and carried out the experiments and data analysis. CLMM provided revision and support for constructing the data analysis models. The manuscript was written by CAH, FLM and MM with contributions from all the authors. FLM provided equipment and expertise in the field of FTIR spectroscopy and chemometrics. PB provided funding for CAH's studentship and expertise in Japanese Knotweed. MM, FLM and JET supervised the project. AA and CMA conducted hormonal analysis.

Conflicts of Interest

The authors declare that there is no conflict of interest.

Acknowledgements

CAH is a member of the Centre for Global Eco-Innovation that is funded by the European Union Regional Development Fund and mediates the collaboration between Lancaster University and Phlorum Ltd. FLM received funding from NIHR Manchester Biomedical Research Centre (NIHR203308). The views expressed are those of the authors and not necessarily those of the NIHR or the Department of Health and Social Care.

References

(1) Anfang, M.; Shani, E. Transport Mechanisms of Plant Hormones. *Curr. Opin. Plant Biol.* **2021**, *63*, 102055. https://doi.org/10.1016/J.PBI.2021.102055.

(2) Blázquez, M. A.; Nelson, D. C.; Weijers, D. Evolution of Plant Hormone Response Pathways. *https://doi.org/10.1146/annurev-arplant-050718-100309* **2020**, *71*, 327–353. https://doi.org/10.1146/ANNUREV-ARPLANT-050718-100309.

(3) Davies, P. J. The Plant Hormones: Their Nature, Occurrence, and Functions. *Plant*

Horm. Biosynthesis, Signal Transduction, Action! **2010**, 1–15. https://doi.org/10.1007/978-1-4020-2686-7_1.

(4) Šimura, J.; Antoniadi, I.; Široká, J.; Tarkowská, D.; Strnad, M.; Ljung, K.; Novák, O. Plant Hormonomics: Multiple Phytohormone Profiling by Targeted Metabolomics. *Plant Physiol.* **2018**, *177* (2), 476. https://doi.org/10.1104/PP.18.00293.

(5) Porfírio, S.; Sonon, R.; Gomes da Silva, M. D. R.; Peixe, A.; Cabrita, M. J.; Azadi, P. Quantification of Free Auxins in Semi-Hardwood Plant Cuttings and Microshoots by Dispersive Liquid–Liquid Microextraction/Microwave Derivatization and GC/MS Analysis. *Anal. Methods* **2016**, *8* (31), 6089–6098. https://doi.org/10.1039/C6AY01289B.

(6) Pradko, A. G.; Litvinovskaya, R. P.; Sauchuk, A. L.; Drach, S. V.; Baranovsky, A. V.; Zhabinskii, V. N.; Mirantsova, T. V.; Khripach, V. A. A New ELISA for Quantification of Brassinosteroids in Plants. *Steroids* **2015**, *97*, 78–86. https://doi.org/10.1016/J.STEROIDS.2014.08.022.

(7) Bosco, R.; Daeseleire, E.; Van Pamel, E.; Scariot, V.; Leus, L. Development of an Ultrahigh-Performance Liquid Chromatography–Electrospray Ionization–Tandem Mass Spectrometry Method for the Simultaneous Determination of Salicylic Acid, Jasmonic Acid, and Abscisic Acid in Rose Leaves. *J. Agric. Food Chem.* **2014**, *62* (27), 6278–6284. https://doi.org/10.1021/JF5023884.

(8) Ge, L.; Peh, C. Y. C.; Yong, J. W. H.; Tan, S. N.; Hua, L.; Ong, E. S. Analyses of Gibberellins by Capillary Electrophoresis–Mass Spectrometry Combined with Solid-Phase Extraction. *J. Chromatogr. A* **2007**, *1159* (1–2), 242–249. https://doi.org/10.1016/J.CHROMA.2007.05.041.

(9) Anagnostopoulos, C. J.; Liapis, K.; Haroutounian, S.; Paspatis, E. Simultaneous

Determination of Different Classes of Plant Growth Regulator in High Water Content Agricultural Products by Liquid Chromatography Tandem Mass Spectrometry and Time of Flight Mass Spectrometry. *J. Liq. Chromatogr. Relat. Technol.* **2013**, *36* (3), 315–335. https://doi.org/10.1080/10826076.2012.657730/SUPPL_FILE/LJLC_A_657730_SUP_26001789.DOC.

(10) Naqvi, S. M. Z. A.; Zhang, Y.; Ahmed, S.; Abdulraheem, M. I.; Hu, J.; Tahir, M. N.; Raghavan, V. Applied Surface Enhanced Raman Spectroscopy in Plant Hormones Detection, Annexation of Advanced Technologies: A Review. *Talanta* **2022**, *236*, 122823. https://doi.org/10.1016/J.TALANTA.2021.122823.

(11) Lew, T. T. S.; Sarojam, R.; Jang, I.-C.; Park, B. S.; Naqvi, N. I.; Wong, M. H.; Singh, G. P.; Ram, R. J.; Shoseyov, O.; Saito, K.; Chua, N.-H.; Strano, M. S. Species-Independent Analytical Tools for next-Generation Agriculture. *Nat. Plants 2020 612* **2020**, *6* (12), 1408–1417. https://doi.org/10.1038/s41477-020-00808-7.

(12) Zhang, C.; Žukauskaitė, A.; Petřík, I.; Pěnčík, A.; Hönig, M.; Grúz, J.; Široká, J.; Novák, O.; Doležal, K. In Situ Characterisation of Phytohormones from Wounded Arabidopsis Leaves Using Desorption Electrospray Ionisation Mass Spectrometry Imaging. *Analyst* **2021**, *146* (8), 2653–2663. https://doi.org/10.1039/D0AN02118K.

(13) Karasov, T. L.; Chae, E.; Herman, J. J.; Bergelson, J. Mechanisms to Mitigate the Trade-Off between Growth and Defense. *Plant Cell* **2017**, *29* (4), 666–680. https://doi.org/10.1105/TPC.16.00931.

(14) Herman, J. J.; Sultan, S. E. Adaptive Transgenerational Plasticity in Plants: Case Studies, Mechanisms, and Implications for Natural Populations. *Front. Plant Sci.* **2011**, *2* (DEC). https://doi.org/10.3389/fpls.2011.00102.

(15) Asif, A.; Baig, M. A.; Siddiqui, M. B. Role of Jasmonates and Salicylates in Plant Allelopathy. **2021**, 115–127. https://doi.org/10.1007/978-3-030-75805-9_6.

(16) Liu, Y.; Oduor, A. M. O.; Dai, Z. C.; Gao, F. L.; Li, J.; Zhang, X.; Yu, F. H. Suppression of a Plant Hormone Gibberellin Reduces Growth of Invasive Plants More than Native Plants. *Oikos* **2021**, *130* (5), 781–789. https://doi.org/10.1111/OIK.07819.

(17) Manoharan, B.; Qi, S. S.; Dhandapani, V.; Chen, Q.; Rutherford, S.; Wan, J. S. H.; Jegadeesan, S.; Yang, H. Y.; Li, Q.; Li, J.; Dai, Z. C.; Du, D. L. Gene Expression Profiling Reveals Enhanced Defense Responses in an Invasive Weed Compared to Its Native Congener During Pathogenesis. *Int. J. Mol. Sci.* **2019**, *20* (19), 4916. https://doi.org/10.3390/IJMS20194916.

(18) Lowry, D. B.; Popovic, D.; Brennan, D. J.; Holeski, L. M. Mechanisms of a Locally Adaptive Shift in Allocation among Growth, Reproduction, and Herbivore Resistance in Mimulus Guttatus*. *Evolution (N. Y).* **2019**, *73* (6), 1168–1181. https://doi.org/10.1111/EVO.13699.

(19) Grossmann, K. Mediation of Herbicide Effects by Hormone Interactions. *J. Plant Growth Regul.* **2003**, *22* (1), 109–122. https://doi.org/10.1007/S00344-003-0020-0/FIGURES/6.

(20) Fennell, M.; Wade, M.; Bacon, K. L. Japanese Knotweed (*Fallopia Japonica*): An Analysis of Capacity to Cause Structural Damage (Compared to Other Plants) and Typical Rhizome Extension. *PeerJ* **2018**, *6*, e5246. https://doi.org/10.7717/peerj.5246.

(21) Santo, P. Assessing Diminution in Value of Residential Properties Affected by Japanese Knotweed. *J. Build. Surv. Apprais. Valuat.* **2017**, *Volume 6* (Number 3), Winter 2017-18, pp. 211-221(11).

(22) Lavoie, C. The Impact of Invasive Knotweed Species (Reynoutria Spp.) on the Environment: Review and Research Perspectives. *Biol. Invasions* **2017**, *19* (8), 2319–2337. https://doi.org/10.1007/s10530-017-1444-y.

(23) van Kleunen, M.; Bossdorf, O.; Dawson, W. The Ecology and Evolution of Alien Plants. *Annu. Rev. Ecol. Evol. Syst.* **2018**, *49* (1), 25–47. https://doi.org/10.1146/annurev-ecolsys-110617-062654.

(24) Parepa, M.; Fischer, M.; Bossdorf, O. Environmental Variability Promotes Plant Invasion. *Nat. Commun.* **2013**, *4* (1), 1–4. https://doi.org/10.1038/ncomms2632.

(25) Urcelay, C.; Austin, A. T. Exotic Plants Get a Little Help from Their Friends. *Science (New York, N.Y.)*. NLM (Medline) May 29, 2020, pp 934–936. https://doi.org/10.1126/science.abc3587.

(26) Liu, Y.; Oduor, A. M. O.; Dai, Z. C.; Gao, F. L.; Li, J.; Zhang, X.; Yu, F. H. Suppression of a Plant Hormone Gibberellin Reduces Growth of Invasive Plants More than Native Plants. *Oikos* **2021**, *130* (5), 781–789. https://doi.org/10.1111/OIK.07819.

(27) Zhang, Y.-Y.; Parepa, M.; Fischer, M.; Bossdorf, O. Epigenetics of Colonizing Species? A Study of Japanese Knotweed in Central Europe. In *Barrett SCH, Colautti RI, Dlugosch KM, Rieseberg LH (Eds) Invasion Genetics*; John Wiley & Sons, Ltd: Chichester, UK, 2016; pp 328–340. https://doi.org/10.1002/9781119072799.ch19.

(28) Richards, C. L.; Schrey, A. W.; Pigliucci, M. Invasion of Diverse Habitats by Few Japanese Knotweed Genotypes Is Correlated with Epigenetic Differentiation. *Ecol. Lett.* **2012**, *15* (9), 1016–1025. https://doi.org/10.1111/j.1461-0248.2012.01824.x.

(29) Rouifed, S.; Byczek, C.; Laffray, D.; Piola, F. Invasive Knotweeds Are Highly Tolerant to Salt Stress. *Environ. Manage.* **2012**, *50*, 1027–1034.

https://doi.org/10.1007/s00267-012-9934-2.

(30) Michalet, S.; Rouifed, S.; Pellassa-Simon, T.; Fusade-Boyer, M.; Meiffren, G.; Nazaret, S.; Piola, F. Tolerance of Japanese Knotweed s.l. to Soil Artificial Polymetallic Pollution: Early Metabolic Responses and Performance during Vegetative Multiplication. *Environ. Sci. Pollut. Res.* **2017**, *24* (26), 20897–20907. https://doi.org/10.1007/s11356-017-9716-8.

(31) Sołtysiak, J. Heavy Metals Tolerance in an Invasive Weed (Fallopia Japonica) under Different Levels of Soils Contamination. *J. Ecol. Eng.* **2020**, *21* (7), 81–91. https://doi.org/10.12911/22998993/125447.

(32) Holm, A. K.; Elameen, A.; Oliver, B. W.; Brandsæter, L. O.; Fløistad, I. S.; Brurberg, M. B. Low Genetic Variation of Invasive Fallopia Spp. in Their Northernmost European Distribution Range. *Ecol. Evol.* **2018**, *8* (1), 755–764. https://doi.org/10.1002/ece3.3703.

(33) Bailey, J. P.; Conolly, A. P. Prize-Winners to Pariahs -A History of Japanese Knotweed s.l. (Polygonaceae) in the British Isles. *Watsonia* **2000**, *23*, 93–110.

(34) Hollingsworth, M. L.; Bailey, J. P. Evidence for Massive Clonal Growth in the Invasive Weed Fallopia Japonica (Japanese Knotweed). *Bot. J. Linn. Soc.* **2000**, *133*, 463–472. https://doi.org/10.1006/bojl.2000.0359.

(35) Skolik, P.; Morais, C. L. M.; Martin, F. L.; McAinsh, M. R. Determination of Developmental and Ripening Stages of Whole Tomato Fruit Using Portable Infrared Spectroscopy and Chemometrics. *BMC Plant Biol.* **2019**, *19* (1), 236. https://doi.org/10.1186/s12870-019-1852-5.

(36) Skolik, P.; McAinsh, M. R.; Martin, F. L. ATR-FTIR Spectroscopy Non-Destructively

Detects Damage-Induced Sour Rot Infection in Whole Tomato Fruit. *Planta* **2019**, *249* (3), 925–939. https://doi.org/10.1007/s00425-018-3060-1.

(37) Morais, C. L. M.; Lima, K. M. G. Principal Component Analysis with Linear and Quadratic Discriminant Analysis for Identification of Cancer Samples Based on Mass Spectrometry. *Artic. J. Braz. Chem. Soc* **2018**, *29* (3), 472–481. https://doi.org/10.21577/0103-5053.20170159.

(38) Morais, C. L. M.; Costa, F. S. L.; Lima, K. M. G. Variable Selection with a Support Vector Machine for Discriminating: Cryptococcus Fungal Species Based on ATR-FTIR Spectroscopy. *Anal. Methods* **2017**, *9* (20), 2964–2970. https://doi.org/10.1039/c7ay00428a.

(39) Mehmood, T.; Liland, K. H.; Snipen, L.; Sæbø, S. A Review of Variable Selection Methods in Partial Least Squares Regression. *Chemom. Intell. Lab. Syst.* **2012**, *118*, 62–69. https://doi.org/10.1016/J.CHEMOLAB.2012.07.010.

(40) Morais, C. L. M.; Lima, K. M. G.; Singh, M.; Martin, F. L. Tutorial: Multivariate Classification for Vibrational Spectroscopy in Biological Samples. *Nature Protocols*. Nature Research July 1, 2020, pp 2143–2162. https://doi.org/10.1038/s41596-020-0322-8.

(41) Met Office. UK Regional Climates. *https://www.metoffice.gov.uk/research/climate/maps-and-data/regional-climates/index* **2019**.

(42) Bailey, J. The Japanese Knotweed Invasion Viewed as a Vast Unintentional Hybridisation Experiment. *Heredity (Edinb).* **2013**. https://doi.org/10.1038/hdy.2012.98.

(43) Smith, H. Light Quality, Photoperception, and Plant Strategy. *Annu. Rev. Plant Physiol.* **1982**, *33* (1), 481–518.

(44) Larsen, D. H.; Woltering, E. J.; Nicole, C. C. S.; Marcelis, L. F. M. Response of Basil Growth and Morphology to Light Intensity and Spectrum in a Vertical Farm. *Front. Plant Sci.* **2020**, *11*, 1893. https://doi.org/10.3389/FPLS.2020.597906/BIBTEX.

(45) Pennisi, G.; Pistillo, A.; Orsini, F.; Cellini, A.; Spinelli, F.; Nicola, S.; Fernandez, J. A.; Crepaldi, A.; Gianquinto, G.; Marcelis, L. F. M. Optimal Light Intensity for Sustainable Water and Energy Use in Indoor Cultivation of Lettuce and Basil under Red and Blue LEDs. *Sci. Hortic. (Amsterdam).* **2020**, *272*, 109508. https://doi.org/10.1016/J.SCIENTA.2020.109508.

(46) Zou, T.; Huang, C.; Wu, P.; Ge, L.; Xu, Y. Optimization of Artificial Light for Spinach Growth in Plant Factory Based on Orthogonal Test. *Plants 2020, Vol. 9, Page 490* **2020**, *9* (4), 490. https://doi.org/10.3390/PLANTS9040490.

(47) Park, Y.; Runkle, E. S. Spectral Effects of Light-Emitting Diodes on Plant Growth, Visual Color Quality, and Photosynthetic Photon Efficacy: White versus Blue plus Red Radiation. *PLoS One* **2018**, *13* (8). https://doi.org/10.1371/JOURNAL.PONE.0202386.

(48) Monaghan, R. M.; Paton, R. J.; Smith, L. C.; Drewry, J. J.; Littlejohn, R. P. The Impacts of Nitrogen Fertilisation and Increased Stocking Rate on Pasture Yield, Soil Physical Condition and Nutrient Losses in Drainage from a Cattle-Grazed Pasture. *New Zeal. J. Agric. Res.* **2005**, *48* (2), 227–240. https://doi.org/10.1080/00288233.2005.9513652.

(49) Dodd, I. C.; Egea, G.; Davies, W. J. Abscisic Acid Signalling When Soil Moisture Is Heterogeneous: Decreased Photoperiod Sap Flow from Drying Roots Limits Abscisic

Acid Export to the Shoots. *Plant. Cell Environ.* **2008**, *31* (9), 1263–1274. https://doi.org/10.1111/J.1365-3040.2008.01831.X.

(50) Albacete, A.; Ghanem, M. E.; Martínez-Andújar, C.; Acosta, M.; Sánchez-Bravo, J.; Martínez, V.; Lutts, S.; Dodd, I. C.; Pérez-Alfocea, F. Hormonal Changes in Relation to Biomass Partitioning and Shoot Growth Impairment in Salinized Tomato (Solanum Lycopersicum L.) Plants. *J. Exp. Bot.* **2008**, *59* (15), 4119–4131. https://doi.org/10.1093/JXB/ERN251.

(51) Groãÿkinsky, D. K.; Albacete, A.; Jammer, A.; Krbez, P.; Van der Graaff, E.; Pfeifhofer, H.; Roitsch, T. A Rapid Phytohormone and Phytoalexin Screening Method for Physiological Phenotyping. *Mol. Plant* **2014**, *7*, 1053–1056. https://doi.org/10.1093/mp/ssu015.

(52) Martin, F. L.; Kelly, J. G.; Llabjani, V.; Martin-Hirsch, P. L.; Patel, I. I.; Trevisan, J.; Fullwood, N. J.; Walsh, M. J. Distinguishing Cell Types or Populations Based on the Computational Analysis of Their Infrared Spectra. *Nat. Protoc.* **2010**, *5* (11), 1748–1760. https://doi.org/10.1038/nprot.2010.133.

(53) Trevisan, J.; Angelov, P. P.; Scott, A. D.; Carmichael, P. L.; Martin, F. L. IRootLab: A Free and Open-Source MATLAB Toolbox for Vibrational Biospectroscopy Data Analysis. *Bioinformatics* **2013**, *29* (8), 1095–1097. https://doi.org/10.1093/bioinformatics/btt084.

(54) Nozahic, V.; Amziane, S. Influence of Sunflower Aggregates Surface Treatments on Physical Properties and Adhesion with a Mineral Binder. *Compos. Part A Appl. Sci. Manuf.* **2012**, *43* (11), 1837–1849. https://doi.org/10.1016/j.compositesa.2012.07.011.

(55) Belfer, S.; Purinson, Y.; Kedem, O. Surface Modification of Commercial Polyamide Reverse Osmosis Membranes by Radical Grafting: An ATR-FTIR Study. *Acta Polym.*

1998, *49* (10–11), 574–582. https://doi.org/10.1002/(sici)1521-4044(199810)49:10/11<574::aid-apol574>3.0.co;2-0.

(56) Shivu, B.; Seshadri, S.; Li, J.; Oberg, K. A.; Uversky, V. N.; Fink, A. L. Distinct β-Sheet Structure in Protein Aggregates Determined by ATR−FTIR Spectroscopy. **2013**. https://doi.org/10.1021/bi400625v.

(57) Jin, N.; Semple, K. T.; Jiang, L.; Luo, C.; Zhang, D.; Martin, F. L. Spectrochemical Analyses of Growth Phase-Related Bacterial Responses to Low (Environmentally-Relevant) Concentrations of Tetracycline and Nanoparticulate Silver. *Analyst* **2018**, *143* (3), 768–776. https://doi.org/10.1039/c7an01800b.

(58) Moskal, P.; Wesełucha-Birczyńska, A.; Łabanowska, M.; Filek, M. Adaxial and Abaxial Pattern of Urtica Dioica Leaves Analyzed by 2DCOS ATR-FTIR as a Function of Their Growth Time and Impact of Environmental Pollution. *Vib. Spectrosc.* **2019**, *104*, 102948. https://doi.org/10.1016/j.vibspec.2019.102948.

(59) Talari, A. C. S.; Martinez, M. A. G.; Movasaghi, Z.; Rehman, S.; Rehman, I. U. Advances in Fourier Transform Infrared (FTIR) Spectroscopy of Biological Tissues. *Appl. Spectrosc. Rev.* **2017**, *52* (5), 456–506. https://doi.org/10.1080/05704928.2016.1230863.

(60) Gorzsas, A. ATR-FTIR Microspectroscopy Brings a Novel Insight Into the Study of Cell Wall Chemistry at the Cellular Level. In *Proceedings of IPSC 2019-2nd International Plant Spectroscopy Conference*; Frontiers Media SA, 2020.

(61) Falcão, L.; Araújo, M. E. M. Tannins Characterization in Historic Leathers by Complementary Analytical Techniques ATR-FTIR, UV-Vis and Chemical Tests. *J. Cult. Herit.* **2013**, *14* (6), 499–508. https://doi.org/10.1016/J.CULHER.2012.11.003.

(62) Morais, C. L. M.; Costa, F. S. L.; Lima, K. M. G. Variable Selection with a Support Vector Machine for Discriminating Cryptococcus Fungal Species Based on ATR-FTIR Spectroscopy. *Anal. Methods* **2017**, *9* (20), 2964–2970. https://doi.org/10.1039/C7AY00428A.

(63) Rana, R.; Herz, K.; Bruelheide, H.; Dietz, S.; Haider, S.; Jandt, U.; Pena, R. Leaf Attenuated Total Reflection Fourier Transform Infrared (ATR-FTIR) Biochemical Profile of Grassland Plant Species Related to Land-Use Intensity. *Ecol. Indic.* **2018**, *84*, 803–810. https://doi.org/10.1016/j.ecolind.2017.09.047.

(64) Sharma, S.; Uttam, K. N. Early Stage Detection of Stress Due to Copper on Maize (Zea Mays L.) by Laser-Induced Fluorescence and Infrared Spectroscopy. *J. Appl. Spectrosc.* **2018**, *85* (4), 771–780. https://doi.org/10.1007/s10812-018-0717-2.

(65) Ajitha, B.; Ashok Kumar Reddy, Y.; Shameer, S.; Rajesh, K. M.; Suneetha, Y.; Sreedhara Reddy, P. Lantana Camara Leaf Extract Mediated Silver Nanoparticles: Antibacterial, Green Catalyst. *J. Photochem. Photobiol. B Biol.* **2015**, *149*, 84–92. https://doi.org/10.1016/j.jphotobiol.2015.05.020.

(66) Geng, Y.; van Klinken, R. D.; Sosa, A.; Li, B.; Chen, J.; Xu, C.-Y. The Relative Importance of Genetic Diversity and Phenotypic Plasticity in Determining Invasion Success of a Clonal Weed in the USA and China. *Front. Plant Sci.* **2016**, *7*, 216. https://doi.org/10.3389/fpls.2016.00213.

(67) Richards, C. L.; Bossdorf, O.; Muth, N. Z.; Gurevitch, J.; Pigliucci, M. Jack of All Trades, Master of Some? On the Role of Phenotypic Plasticity in Plant Invasions. *Ecol. Lett.* **2006**, *9* (8), 981–993. https://doi.org/10.1111/j.1461-0248.2006.00950.x.

(68) Butler, H. J.; McAinsh, M. R.; Adams, S.; Martin, F. L. Application of Vibrational Spectroscopy Techniques to Non-Destructively Monitor Plant Health and

Development. *Anal. Methods* **2015**, *7* (10), 4059–4070. https://doi.org/10.1039/C5AY00377F.

(69) Holden, C. A.; Morais, C. L. M.; Taylor, J. E.; Martin, F. L.; Beckett, P.; McAinsh, M. Regional Differences in Clonal Japanese Knotweed Revealed by Chemometrics-Linked Attenuated Total Reflection Fourier-Transform Infrared Spectroscopy. *BMC Plant Biol. 2021 211* **2021**, *21* (1), 1–20. https://doi.org/10.1186/S12870-021-03293-Y.

(70) Traoré, M.; Kaal, J.; Martínez Cortizas, A. Differentiation between Pine Woods According to Species and Growing Location Using FTIR-ATR. *Wood Sci. Technol.* **2018**, *52* (2), 487–504. https://doi.org/10.1007/s00226-017-0967-9.

(71) Holden, C. A.; Bailey, J. P.; Taylor, J. E.; Martin, F.; Beckett, P.; McAinsh, M. Know Your Enemy: Application of ATR-FTIR Spectroscopy to Invasive Species Control. *PLoS One* **2022**, *17* (1), e0261742. https://doi.org/10.1371/JOURNAL.PONE.0261742.

(72) Wolters, H.; Jürgens, G. Survival of the Flexible: Hormonal Growth Control and Adaptation in Plant Development. *Nat. Rev. Genet.* **2009**, *10* (5), 305–317. https://doi.org/10.1038/NRG2558.

(73) Spalding, K.; Bonnier, F.; Bruno, C.; Blasco, H.; Board, R.; Benz-de Bretagne, I.; Byrne, H. J.; Butler, H. J.; Chourpa, I.; Radhakrishnan, P.; Baker, M. J. Enabling Quantification of Protein Concentration in Human Serum Biopsies Using Attenuated Total Reflectance – Fourier Transform Infrared (ATR-FTIR) Spectroscopy. *Vib. Spectrosc.* **2018**, *99*, 50–58. https://doi.org/10.1016/j.vibspec.2018.08.019.

(74) Wagner, H.; Liu, Z.; Langner, U.; Stehfest, K.; Wilhelm, C. The Use of FTIR Spectroscopy to Assess Quantitative Changes in the Biochemical Composition of

Microalgae. *J. Biophotonics* **2010**, *3* (8–9), 557–566. https://doi.org/10.1002/jbio.201000019.

(75) Butler, H. J.; Martin, F. L.; Roberts, M. R.; Adams, S.; McAinsh, M. R. Observation of Nutrient Uptake at the Adaxial Surface of Leaves of Tomato (*Solanum Lycopersicum*) Using Raman Spectroscopy. *Anal. Lett.* **2020**, *53* (4), 536–562. https://doi.org/10.1080/00032719.2019.1658199.

(76) Strong, R.; Martin, F. L.; Jones, K. C.; Shore, R. F.; Halsall, C. J. Subtle Effects of Environmental Stress Observed in the Early Life Stages of the Common Frog, Rana Temporaria. *Sci. Rep.* **2017**, *7* (1), 1–13. https://doi.org/10.1038/srep44438.

(77) Heap, B.; Holden, C.; Taylor, J.; McAinsh, M. <scp>ROS</Scp> Crosstalk in Signalling Pathways. In *eLS*; Wiley, 2020; pp 1–9. https://doi.org/10.1002/9780470015902.a0025271.

(78) Bharath, P.; Gahir, S.; Raghavendra, A. S. Abscisic Acid-Induced Stomatal Closure: An Important Component of Plant Defense Against Abiotic and Biotic Stress. *Front. Plant Sci.* **2021**, *12*, 324. https://doi.org/10.3389/FPLS.2021.615114/BIBTEX.

(79) Maruri-López, I.; Aviles-Baltazar, N. Y.; Buchala, A.; Serrano, M. Intra and Extracellular Journey of the Phytohormone Salicylic Acid. *Front. Plant Sci.* **2019**, *0*, 423. https://doi.org/10.3389/FPLS.2019.00423.

(80) Saleem, M.; Fariduddin, Q.; Castroverde, C. D. M. Salicylic Acid: A Key Regulator of Redox Signalling and Plant Immunity. *Plant Physiol. Biochem.* **2021**, *168*, 381–397. https://doi.org/10.1016/J.PLAPHY.2021.10.011.

(81) Zheng, W.; Wang, S. Y. Antioxidant Activity and Phenolic Compounds in Selected Herbs. *J. Agric. Food Chem.* **2001**, *49* (11), 5165–5170.

https://doi.org/10.1021/JF010697N.

(82) Heredia-Guerrero, J. A.; Benítez, J. J.; Domínguez, E.; Bayer, I. S.; Cingolani, R.; Athanassiou, A.; Heredia, A. Infrared and Raman Spectroscopic Features of Plant Cuticles: A Review. *Front. Plant Sci.* **2014**, *5*, 305. https://doi.org/10.3389/fpls.2014.00305.

(83) Ord, J.; Butler, H. J.; McAinsh, M. R.; Martin, F. L. Spectrochemical Analysis of Sycamore (Acer Pseudoplatanus) Leaves for Environmental Health Monitoring. *Analyst* **2016**, *141* (10), 2896–2903. https://doi.org/10.1039/C6AN00392C.

(84) Liu, X.; Renard, C. M. G. C.; Bureau, S.; Le Bourvellec, C. Revisiting the Contribution of ATR-FTIR Spectroscopy to Characterize Plant Cell Wall Polysaccharides. *Carbohydr. Polym.* **2021**, *262*, 117935. https://doi.org/10.1016/J.CARBPOL.2021.117935.

(85) Courbier, S.; Grevink, S.; Sluijs, E.; Bonhomme, P.-O.; Kajala, K.; Wees, S. C. M. Van; Pierik, R. Far-Red Light Promotes Botrytis Cinerea Disease Development in Tomato Leaves via Jasmonate-Dependent Modulation of Soluble Sugars. *Plant. Cell Environ.* **2020**, *43* (11), 2769–2781. https://doi.org/10.1111/PCE.13870.

(86) van der Weijde, T.; Huxley, L. M.; Hawkins, S.; Sembiring, E. H.; Farrar, K.; Dolstra, O.; Visser, R. G. F.; Trindade, L. M. Impact of Drought Stress on Growth and Quality of Miscanthus for Biofuel Production. *GCB Bioenergy* **2017**, *9* (4), 770–782. https://doi.org/10.1111/GCBB.12382.

(87) Gfeller, A.; Dubugnon, L.; Liechti, R.; Farmer, E. E. Jasmonate Biochemical Pathway. *Sci. Signal.* **2010**, *3* (109). https://doi.org/10.1126/SCISIGNAL.3109CM3/ASSET/57BCEEBB-B6E4-4299-8646-8E4F84042400/ASSETS/GRAPHIC/3109CM3-F3.JPEG.

(88) Zhu, J.; Agyekum, A. A.; Kutsanedzie, F. Y. H.; Li, H.; Chen, Q.; Ouyang, Q.; Jiang, H. Qualitative and Quantitative Analysis of Chlorpyrifos Residues in Tea by Surface-Enhanced Raman Spectroscopy (SERS) Combined with Chemometric Models. *LWT* **2018**, *97*, 760–769. https://doi.org/10.1016/J.LWT.2018.07.055.

(89) Romera-Fernández, M.; Berrueta, L. A.; Garmón-Lobato, S.; Gallo, B.; Vicente, F.; Moreda, J. M. Feasibility Study of FT-MIR Spectroscopy and PLS-R for the Fast Determination of Anthocyanins in Wine. *Talanta* **2012**, *88*, 303–310. https://doi.org/10.1016/J.TALANTA.2011.10.045.

(90) Bensemmane, N.; Bouzidi, N.; Daghbouche, Y.; Garrigues, S.; de la Guardia, M.; El Hattab, M. Quantification of Phenolic Acids by Partial Least Squares Fourier-Transform Infrared (PLS-FTIR) in Extracts of Medicinal Plants. *Phytochem. Anal.* **2021**, *32* (2), 206–221. https://doi.org/10.1002/PCA.2974.

(91) Netting, A. G.; Theobald, J. C.; Dodd, I. C. Xylem Sap Collection and Extraction Methodologies to Determine in Vivo Concentrations of ABA and Its Bound Forms by Gas Chromatography-Mass Spectrometry (GC-MS). *Plant Methods* **2012**, *8* (1), 1–14. https://doi.org/10.1186/1746-4811-8-11/FIGURES/8.

(92) Wang, C.; Liu, Y.; Li, S.-S.; Han, G.-Z. Insights into the Origin and Evolution of the Plant Hormone Signaling Machinery. *Plant Physiol.* **2015**, *167* (3), 872–886. https://doi.org/10.1104/PP.114.247403.

Footnotes

† Electronic supplementary information (ESI):

- **Table S1:** Lighting conditions within each Snijder cabinet.

- **Figure S1:** Spectra from a) 'Light' (LC, LD, LN, LLN) b) 'Shade' (SC, SD, SN, SLN) cabinets, providing red: far-red ratios of 5.6 and 0.4 respectively.
- **Table S2:** Reagents used for Hoagland's solution.
- **Figure S2:** Chromatogram and mass spectra for the hormone salicylic acid
- **Table S3:** Hormone descriptions and molecular ion masses
- **Figure S3: (a)** Raw and **(b)** pre-processed class means spectra in the fingerprint region from xylem sap, **(c)** Raw and **(d)** pre-processed (Savitzky–Golay 2nd differentiation, n=9, and vector normalisation) class means spectra in the fingerprint region from freeze-dried ground leaves.
- **Table S4:** SVM parameters for classification.
- **Figure S4:** Loadings from spectra of a) xylem sap and b) freeze-dried ground leaf samples
- **Table S5:** PCA-loadings and biomarkers: key wavenumbers and compounds, which differentiate spectral profiles of plants from different growth conditions for both xylem sap and freeze-dried ground sample types.
- **Figure S5:** Hormone profiles from xylem sap in ng·ml^{-1} sap for a) 1-amino-cyclopropanecarboxylic acid (ACC), b) trans-Zeatin (tZ), c) isopentyl-adenine (iP), d) salicylic acid (SA), e) abscisic acid (ABA), f) jasmonic acid (JA), g) gibberellin A1 (GA_1), gibberellin A4 (GA_4), gibberellic acid (GA_3), *trans*-zeatin riboside (tZR), and indole-3-acetic acid (IAA).
- **Figure S6:** Hormone profiles from freeze-dried ground leaves ng·g^{-1} dry weight for a) 1-amino-cyclopropanecarboxylic acid (ACC), b) trans-Zeatin (tZ), c) isopentyl-adenine (iP), d) salicylic acid (SA), e) abscisic acid (ABA), f) jasmonic acid (JA), g) gibberellin A1 (GA_1), gibberellin A4 (GA_4), gibberellic acid (GA_3), *trans*-zeatin riboside (tZR), and indole-3-acetic acid (IAA).

- **Figure S7:** PLS regression graphs for prediction of plant hormones from xylem sap. Validation was performed by Monte-Carlo cross-validation with 20% of samples left-out for validation during 1000 iterations. All models were built using 10 latent variables.
- **Figure S8:** PLSR regression coefficients for prediction of plant hormones from xylem sap.
- **Figure S9:** PLS regression graphs for prediction of plant hormones from freeze-dried ground leaves. Validation was performed by Monte-Carlo cross-validation with 20% of samples left-out for validation during 1000 iterations. All models were built using 10 latent variables.
- **Figure S10:** PLSR regression coefficients for prediction of plant hormones from freeze-dried ground leaves.
- **Table S6:** Number of latent variables (LVs) used to build the PLSR models between different types of treatment and hormone levels for xylem sap and freeze-dried ground (FDG) leaves. Higher number of LVs represents higher model complexity.
- **Data S1:** Hormone concentrations measured by ultra-high-performance liquid chromatography-high-resolution mass spectrometry and spectral absorbances measured by attenuated total reflection Fourier-transform infrared spectroscopy for freeze-dried ground leaf and xylem sap samples.

REVIEWER REPORT(S):

Referee: 1

Comments to the Author

Having reconsidered the analysis of Figure 4, the text (lines 495- 563) following this statement "The regression coefficients in Figure 4 aid to identify key spectral wavenumbers used in the model creation for tZ concentration prediction." is not clearly well supported, and especially the repeated assignment of precise wavenumber values to features in the spectrum which appear to be quite noisy.

We have amended the manuscript to clarify this issue (lines 496-578). In addition, we have modified Figure 4 by marking the main wavenumbers associated with largest weights during the regression model, which is related with the increase or decrease of the hormone concentration. Furthermore, the "noisy" aspect is due to the spectral pre-processing – the 2nd derivative. The 2nd derivative is the slope of the slope of the absorbance (x) at certain wavenumber (w): $\frac{d^2x}{dw^2}$; which has a "noisy" appearance given the spectral resolution. However, this pre-processing magnifies the differences between the spectra since small differences in the original absorbance is now much amplified. Since the PLS regression model was built with the pre-processed data, the regression coefficient will have the same aspect. The PLS regression coefficients help to identify key spectral markers since those coefficients with larger values (either positive or negative) have larger weight in the regression. For example, the hormone concentration prediction (y) of a test sample (x_{test}) is given by:

$$y = x_{test} \times b$$

where b are the regression coefficients. Therefore, those regression coefficients are directly related to the weight of each wavenumber towards the hormone concentration.

The precise wavenumber values reported in the text are tentative assignments based on the literature, which match some of the regression coefficients with larger weights for each hormone and sample type.

Electronic Supplimentary Information

Attenuated total reflection Fourier-transform infrared spectroscopy for the prediction of hormone concentrations in plants

Claire A Holden[1], Martin McAinsh[1], Jane E Taylor[1], Paul Beckett[2], Alfonso Albacete[3,4], Cristina Martínez-Andújar[4], Camilo L. M. Morais[5,6], Francis L Martin[7,8]*

[1] Lancaster Environment Centre, Lancaster University, UK

[2] Phlorum Ltd, UK

[3] Institute for Agro-Environmental Research and Development of Murcia (IMIDA), Department of Plant Production and Agrotechnology, C/ Mayor s/n, E-30150 La Alberca, Murcia, Spain

[4] CEBAS-CSIC. Department of Plant Nutrition. Campus Universitario de Espinardo, E-30100 Murcia, Spain

[5] Center for Education, Science and Technology of the Inhamuns Region, State University of Ceará, Tauá 63660-000, Brazil

[6] Graduate Program in Chemistry, Institute of Chemistry, Federal University of Rio Grande do Norte, Natal 59072-970, Brazil

[7] Department of Cellular Pathology, Blackpool Teaching Hospitals NHS Foundation Trust, Whinney Heys Road, Blackpool FY3 8NR, UK

[8] Biocel UK Ltd., Hull HU10 6TS, UK

*Corresponding author: Francis L Martin; Email: francis.martin2@nhs.net

Table S1: Lighting conditions within each Snijder cabinet

Light Quality	**'Light' Groups: LC, LD, LN and LLN**	**'Shade' Groups: SC, SD, SN and SLN**
PFD-R(700-780 nm)	72.51	49.28
PFD-FR(600-700 nm)	12.89	116.5
photosynthetic photon flux density PPFD(400-700 nm)	189.8	124.7
PFD-UV(380-400 nm)	0.5677	0.4402
PFD-B(400-500 nm)	33.93	21.58
PFD-G(500-600 nm)	83.40	53.87
peak wavelength λp / nm	545	741
peak wavelength value λpV / $mWm^{-2}nm^{-1}$	827.7	576.0
Irradiance	43.2	45.8
Illuminance/ lux.	15128	9617

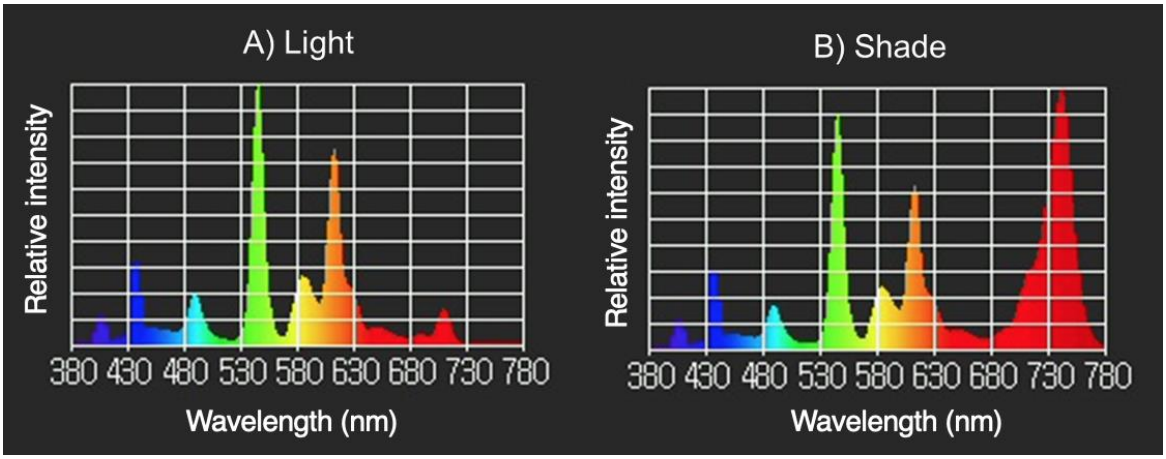

Figure S1: Spectra from a) 'Light' b) 'Shade' cabinets, providing red: far-red ratios of 5.6 and 0.4 respectively.

Table S2: Reagents used for Hoagland's solution. Full strength Hoagland's solution was made using 100 mL of solution A, 100 mL of solution B and 10 mL of solution C in 10 L of deionised water.

Solution	**Reagent**	**Concentration/ gL^{-1}**
A (100 mL)	NH_4NO_3	8.000
	$Ca(NO_3)_2.4H_2O$	82.600
	KNO_3	35.700
B (100 mL)	KNO_3	5.000
	KH_2PO_4	27.400
	$MgSO_4.7H_2O$ *added first	24.600
	$MnSO_4.5H_2O$	0.053
	H_3BO_3	0.140
	$CuSO_4.5H_2O$	0.015
	$(NH_4)_6Mo_7O_{24}.4H_2O$	0.008
	$ZnSO_4.7H_2O$	0.060
C (10 mL)	Fe-EDTA	36.71

a)

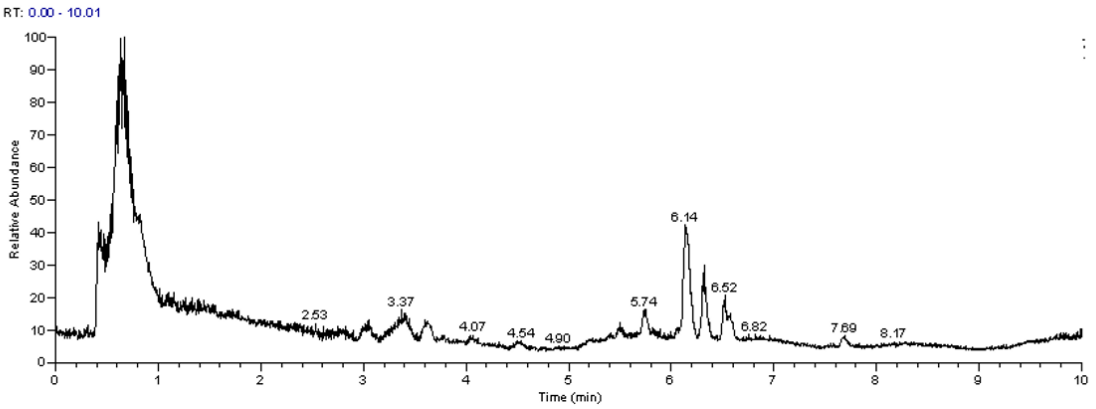

Quan Component's Peak Report

Component Name: SA

b)

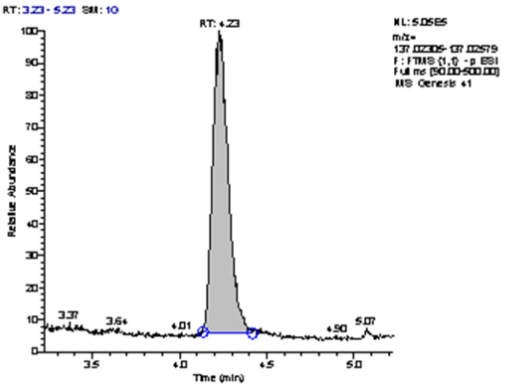

Figure S2: Total ion current and mass chromatogram (m/z 137.02442) for salicylic acid.

Table S3: Hormone descriptions and molecular ion masses

Hormone class	**Abbreviation**	**Hormone**	**Molecular formula**	**[M-H]$^-$**
Ethylene precursor	ACC	1-Aminocyclopropane-1-carboxylic acid	$C_4H_7NO_2$	100.04040
Cytokinins	t-Z	*trans*-Zeatin	$C_{10}H_{13}N_5O$	218.10473
	t-ZR	*trans*-Zeatin riboside	$C_{15}H_{21}N_5O_5$	350.14699
	iP	Isopentenyladenine	$C_{10}H_{13}N_5$	202.10982
Gibberellins	GA1	Gibberellin A1	$C_{19}H_{24}O_6$	347.15001
	GA3	Gibberellin A3	$C_{19}H_{22}O_6$	345.13436
	GA4	Gibberellin A4	$C_{19}H_{24}O_5$	331.15510
Auxins	IAA	Indole-3-acetic acid	$C_{10}H_9NO_2$	174.05605
Abscisic acid	ABA	Abscisic acid	$C_{15}H_{20}O_4$	263.12888
Salicylates	SA	Salicylic acid	$C_7H_6O_3$	137.02442
Jasmonates	JA	Jasmonic acid	$C_{12}H_{18}O_3$	209.11832

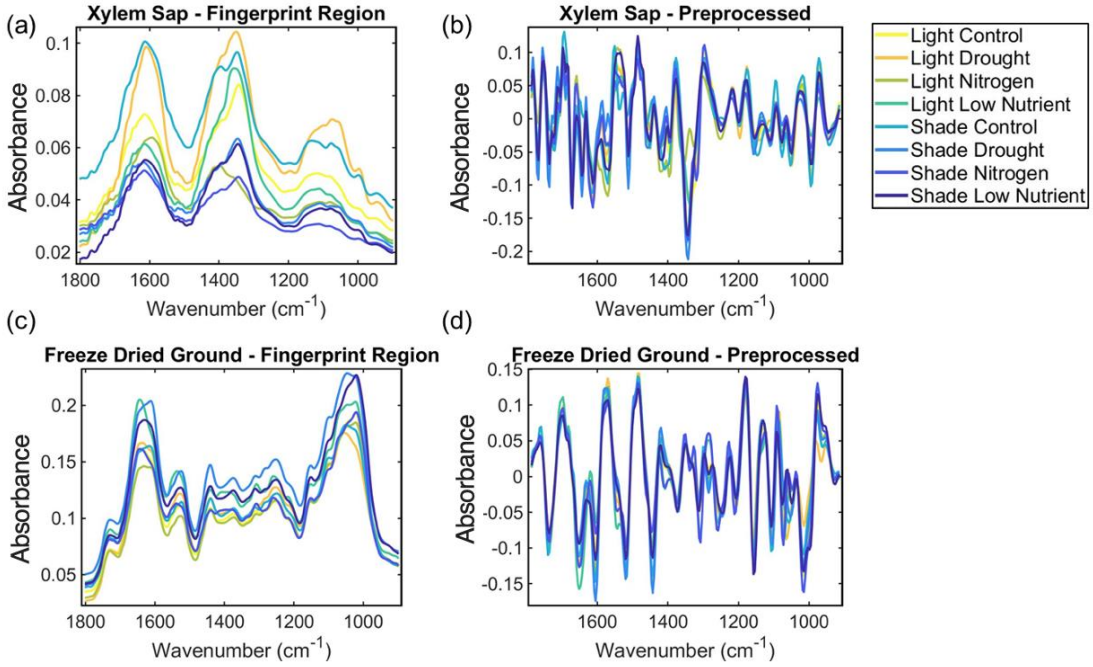

Figure S3: (a) Raw and **(b)** pre-processed class means spectra in the fingerprint region from xylem sap, **(c)** Raw and **(d)** pre-processed (Savitzky–Golay 2nd differentiation, *n*=9, and vector normalisation) class means spectra in the fingerprint region from freeze-dried ground leaves. Each class is grouped by treatment; Light Control (LC), Light Drought (LD), Light Nitrogen (LN), Light Low Nitrogen (LLN), Shade Control (SC), Shade Drought (SD), Shade Nitrogen (SN) and Shade Low Nitrogen (SLN).

Table S4: SVM parameters for classification

	Cost	Gamma (γ)	Number of support vectors (N_{SV})
Xylem Sap	31.6228	3.1623	314
Freeze-dried ground leaves	100	3.1623	194

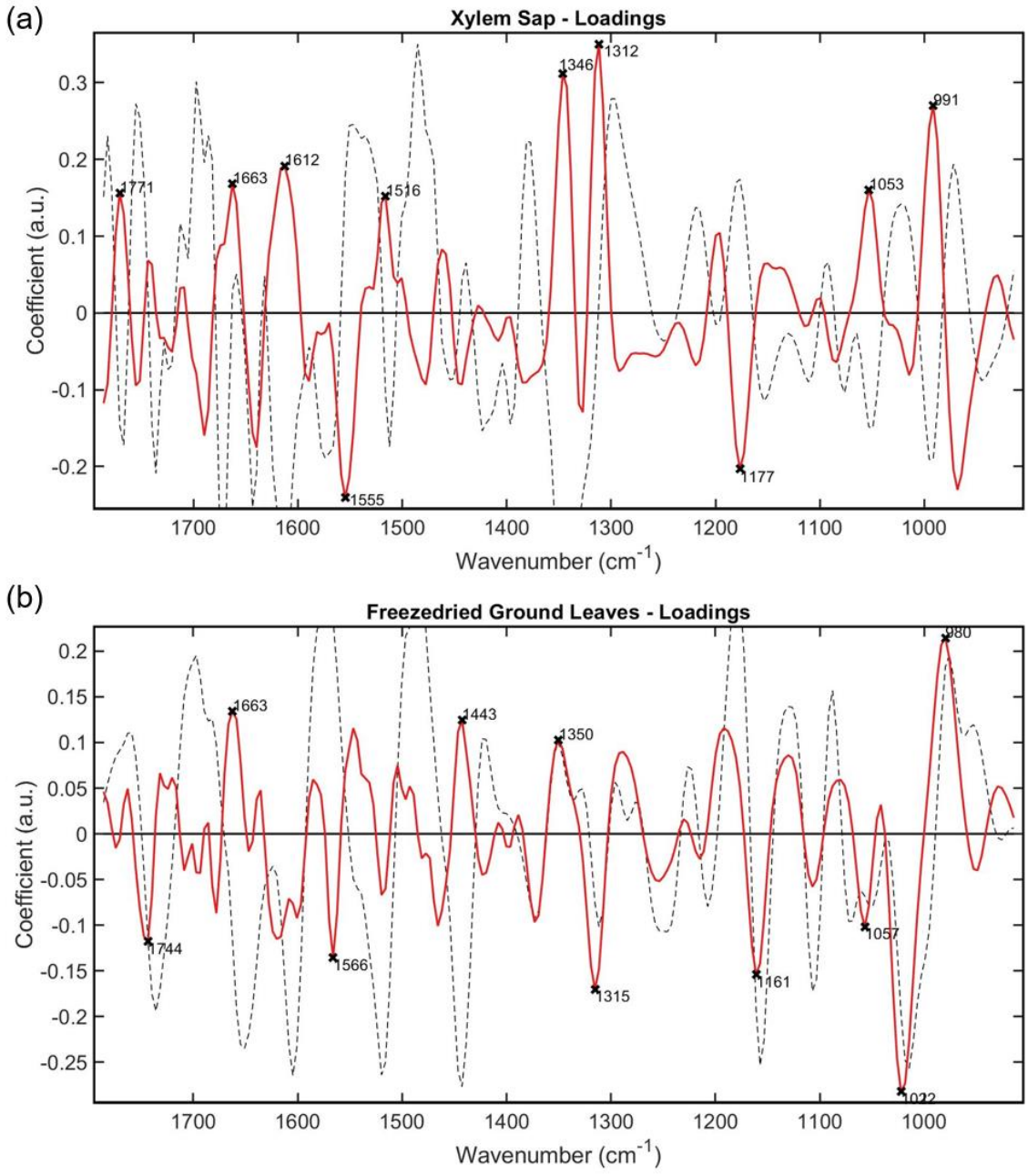

Figure S4: Loadings from spectra of a) xylem sap and b) freeze-dried ground leaf samples. These are the key wavenumbers which differentiate spectral profiles of different treatment groups from one another. The red line represents the PCA loadings and the black-dashed line represents the total mean spectrum, scaled to fit.

Table S5: PCA-loadings and biomarkers: key wavenumbers and compounds, which differentiate ATR-FTIR spectral profiles of plants from different growth conditions for both xylem sap and freeze-dried ground sample types.

Sample Type	Wavelength / cm	Tentative Molecular Assignment	Reference
Xylem sap	1770.65	v_1 symmetric stretching of C=O in the carboxylic acid of pectin or ester bond of triacylglycerol	(Nozahic and Amziane, 2012)
	1662.64	The N-C=O group of proteins. Amide I vibrations, specifically associated with disordered secondary structures or turns.	(Belfer *et al.*, 1998; Shivu *et al.*, 2013)
	1612.49	Amide I	(Jin *et al.*, 2018)
	1554.62	C-N stretching and N-H bending (Amide II vibration); C-O-O^- asymmetric stretching of proteins and glutamate	(Moskal *et al.*, 2019)
	1516.05	Amide II vibrations of proteins	(Talari *et al.*, 2017)
	1346.31	Cellulose	(Gorzsas, 2020)
	1311.59	Amide III vibrations of proteins	(Talari *et al.*, 2017)
	1176.58	C–O stretch vibration of tannins	(Falcão and Araújo, 2013)
	1053.13	Starch, *v*C–O and δC–O of carbohydrates	(Talari *et al.*, 2017; Jin *et al.*, 2018)
	991.41	C–O ribose	(Camilo L. M. Morais *et al.*, 2017)
Freeze-dried ground leaves	1743.53	Ester C=O stretch: triglycerides	(Talari *et al.*, 2017)
	1662.52	The N-C=O group of proteins. Amide I vibrations, specifically associated with disordered secondary structures or turns.	(Belfer *et al.*, 1998; Shivu *et al.*, 2013)
	1566.09	N-H bending; C-N stretching (Amide II band of proteins)	(Rana *et al.*, 2018)
	1442.65	Pectin	(Sharma and Uttam, 2018)
	1350.08	Phosphodiester stretching bands region (for absorbances due to starch)	(Talari *et al.*, 2017)
	1315.36	Cellulose	(Sharma and Uttam, 2018)
	1161.06	C–OH groups of serine, threonine and tyrosine of proteins, C-O stretching and hydrogen bonding	(Talari *et al.*, 2017)
	1056.92	Stretching C–O deoxyribose	(Talari *et al.*, 2017)
	1022.2	Starch	(Talari *et al.*, 2017)
	979.769	C-OH stretching of secondary alcohols and C-O-C vibrations of polysaccharides	(Ajitha *et al.*, 2015)

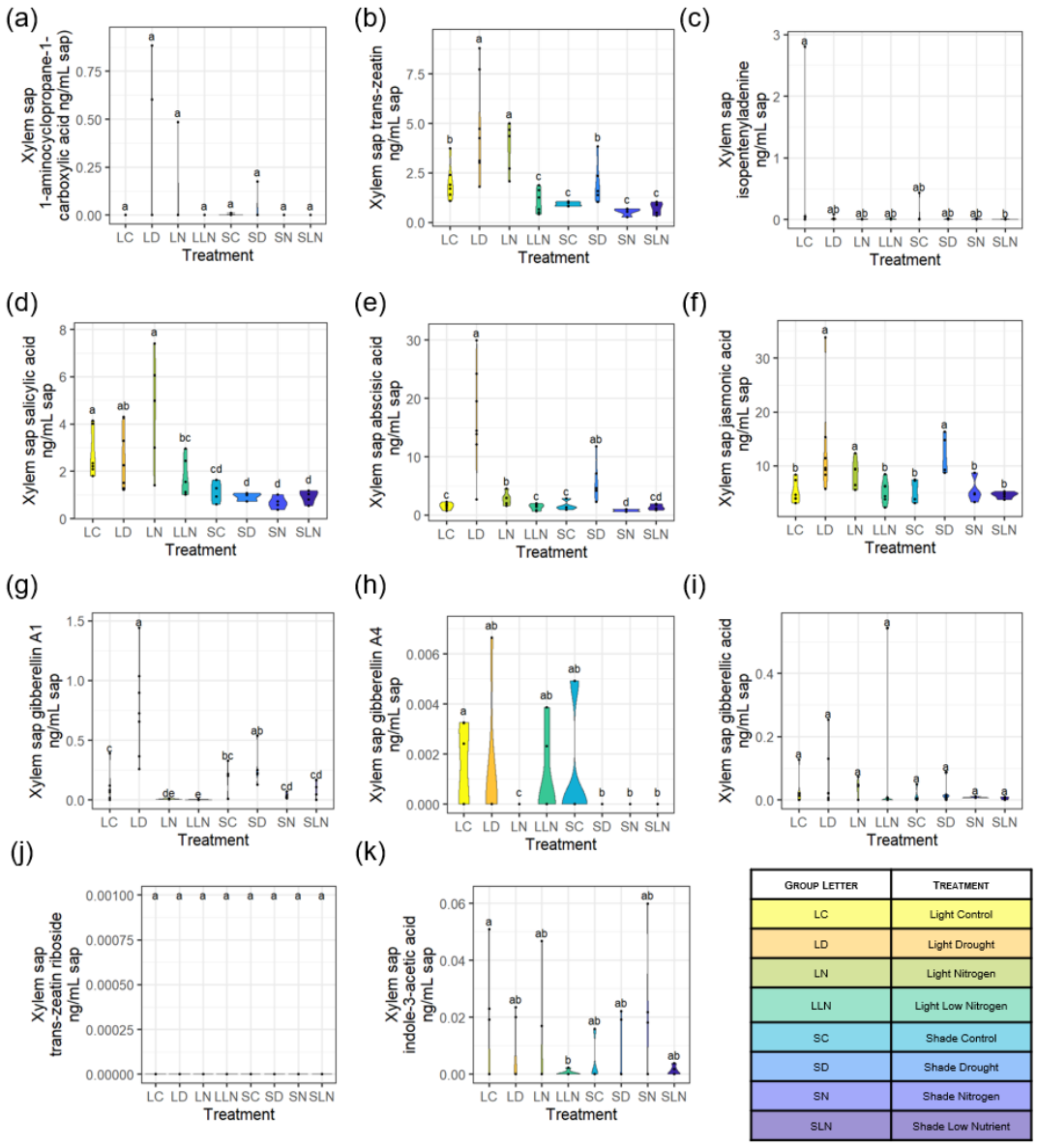

Figure S5: Hormone profiles from xylem sap measured using UHPLC– HRMS in ng·ml^{-1} sap for a) 1-amino-cyclopropanecarboxylic acid (ACC), b) *trans*-Zeatin (tZ), c) isopentyl-adenine (iP), d) salicylic acid (SA), e) abscisic acid (ABA), f) jasmonic acid (JA), g) gibberellin A1 (GA_1), gibberellin A4 (GA_4), gibberellic acid (GA_3), *trans*-zeatin riboside (tZR), and indole-3-acetic acid (IAA). ABA concentration was highest in the drought categories; LD had ~17 ng·ml^{-1} sap of ABA compared with SD which had ~7 ng·ml^{-1} sap, whilst the other categories ranged between ~1 and 3 ng·ml^{-1} sap. Shade plants had lower xylem SA levels than light ones, in the range of 0.7-1.1 ng·ml^{-1} sap compared with 1.6-4.5 ng·ml^{-1} sap respectively. Xylem sap levels of GA_1 were approximately three times higher in LD than most other treatment groups, although this was not significantly different to the other drought category, SD, due to high variation.

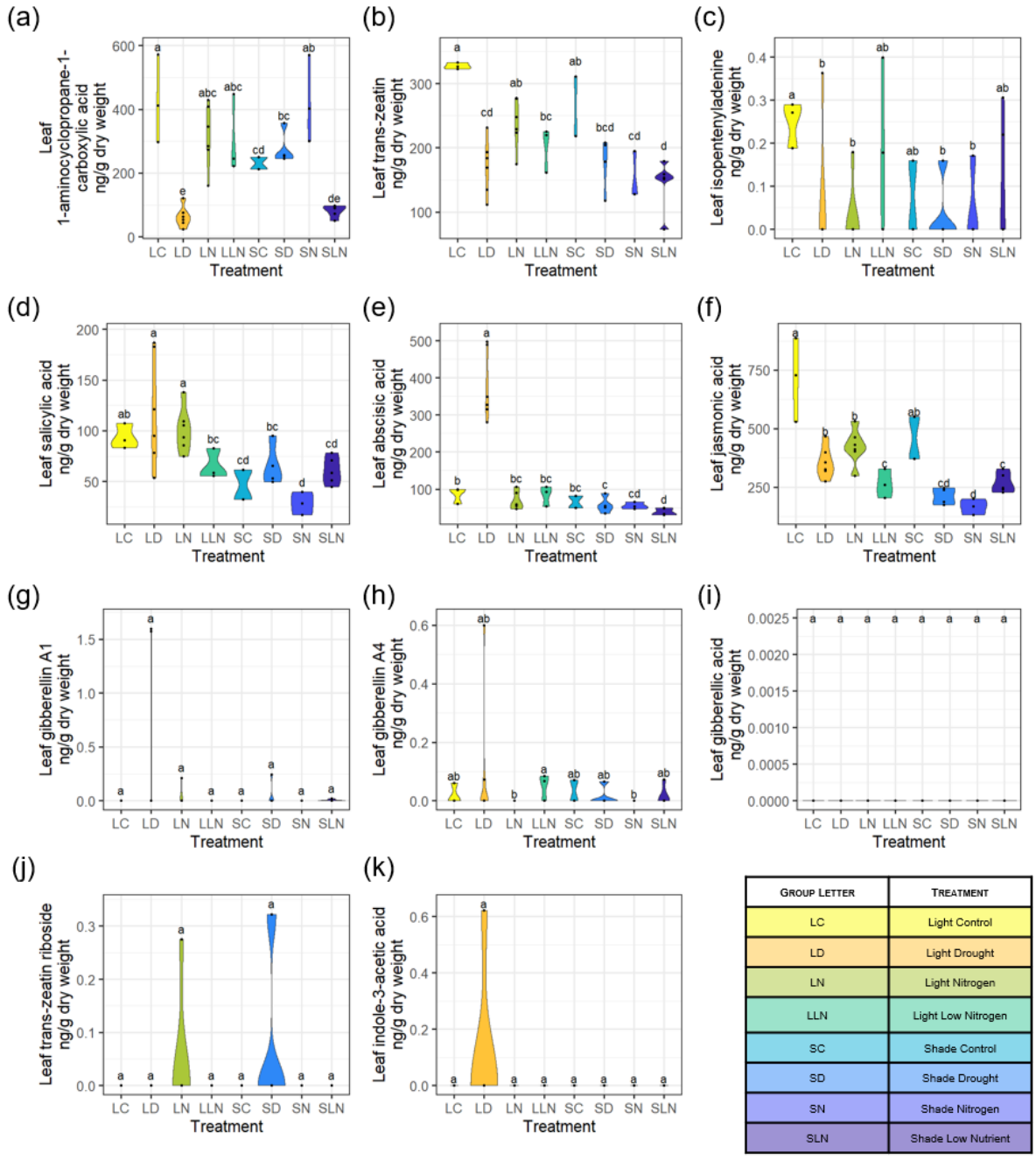

Figure S6: Hormone profiles from freeze-dried ground leaves measured using UHPLC–HRMS in ng·g^{-1} dry weight for a) 1-amino-cyclopropanecarboxylic acid (ACC), b) *trans*-Zeatin (tZ), c) isopentyl-adenine (iP), d) salicylic acid (SA), e) abscisic acid (ABA), f) jasmonic acid (JA), g) gibberellin A1 (GA_1), gibberellin A4 (GA_4), gibberellic acid (GA_3), *trans*-zeatin riboside (tZR), and indole-3-acetic acid (IAA). Leaf ABA levels (Figure S5) were approximately quadruple in LD than those of the other categories. Plants grown under LC treatment category registered approximately 4.5-fold higher of leaf tZ than those in SLN. Leaf JA concentration was significantly higher in the light control group LC (~710 ng·g^{-1} dry weight) compared to all other groups (ranging 170-420 ng·g^{-1} dry weight), except the shade control group SC (~460 ng·g^{-1} dry weight). The highest iP hormone concentration was found in leaves of category LC, at 0.25 ng·g^{-1} dry weight. This value was significantly higher compared to groups LD, LN, SD, SN (ranging 0.03-0.6 ng·g^{-1} dry weight), with the other groups falling in between.

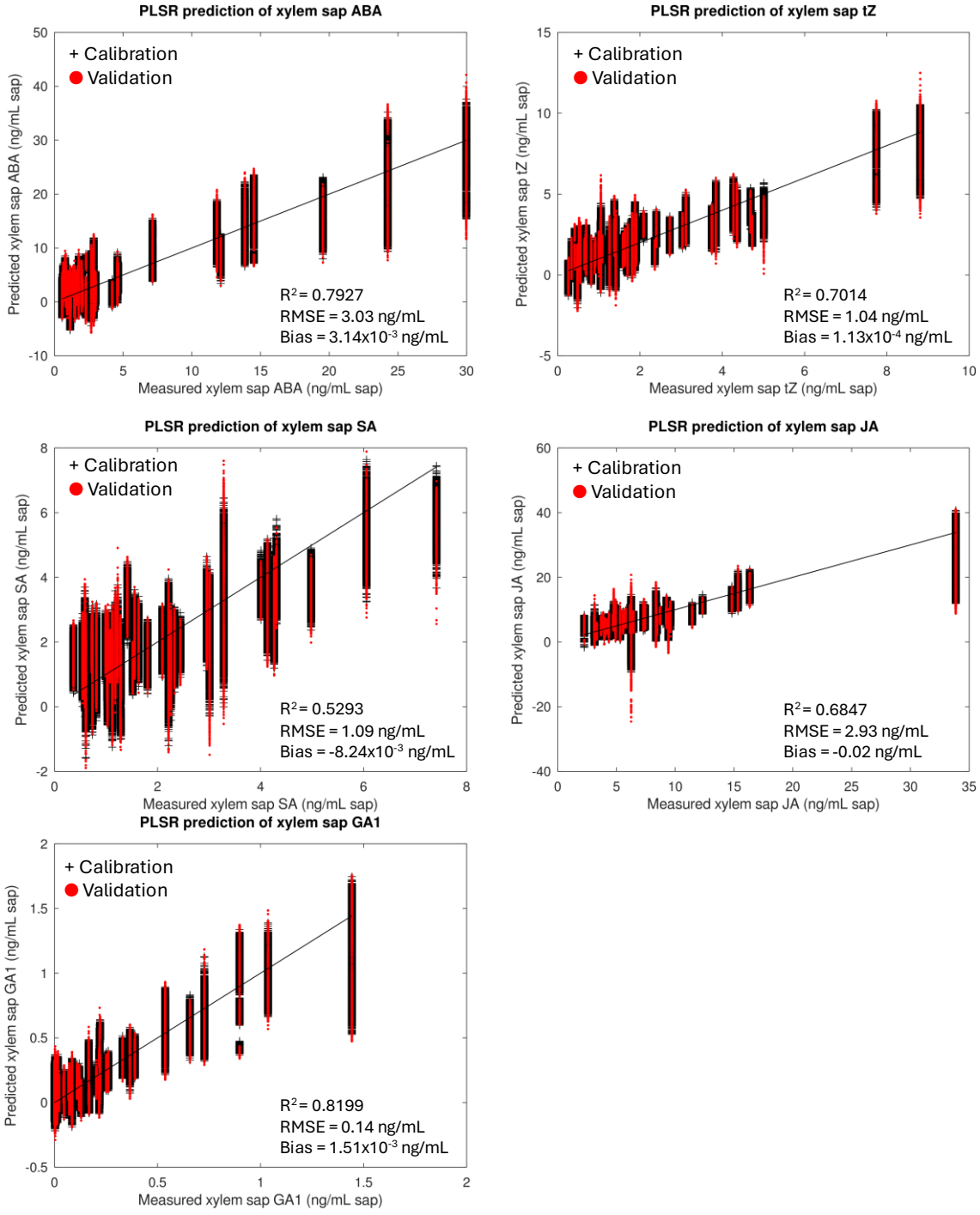

Figure S7: PLS regression graphs for prediction of plant hormones from xylem sap. Validation was performed by Monte-Carlo cross-validation with 20% of samples left-out for validation during 1000 iterations. All models were built using 10 latent variables.

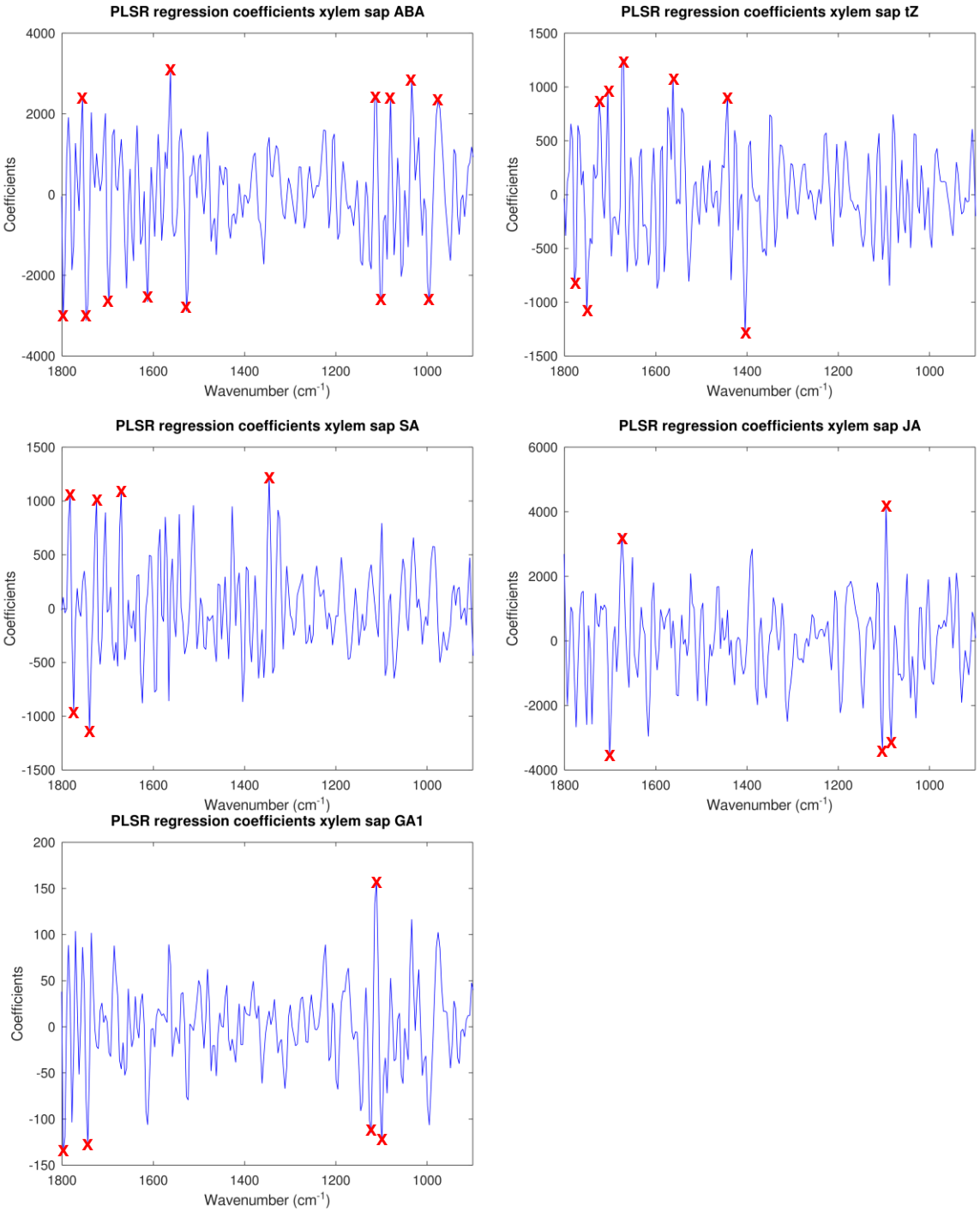

Figure S8: PLSR regression coefficients for prediction of plant hormones from xylem sap. Main wavenumbers are marked with a red X.

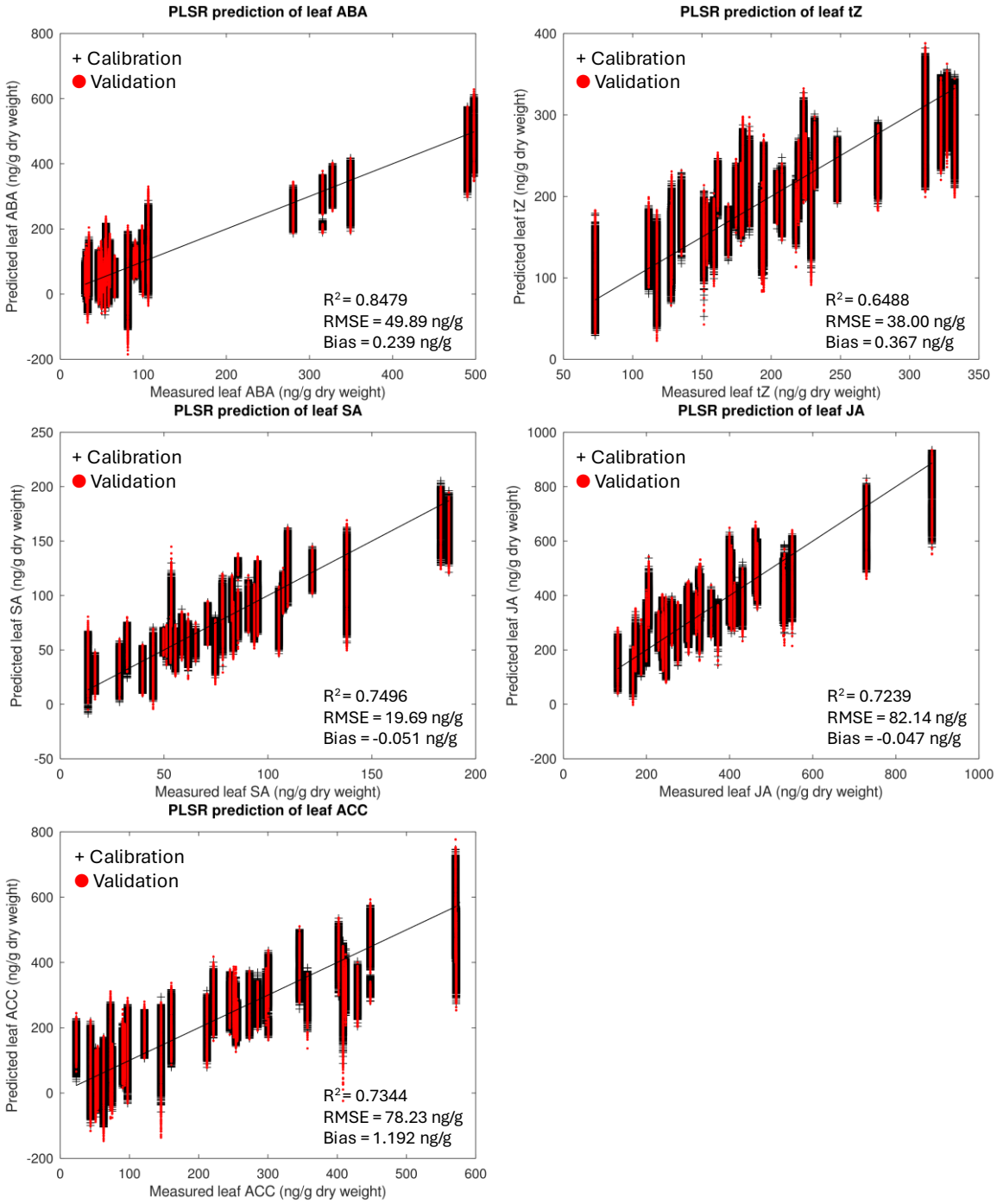

Figure S9: PLS regression graphs for prediction of plant hormones from freeze-dried ground leaves. Validation was performed by Monte-Carlo cross-validation with 20% of samples left-out for validation during 1000 iterations. All models were built using 10 latent variables.

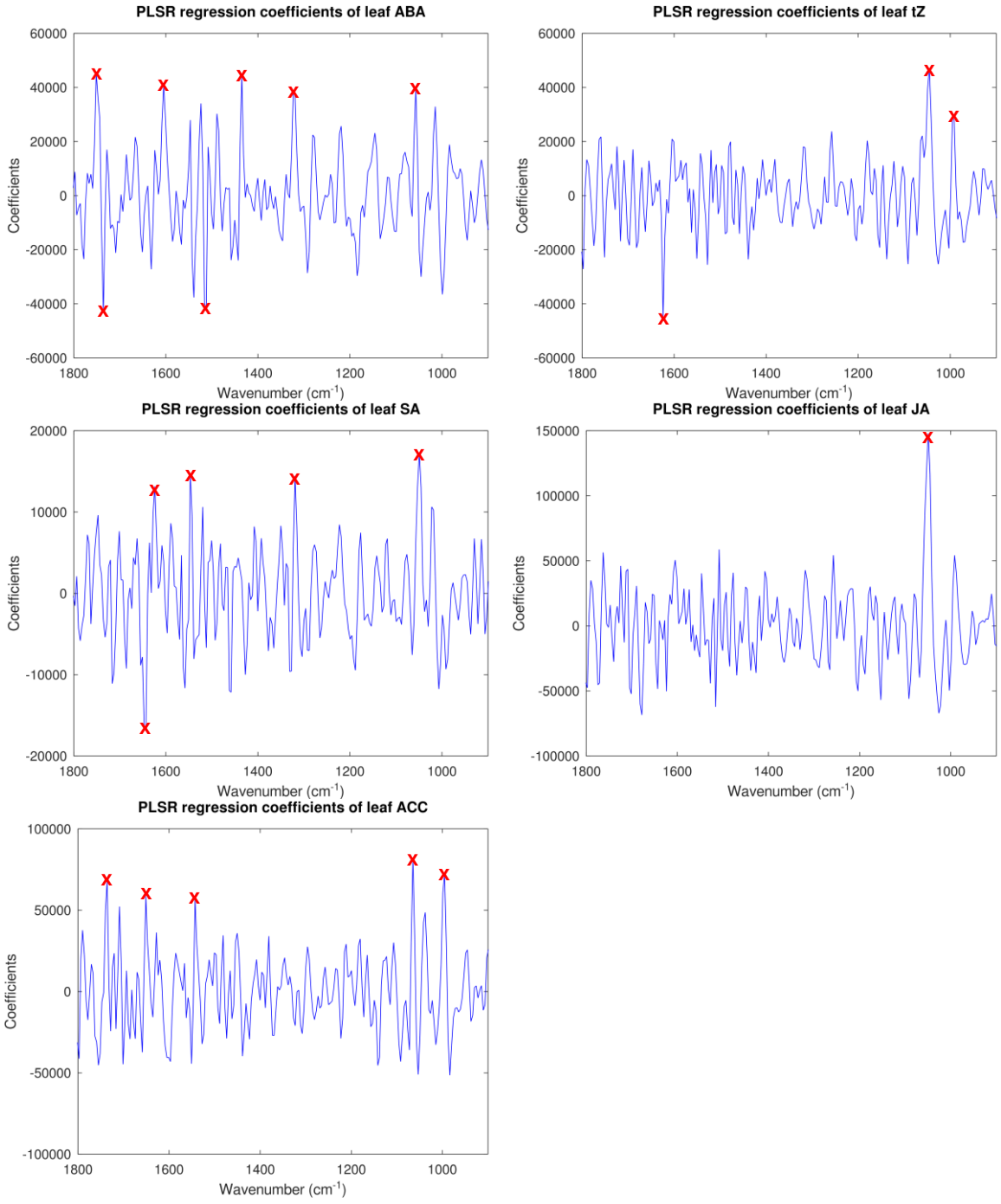

Figure S10: PLSR regression coefficients for prediction of plant hormones from freeze-dried ground leaves. Main wavenumbers are marked with a red X.

Xylem Sap Number of LVs	tz	iP	GA1	GA3	GA4	IAA	ABA	JA	SA
Light Control	6	8	9	NA	6	6	8	7	7
Light Drought	9	4	10	9	NA	NA	10	10	9
Light Nitrogen	6	4	8	5	NA	NA	6	5	5
Light Low Nutrient	7	7	9	NA	NA	NA	9	7	10
Shade Control	7	6	5	5	NA	NA	4	4	4
Shade Drought	3	NA	5	7	NA	NA	5	7	7
Shade Nitrogen	7	7	7	5	NA	6	7	6	7
Shade Low Nutrient	7	NA	7	NA	NA	NA	7	6	6

FDG Leaves Number of LVs	ACC	tz	ABA	JA	SA
Light Control	5	5	7	5	5
Light Drought	7	7	7	6	9
Light Nitrogen	8	8	9	7	7
Light Low Nutrient	5	4	4	5	5
Shade Control	3	5	2	4	4
Shade Drought	5	5	5	5	4
Shade Nitrogen	4	4	4	5	3
Shade Low Nutrient	7	6	6	8	6

Table S6: Number of latent variables (LVs) used to build the PLSR models between different types of treatment and hormone levels for xylem sap and freeze-dried ground (FDG) leaves. Higher number of LVs represents higher model complexity.

Electronic Supplimentary Information

Attenuated total reflection Fourier-transform infrared spectroscopy for the prediction of hormone concentrations in plants

Claire A Holden[1], Martin McAinsh[1], Jane E Taylor[1], Paul Beckett[2], Alfonso Albacete[3,4], Cristina Martínez-Andújar[4], Camilo L. M. Morais[5,6], Francis L Martin[7,8]*

[1] Lancaster Environment Centre, Lancaster University, UK

[2] Phlorum Ltd, UK

[3] Institute for Agro-Environmental Research and Development of Murcia (IMIDA), Department of Plant Production and Agrotechnology, C/ Mayor s/n, E-30150 La Alberca, Murcia, Spain

[4] CEBAS-CSIC. Department of Plant Nutrition. Campus Universitario de Espinardo, E-30100 Murcia, Spain

[5] Center for Education, Science and Technology of the Inhamuns Region, State University of Ceará, Tauá 63660-000, Brazil

[6] Graduate Program in Chemistry, Institute of Chemistry, Federal University of Rio Grande do Norte, Natal 59072-970, Brazil

[7] Department of Cellular Pathology, Blackpool Teaching Hospitals NHS Foundation Trust, Whinney Heys Road, Blackpool FY3 8NR, UK

[8] Biocel UK Ltd., Hull HU10 6TS, UK

*Corresponding author: Francis L Martin; Email: francis.martin2@nhs.net

Table S1: Lighting conditions within each Snijder cabinet

Light Quality	**'Light' Groups: LC, LD, LN and LLN**	**'Shade' Groups: SC, SD, SN and SLN**
PFD-R$_{(700\text{-}780\ nm)}$	72.51	49.28
PFD-FR$_{(600\text{-}700\ nm)}$	12.89	116.5
photosynthetic photon flux density PPFD$_{(400\text{-}700\ nm)}$	189.8	124.7
PFD-UV$_{(380\text{-}400\ nm)}$	0.5677	0.4402
PFD-B$_{(400\text{-}500\ nm)}$	33.93	21.58
PFD-G$_{(500\text{-}600\ nm)}$	83.40	53.87
peak wavelength λp / nm	545	741
peak wavelength value λpV / mWm^{-2}nm^{-1}	827.7	576.0
Irradiance	43.2	45.8
Illuminance/ lux.	15128	9617

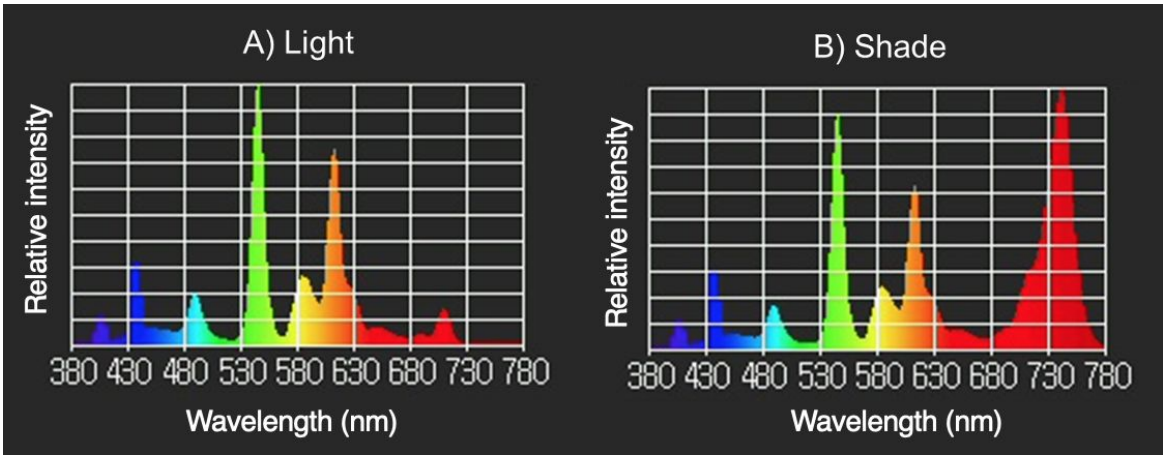

Figure S1: Spectra from a) 'Light' b) 'Shade' cabinets, providing red: far-red ratios of 5.6 and 0.4 respectively.

Table S2: Reagents used for Hoagland's solution. Full strength Hoagland's solution was made using 100 mL of solution A, 100 mL of solution B and 10 mL of solution C in 10 L of deionised water.

Solution	**Reagent**	**Concentration/ gL^{-1}**
A (100 mL)	NH_4NO_3	8.000
	$Ca(NO_3)_2.4H_2O$	82.600
	KNO_3	35.700
B (100 mL)	KNO_3	5.000
	KH_2PO_4	27.400
	$MgSO_4.7H_2O$ *added first	24.600
	$MnSO_4.5H_2O$	0.053
	H_3BO_3	0.140
	$CuSO_4.5H_2O$	0.015
	$(NH_4)_6Mo_7O_{24}.4H_2O$	0.008
	$ZnSO_4.7H_2O$	0.060
C (10 mL)	Fe-EDTA	36.71

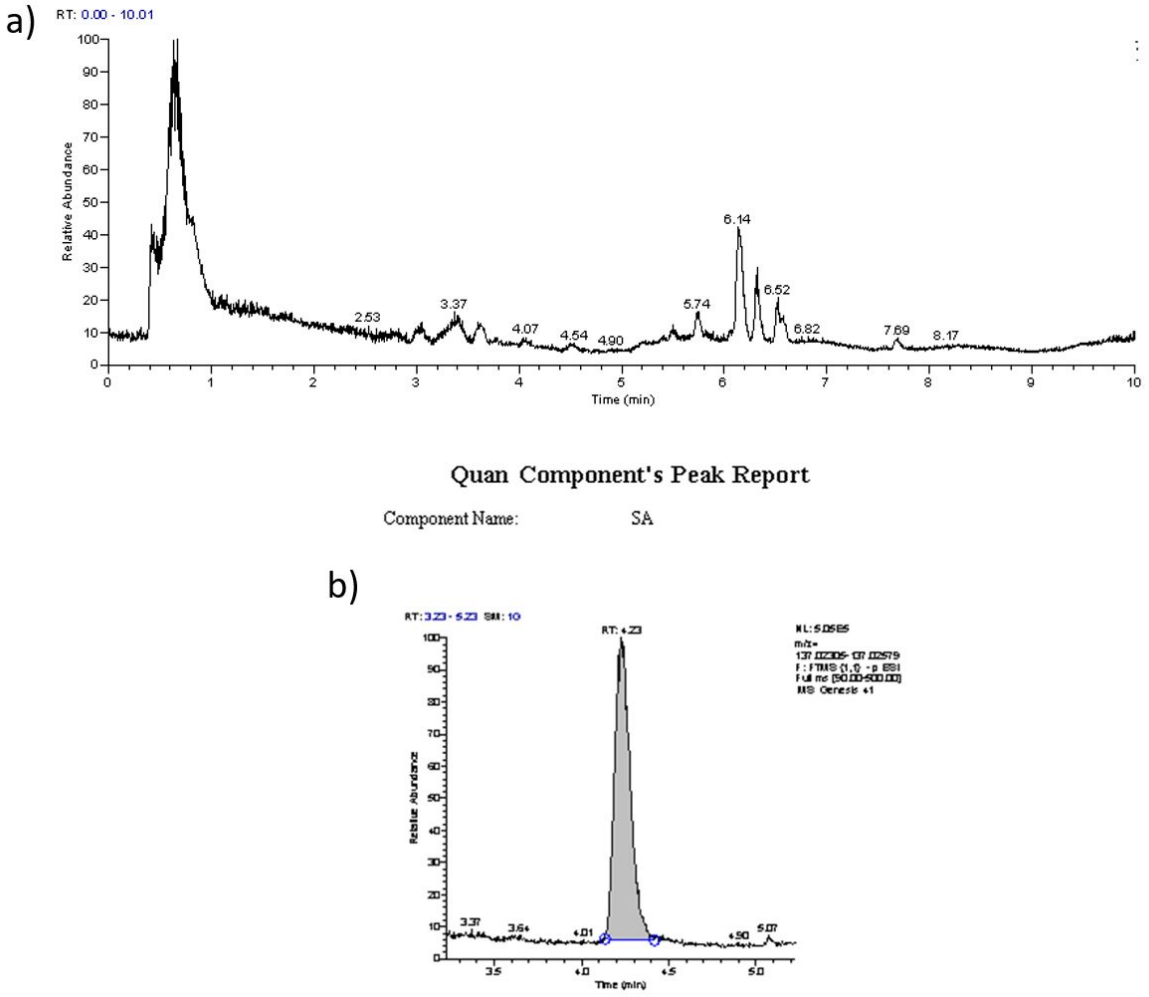

Figure S2: Total ion current and mass chromatogram (m/z 137.02442) for salicylic acid.

Table S3: Hormone descriptions and molecular ion masses

Hormone class	**Abbreviation**	**Hormone**	**Molecular formula**	**[M-H]⁻**
Ethylene precursor	ACC	1-Aminocyclopropane-1-carboxylic acid	$C_4H_7NO_2$	100.04040
Cytokinins	t-Z	*trans*-Zeatin	$C_{10}H_{13}N_5O$	218.10473
	t-ZR	*trans*-Zeatin riboside	$C_{15}H_{21}N_5O_5$	350.14699
	iP	Isopentenyladenine	$C_{10}H_{13}N_5$	202.10982
Gibberellins	GA1	Gibberellin A1	$C_{19}H_{24}O_6$	347.15001
	GA3	Gibberellin A3	$C_{19}H_{22}O_6$	345.13436
	GA4	Gibberellin A4	$C_{19}H_{24}O_5$	331.15510
Auxins	IAA	Indole-3-acetic acid	$C_{10}H_9NO_2$	174.05605
Abscisic acid	ABA	Abscisic acid	$C_{15}H_{20}O_4$	263.12888
Salicylates	SA	Salicylic acid	$C_7H_6O_3$	137.02442
Jasmonates	JA	Jasmonic acid	$C_{12}H_{18}O_3$	209.11832

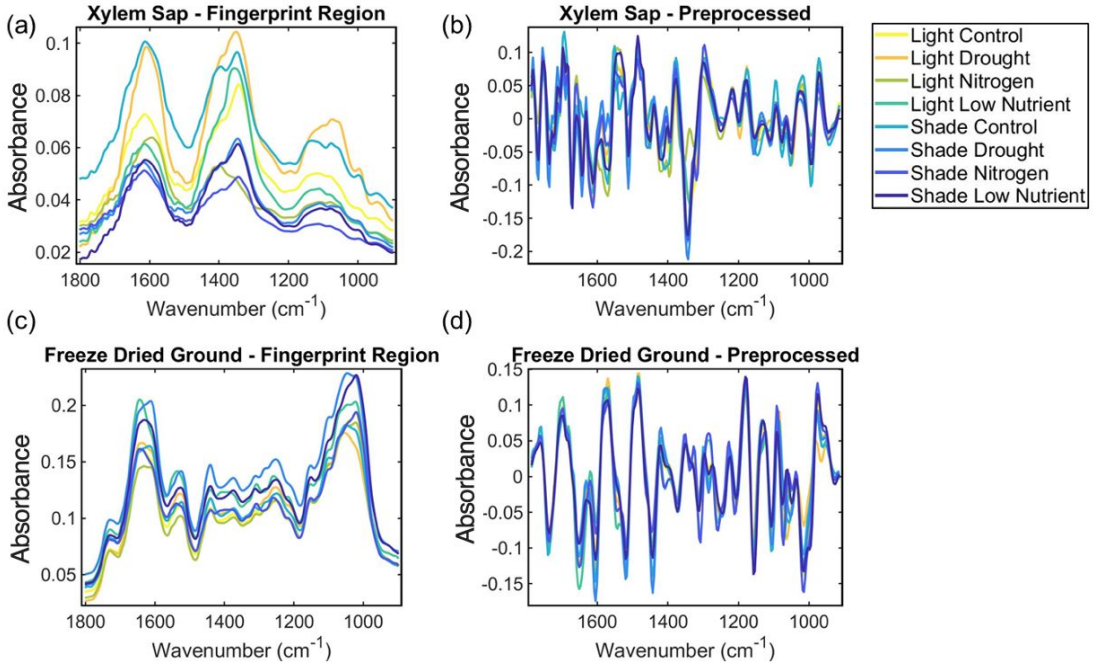

Figure S3: (a) Raw and **(b)** pre-processed class means spectra in the fingerprint region from xylem sap, **(c)** Raw and **(d)** pre-processed (Savitzky–Golay 2nd differentiation, *n*=9, and vector normalisation) class means spectra in the fingerprint region from freeze-dried ground leaves. Each class is grouped by treatment; Light Control (LC), Light Drought (LD), Light Nitrogen (LN), Light Low Nitrogen (LLN), Shade Control (SC), Shade Drought (SD), Shade Nitrogen (SN) and Shade Low Nitrogen (SLN).

Table S4: SVM parameters for classification

	Cost	Gamma (γ)	Number of support vectors (N_{SV})
Xylem Sap	31.6228	3.1623	314
Freeze-dried ground leaves	100	3.1623	194

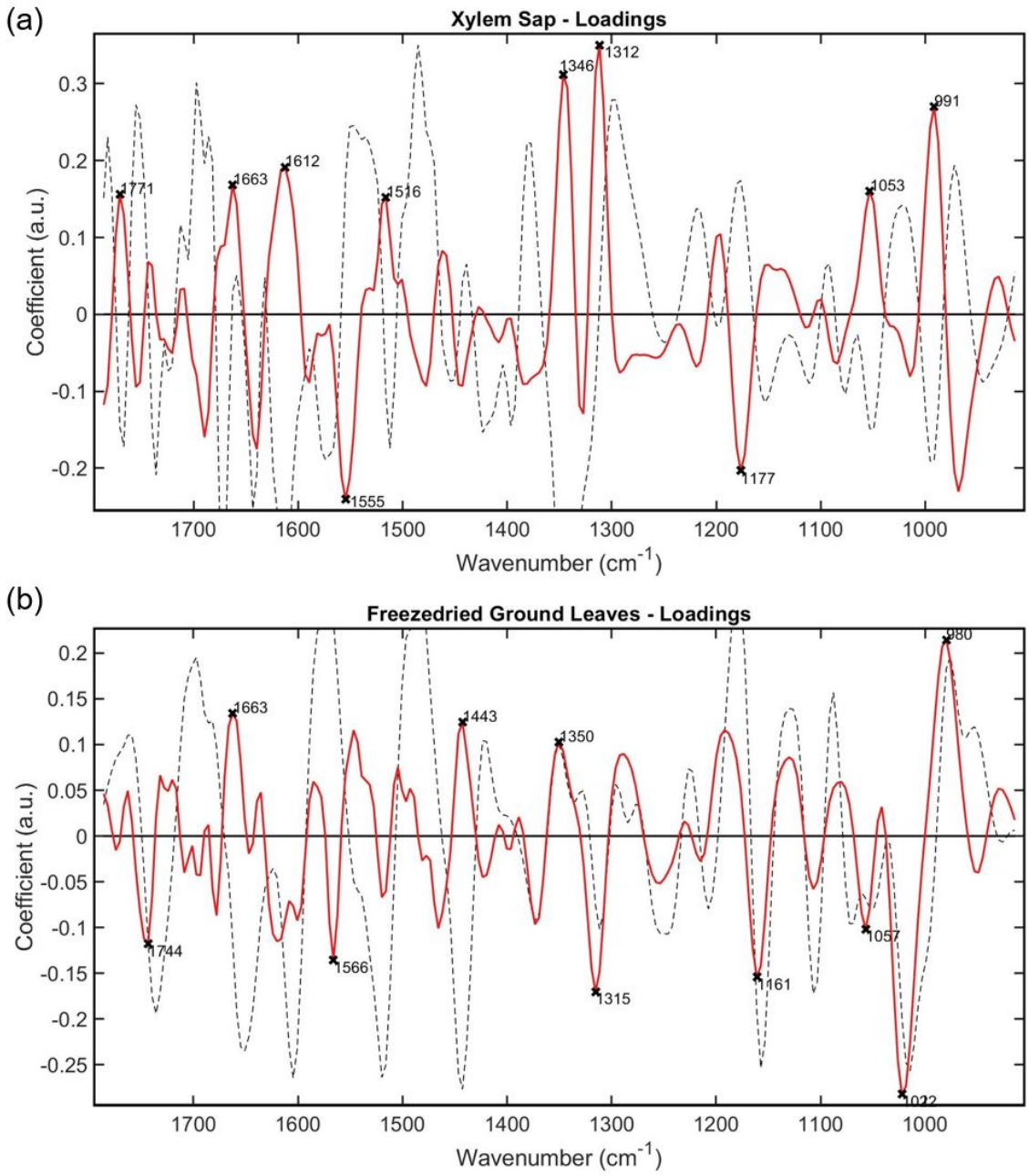

Figure S4: Loadings from spectra of a) xylem sap and b) freeze-dried ground leaf samples. These are the key wavenumbers which differentiate spectral profiles of different treatment groups from one another. The red line represents the PCA loadings and the black-dashed line represents the total mean spectrum, scaled to fit.

Table S5: PCA-loadings and biomarkers: key wavenumbers and compounds, which differentiate ATR-FTIR spectral profiles of plants from different growth conditions for both xylem sap and freeze-dried ground sample types.

Sample Type	Wavelength / cm	Tentative Molecular Assignment	Reference
Xylem sap	1770.65	v_1 symmetric stretching of C=O in the carboxylic acid of pectin or ester bond of triacylglycerol	(Nozahic and Amziane, 2012)
	1662.64	The N-C=O group of proteins. Amide I vibrations, specifically associated with disordered secondary structures or turns.	(Belfer *et al.*, 1998; Shivu *et al.*, 2013)
	1612.49	Amide I	(Jin *et al.*, 2018)
	1554.62	C-N stretching and N-H bending (Amide II vibration); C-O-O^- asymmetric stretching of proteins and glutamate	(Moskal *et al.*, 2019)
	1516.05	Amide II vibrations of proteins	(Talari *et al.*, 2017)
	1346.31	Cellulose	(Gorzsas, 2020)
	1311.59	Amide III vibrations of proteins	(Talari *et al.*, 2017)
	1176.58	C–O stretch vibration of tannins	(Falcão and Araújo, 2013)
	1053.13	Starch, *v*C–O and δC–O of carbohydrates	(Talari *et al.*, 2017; Jin *et al.*, 2018)
	991.41	C–O ribose	(Camilo L. M. Morais *et al.*, 2017)
Freeze-dried ground leaves	1743.53	Ester C=O stretch: triglycerides	(Talari *et al.*, 2017)
	1662.52	The N-C=O group of proteins. Amide I vibrations, specifically associated with disordered secondary structures or turns.	(Belfer *et al.*, 1998; Shivu *et al.*, 2013)
	1566.09	N-H bending; C-N stretching (Amide II band of proteins)	(Rana *et al.*, 2018)
	1442.65	Pectin	(Sharma and Uttam, 2018)
	1350.08	Phosphodiester stretching bands region (for absorbances due to starch)	(Talari *et al.*, 2017)
	1315.36	Cellulose	(Sharma and Uttam, 2018)
	1161.06	C–OH groups of serine, threonine and tyrosine of proteins, C-O stretching and hydrogen bonding	(Talari *et al.*, 2017)
	1056.92	Stretching C–O deoxyribose	(Talari *et al.*, 2017)
	1022.2	Starch	(Talari *et al.*, 2017)
	979.769	C-OH stretching of secondary alcohols and C-O-C vibrations of polysaccharides	(Ajitha *et al.*, 2015)

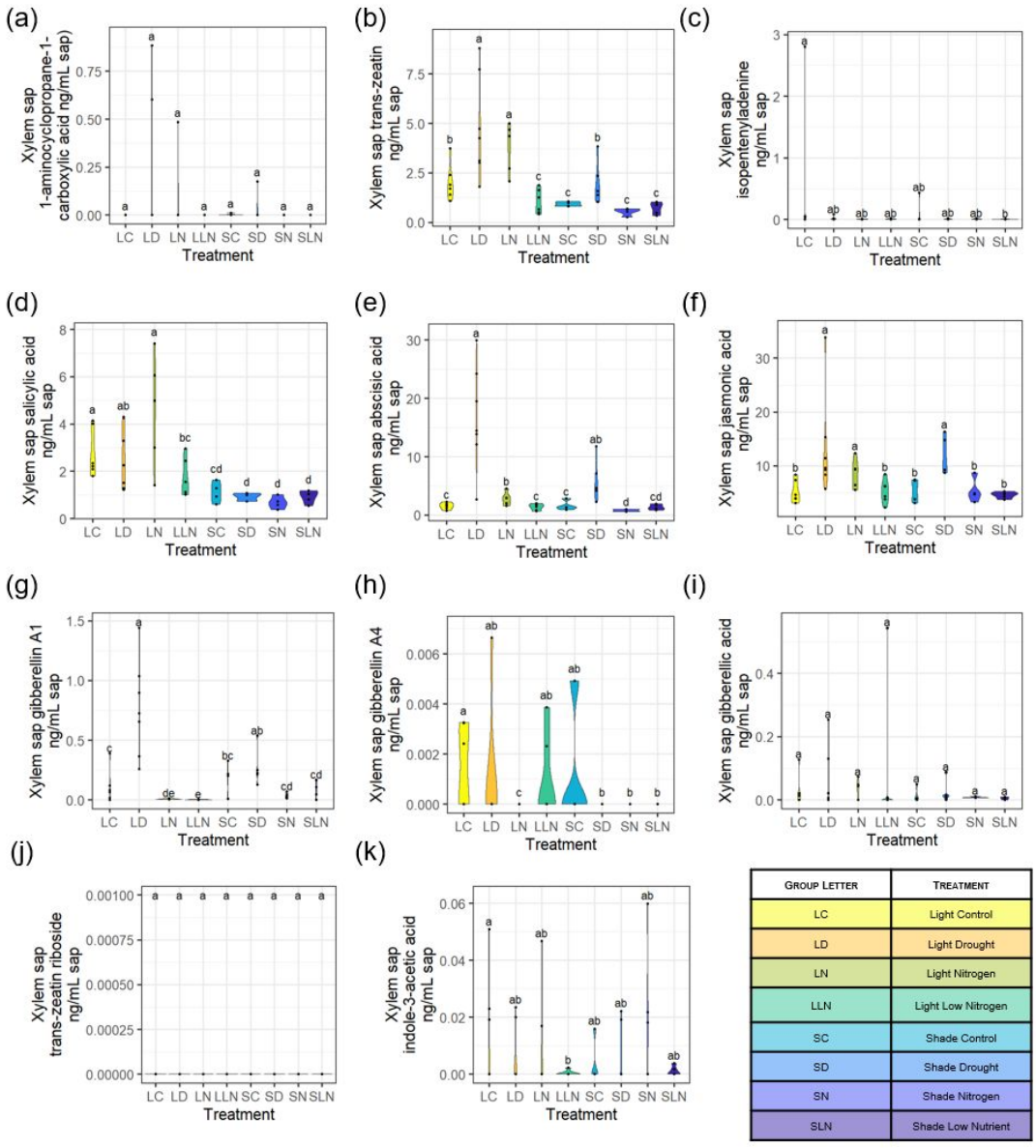

Figure S5: Hormone profiles from xylem sap measured using UHPLC– HRMS in ng·ml^{-1} sap for a) 1-amino-cyclopropanecarboxylic acid (ACC), b) *trans*-Zeatin (tZ), c) isopentyl-adenine (iP), d) salicylic acid (SA), e) abscisic acid (ABA), f) jasmonic acid (JA), g) gibberellin A1 (GA_1), gibberellin A4 (GA_4), gibberellic acid (GA_3), *trans*-zeatin riboside (tZR), and indole-3-acetic acid (IAA). ABA concentration was highest in the drought categories; LD had ~17 ng·ml^{-1} sap of ABA compared with SD which had ~7 ng·ml^{-1} sap, whilst the other categories ranged between ~1 and 3 ng·ml^{-1} sap. Shade plants had lower xylem SA levels than light ones, in the range of 0.7-1.1 ng·ml^{-1} sap compared with 1.6-4.5 ng·ml^{-1} sap respectively. Xylem sap levels of GA_1 were approximately three times higher in LD than most other treatment groups, although this was not significantly different to the other drought category, SD, due to high variation.

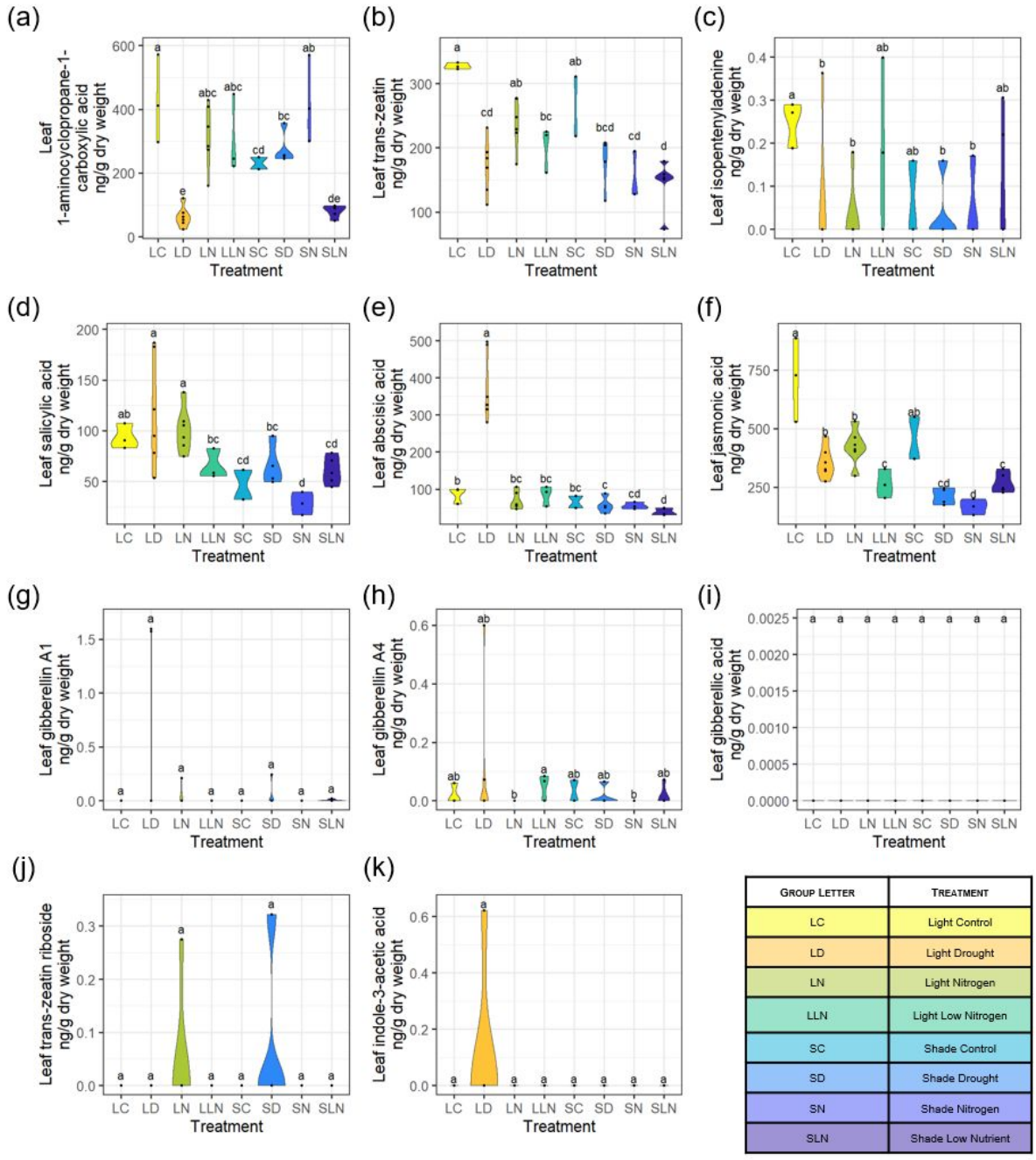

Figure S6: Hormone profiles from freeze-dried ground leaves measured using UHPLC–HRMS in ng·g^{-1} dry weight for a) 1-amino-cyclopropanecarboxylic acid (ACC), b) *trans*-Zeatin (tZ), c) isopentyl-adenine (iP), d) salicylic acid (SA), e) abscisic acid (ABA), f) jasmonic acid (JA), g) gibberellin A1 (GA_1), gibberellin A4 (GA_4), gibberellic acid (GA_3), *trans*-zeatin riboside (tZR), and indole-3-acetic acid (IAA). Leaf ABA levels (Figure S5) were approximately quadruple in LD than those of the other categories. Plants grown under LC treatment category registered approximately 4.5-fold higher of leaf tZ than those in SLN. Leaf JA concentration was significantly higher in the light control group LC (~710 ng·g^{-1} dry weight) compared to all other groups (ranging 170-420 ng·g^{-1} dry weight), except the shade control group SC (~460 ng·g^{-1} dry weight). The highest iP hormone concentration was found in leaves of category LC, at 0.25 ng·g^{-1} dry weight. This value was significantly higher compared to groups LD, LN, SD, SN (ranging 0.03-0.6 ng·g^{-1} dry weight), with the other groups falling in between.

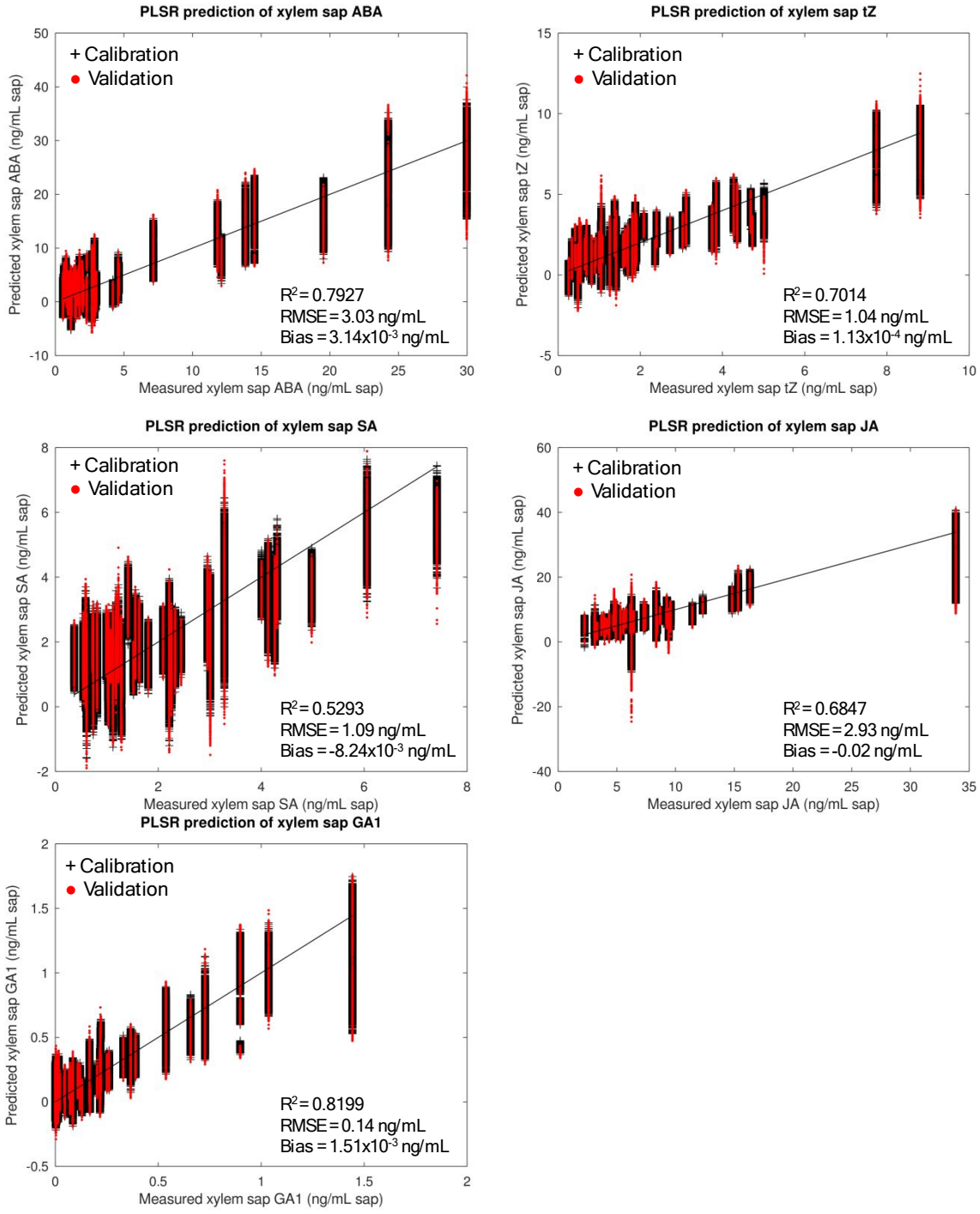

Figure S7: PLS regression graphs for prediction of plant hormones from xylem sap. Validation was performed by Monte-Carlo cross-validation with 20% of samples left-out for validation during 1000 iterations. All models were built using 10 latent variables.

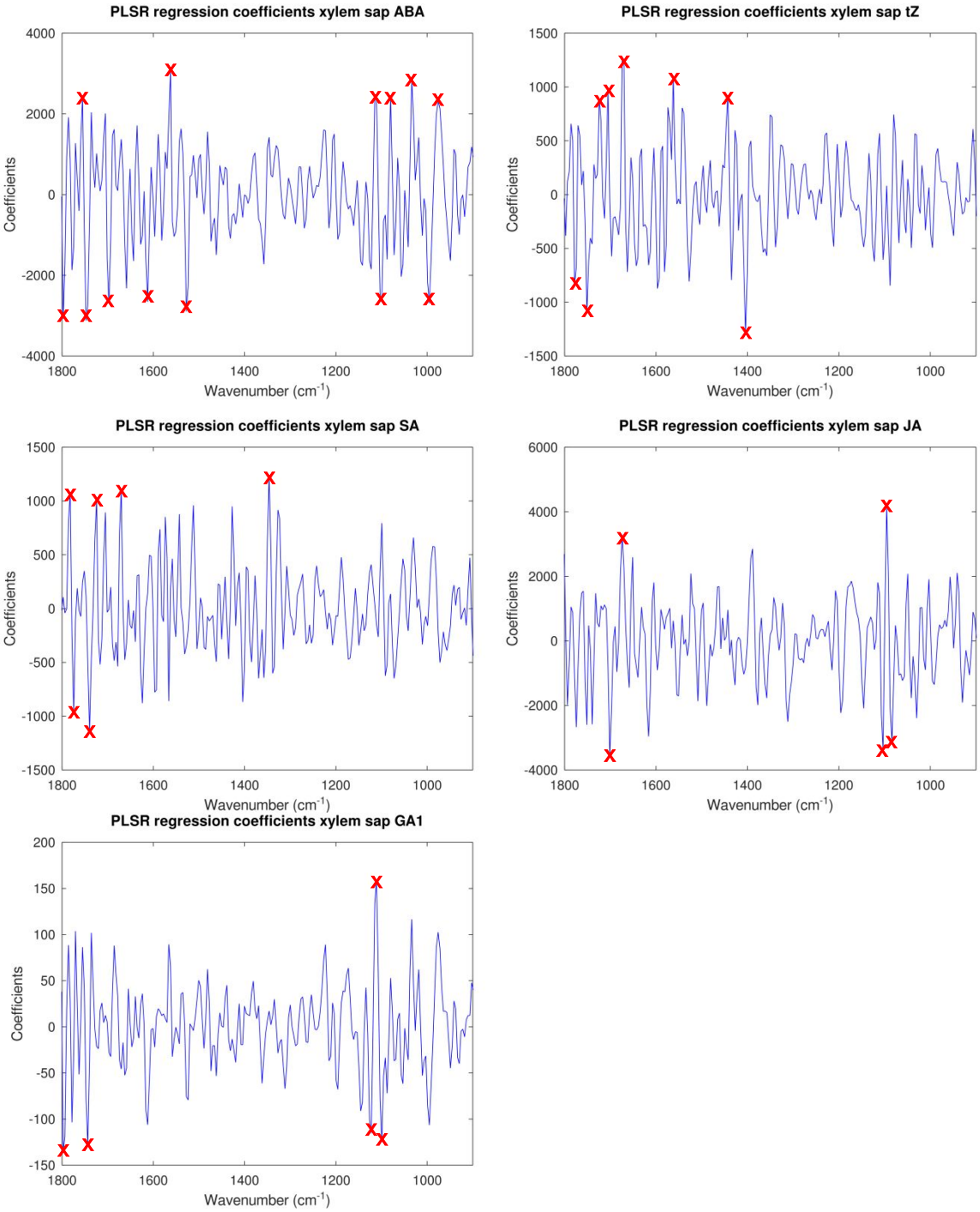

Figure S8: PLSR regression coefficients for prediction of plant hormones from xylem sap. Main wavenumbers are marked with a red X.

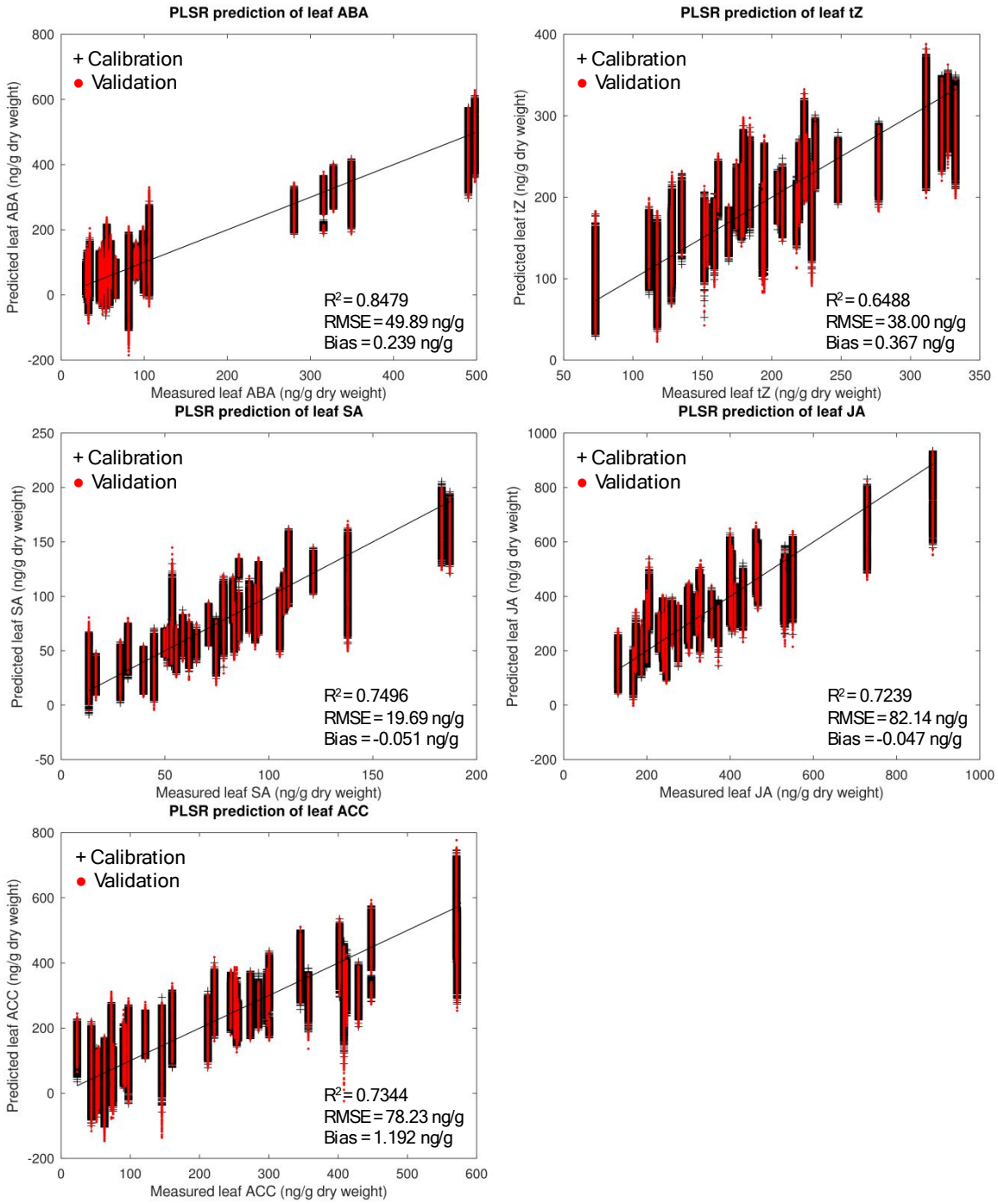

Figure S9: PLS regression graphs for prediction of plant hormones from freeze-dried ground leaves. Validation was performed by Monte-Carlo cross-validation with 20% of samples left-out for validation during 1000 iterations. All models were built using 10 latent variables.

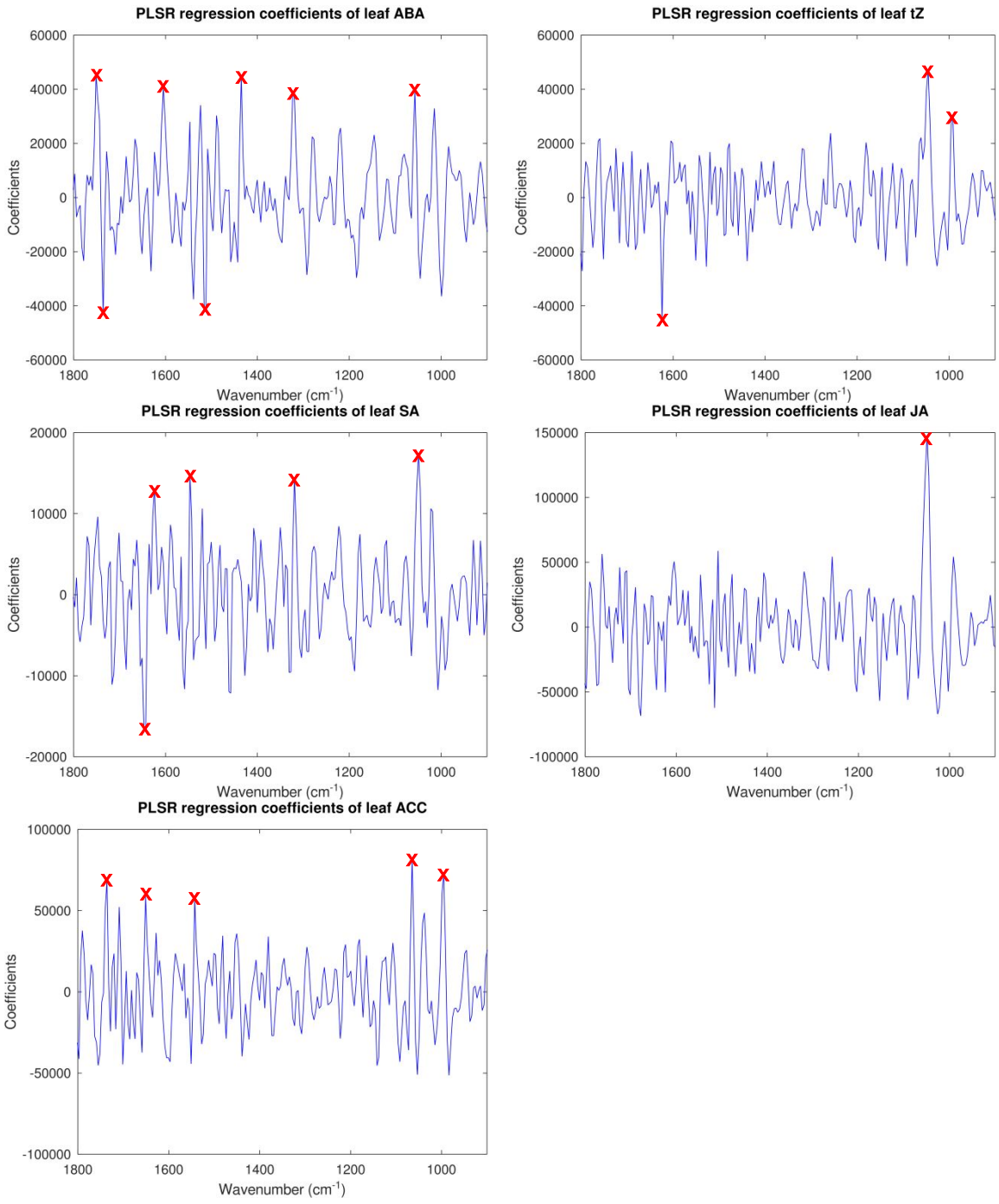

Figure S10: PLSR regression coefficients for prediction of plant hormones from freeze-dried ground leaves. Main wavenumbers are marked with a red X.

Xylem Sap Number of LVs	tz	iP	GA1	GA3	GA4	IAA	ABA	JA	SA
Light Control	6	8	9	NA	6	6	8	7	7
Light Drought	9	4	10	9	NA	NA	10	10	9
Light Nitrogen	6	4	8	5	NA	NA	6	5	5
Light Low Nutrient	7	7	9	NA	NA	NA	9	7	10
Shade Control	7	6	5	5	NA	NA	4	4	4
Shade Drought	3	NA	5	7	NA	NA	5	7	7
Shade Nitrogen	7	7	7	5	NA	6	7	6	7
Shade Low Nutrient	7	NA	7	NA	NA	NA	7	6	6

FDG Leaves Number of LVs	ACC	tz	ABA	JA	SA
Light Control	5	5	7	5	5
Light Drought	7	7	7	6	9
Light Nitrogen	8	8	9	7	7
Light Low Nutrient	5	4	4	5	5
Shade Control	3	5	2	4	4
Shade Drought	5	5	5	5	4
Shade Nitrogen	4	4	4	5	3
Shade Low Nutrient	7	6	6	8	6

Table S6: Number of latent variables (LVs) used to build the PLSR models between different types of treatment and hormone levels for xylem sap and freeze-dried ground (FDG) leaves. Higher number of LVs represents higher model complexity.

1. Growth of invasive Japanese knotweed under different environmental conditions

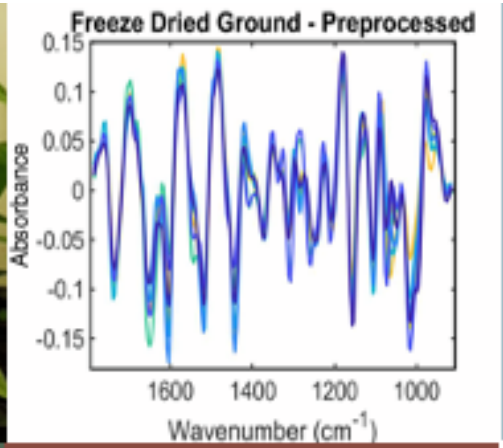

2. Spectral acquisition, pre-processing, and chemometric analysis of freeze-dried leaves and xylem sap

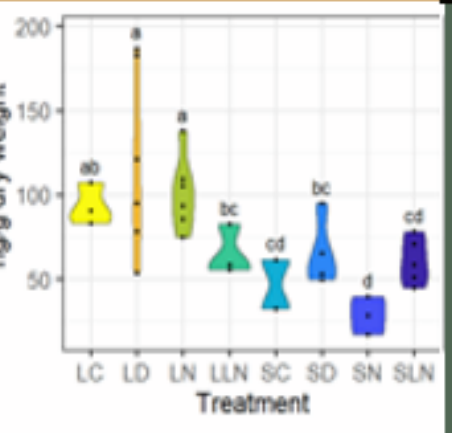

3. Measurement of hormone concentrations using ultra-high-performance liquid chromatography-high-resolution mass spectrometry

2. Spectral acquisition, pre-processing, and chemometric analysis of freeze-dried leaves and xylem sap

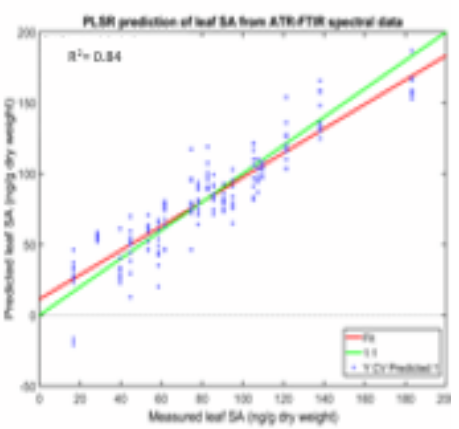

Attenuated total reflection Fourier-transform infrared spectroscopy for the prediction of hormone concentrations in plants

Claire A Holden[1], Martin McAinsh[1], Jane E Taylor[1], Paul Beckett[2], Alfonso Albacete[3,4], Cristina Martínez-Andújar[4], Camilo L. M. Morais[5,6], Francis L Martin[7,8]*

[1] Lancaster Environment Centre, Lancaster University, UK

[2] Phlorum Ltd, UK

[3] Institute for Agro-Environmental Research and Development of Murcia (IMIDA), Department of Plant Production and Agrotechnology, C/ Mayor s/n, E-30150 La Alberca, Murcia, Spain

[4] CEBAS-CSIC. Department of Plant Nutrition. Campus Universitario de Espinardo, E-30100 Murcia, Spain

[5] Center for Education, Science and Technology of the Inhamuns Region, State University of Ceará, Tauá 63660-000, Brazil

[6] Graduate Program in Chemistry, Institute of Chemistry, Federal University of Rio Grande do Norte, Natal 59072-970, Brazil

[7] Department of Cellular Pathology, Blackpool Teaching Hospitals NHS Foundation Trust, Whinney Heys Road, Blackpool FY3 8NR, UK

[8] Biocel UK Ltd., Hull HU10 6TS, UK

***Corresponding author:** Francis L Martin; Email: francis.martin2@nhs.net

Spectroscopy-based environmental metabolomics

ToC graphic

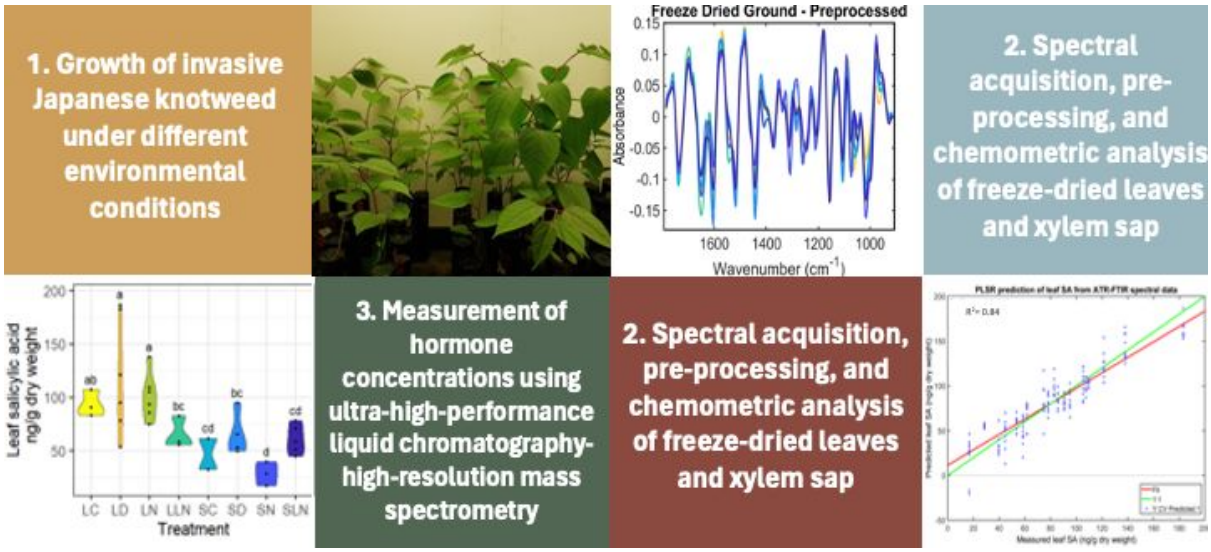

Analysis with ATR-FTIR spectroscopy combined with chemometrics methods facilitates determination of hormone concentrations in Japanese knotweed samples under different environmental conditions.

Abstract

Plant hormones are important in the control of physiological and developmental processes including seed germination, senescence, flowering, stomatal aperture, and ultimately the overall growth and yield of plants. Many currently available methods to quantify such growth regulators quickly and accurately require extensive sample purification using complex analytic techniques. Herein we used ultra-performance liquid chromatography-high-resolution mass spectrometry (UHPLC-HRMS) to create and validate the prediction of hormone concentrations made using attenuated total reflection Fourier-transform infrared (ATR-FTIR) spectral profiles of both freeze-dried ground leaf tissue and extracted xylem sap of Japanese knotweed (*Reynoutria japonica*) plants grown under different environmental conditions. In addition to these predictions made with partial least squares regression, further analysis of spectral data was performed using chemometric techniques, including principal component analysis, linear discriminant analysis, and support vector machines (SVM). Plants grown in different environments had sufficiently different biochemical profiles, including plant hormonal compounds, to allow successful differentiation by ATR-FTIR spectroscopy coupled with SVM. ATR-FTIR spectral biomarkers highlighted a range of biomolecules responsible for the differing spectral signatures between growth environments, such as triacylglycerol, proteins and amino acids, tannins, pectin, polysaccharides such as starch and cellulose, DNA and RNA. Using partial least squares regression, we show the potential for accurate prediction of plant hormone concentrations from ATR-FTIR spectral profiles, calibrated with hormonal data quantified by UHPLC-HRMS. The application of ATR-FTIR spectroscopy and chemometrics offers accurate prediction of hormone concentrations in plant samples, with advantages over existing approaches.

Introduction

As sessile organisms, plants rely on signalling molecules such as plant hormones to enable them to react appropriately to their environment; they contribute to a plastic adaptive response, regulating plant growth and stress tolerance [1], and plants grown under different environmental conditions show significant differences in hormone profiles [2,3]. Plant hormones include: ethylene, auxin, gibberellins (GAs), cytokinins (CKs), abscisic acid (ABA), salicylic acid (SA), strigolactones (SLs), brassinosteroids (BRs) and jasmonic acid (JA) [1,3]. Plant hormone identification is challenging due to their low concentrations, ranging stabilities and similar core structures, including isomers with the same MS fragmentation patterns (e.g. cis- and trans-zeatin, topolin isomers, brassinolide and 24-epibrassinolide [24-epiBL], and castasterone and 24-epicastasterone; Šimura *et al.*, 2018). Current methods for plant hormone analysis include: gas chromatography-mass spectrometry (GC-MS), capillary electrophoresis-mass spectroscopy (CE-MS) [5], enzyme-linked immune sorbent assay (ELISA) [6], ultra-performance liquid chromatography-mass spectrometry (UPLC-MS) [7], high performance liquid chromatography-mass spectrometry (HPLC-MS) [8] and liquid chromatography-ultraviolet detection (LC-UV) [9]. Liquid chromatography is a versatile method that allows the separation of compounds of a wide range of polarity, but these classical chromatographic techniques require destruction of the plant and lengthy sample preparation. More recently the research focus has shifted towards the development of non-destructive spectroscopic techniques for plant hormone detection, such as Raman spectroscopy [10,11] and desorption electrospray ionisation mass spectrometry imaging (DESI-MSI)[12].

Plant hormones control a range of complex physiological and developmental processes including seed germination, senescence, flowering, and stomatal control, and affect overall plant growth and crop yield [1]. Antagonistic hormonal crosstalk also regulates numerous

factors influencing the success of invasive alien species (IAS), for example, the trade-off between growth and defence [13], adaptive transgenerational plasticity [14], and the biosynthesis of allelopathic chemicals [15]. The importance of hormonal regulation in plant invasions has been demonstrated in the differential biomass allocation [16] and defence responses [17] of invasive and native plants, and in locally adaptive chromosomal inversion in invasive plants [18]. Additionally, many herbicides used for the control of IAS are plant hormone analogues or interfere with hormonal signalling and synthesis pathways [19]. IAS have significant negative socio-economic [20,21] and environmental [22] impacts and therefore it is critical to gain an increased understanding of the factors, including the role of plant hormones, that enable the invasiveness and superior growth performance of these species [23–26].

Japanese knotweed (*Reynoutria japonica*) is an IAS found across a broad geographic range, colonising diverse habitats including riparian wetlands, urban transport courses, and coastal areas [27,28]. It is very tolerant to abiotic stress, occupying extreme environments such as salt marshes [29] and metal-polluted soil [30,31]. Although its habitats are diverse, Japanese knotweed exhibits minimal genetic variation in Central Europe [27], Norway [32] and the USA [28], and exists as a female clone in the United Kingdom from a single introduction [33,34]. The ecological adaptability of Japanese knotweed as an invasive weed renders this species an ideal model for investigating the contribution of plant hormones to IAS invasiveness through a concatenated approach combining ultra-performance liquid chromatography-high resolution mass spectrometry (UHPLC-HRMS) and attenuated total reflection Fourier-transform infrared (ATR-FTIR) spectral data.

In this study we used UHPLC-HRMS to quantitatively measure the concentrations of a set of plant hormones at nanogram per millilitre concentrations: the active CKs *trans*-Zeatin (t-Z), *trans*-zeatin riboside (tZR) and isopentyl-adenine (iP), the active GAs gibberellin A1 (GA_1), gibberellin A4 (GA_4), gibberellin A3 (GA_3), the active auxin indole-3-acetic acid (IAA),

ABA, JA, SA, and the ethylene precursor 1-amino-cyclopropane-1-carboxylic acid (ACC); and compared these measured concentrations to those predicted from ATR-FTIR spectral profiles of both xylem sap and freeze-dried ground leaves. ATR-FTIR spectroscopy employs infrared (IR) light to alter the molecular vibrations of a sample, providing information on the compounds within. It is a rapid analytical technique well-suited to environmental monitoring with the advantages of a high degree of specificity and sensitivity, minimal sample preparation, and portable enough for use in the field. It can be used non-destructively on whole plant tissues, even *in planta* [35,36]. We used chemometric algorithms to allow further information to be gained from the absorbance profiles, such as molecular biomarkers associated with the plants' environments. Chemometric techniques used included principal component analysis (PCA), PCA in combination with linear discriminant analysis (LDA), support vector machines (SVMs), and partial least squares regression (PLSR) [37–39]. These highlighted a range of biomolecules responsible for the differing IR spectral signatures between growth environments, such as triacylglycerol, proteins and amino acids, tannins, pectin, polysaccharides such as starch and cellulose, deoxyribonucleic acid (DNA) and ribonucleic acid (RNA) [40]. PLSR comparison of the ATR-FTIR spectral data with the quantitative data from UHPLC– HRMS analysis allowed the effect of each hormone on the spectral absorbances to be viewed in isolation. Key wavenumbers within the mid-infrared fingerprint region were identified for prediction of plant hormone concentrations using ATR-FTIR spectroscopy; predominantly in the region of 1200-1000 cm^{-1} for leaf samples and 1600-1500 cm^{-1} for xylem sap samples. In leaf samples these often related to polysaccharide molecules, whilst in xylem compounds these key wavenumbers were more commonly associated with nucleic acids and bases. Predictive models were built to consider the concentrations of each hormone in turn and also to detect concentrations of several different hormones at once.

Materials and Methods

Plant growth

Japanese knotweed readily reproduces asexually from small fragments of an underground storage organ called a rhizome, which has a woody root-like structure. Rhizomes were collected from a site on the River Wyre, Google map reference 53.94977780, -2.75541670, with landowner permission from Lancashire County Council. Ninety fragments of rhizome (10-50 g, volume 2-58 cm^3) were planted in fertilized organic loam (John Innes No. 1, J. Arthur Bowers, UK) in cylindrical pots designed to tightly fit in a Scholander-type pressure chamber (Soil Moisture Equipment Corp., Santa Barbara, CA, USA) measuring 6.5 cm in diameter and 23 cm in length with a volume of 763.2 cm^3, and featured a stainless-steel mesh (0.7 mm aperture) at the base to assist drainage. Pots were placed in one of two climate-controlled cabinets (Microclima 1750, Snijders Scientific BV, Netherlands) at 80% humidity, 16 h of photoperiod, and 19/11°C day/night temperature where the treatments were applied and plants were grown for a total of fifty days before harvesting. The long photoperiod and temperature range were selected to simulate an average British Summer in the areas where Japanese knotweed usually colonises, using a comparison of temperature maps from the Met Office [41] and a distribution map of Japanese knotweed in the British Isles [42].

Treatments

Rhizome fragments were divided into eight treatment groups to give an even split of rhizome masses in each group. The treatments applied were: Light Control ‘LC’, Light Drought ‘LD’, Light Nitrogen ‘LN’, Light Low Nutrient ‘LLN’, Shade Control ‘SC’, Shade Drought ‘SD’, Shade Nitrogen ‘SN’ and Shade Low Nutrient ‘SLN’. Four groups were placed in each of two growth cabinets. In both cabinets, the light emitted from the two high-pressure sodium lamps (SON-T 400 W, Philips Lighting, Eindhoven, The Netherlands) was reduced using a LEE 209 filter (LEE Filters Worldwide, Andover, Hampshire, UK). In one cabinet, a matrix

of far-red LEDs (EPILEDS, 740-745 nm) distributed in five rows 30 cm apart was used to decrease the red: far-red ratio (R:FR) to simulate shading. Wavelengths emitted were measured using an UPRtek (Taiwan) PG100N light spectrometer. The resultant combined light conditions (see Table S1†) resulted in a 'light' treatment with a R:FR of 5.6 and a 'shade' treatment with a R:FR of 0.4 (see Figure S1† for the spectral profile). Plants were shuffled weekly within each cabinet to minimise positional effects from the LED matrix pattern. The R:FR of natural sunlight during the day is approximately 1.15 [43] and the R:FR of 0.4 in the shade treatment was chosen to replicate that found within vegetative canopies such as sugar beet, deciduous woodland, coniferous woodland and tropical rainforest [43]. In both cases, the photosynthetic photon flux density (PPFD) was between 124.7 and 189.8 $\mu mol \cdot m^{-2} \cdot s^{-1}$ which is typical of growth cabinet studies [44–47].

Plants were provided with water (75 mL/pot / 48 h), apart from LD and SD in which water was withheld for 7 days prior to harvest. Once a week, four groups (LC, LD, SC, SD) were watered with 75 mL Hoagland solution to provide both nitrogen and micronutrients, see Table S2† for details. LN and SN were fed with the commonly used agricultural dose of 50 $kg\ ha^{-1}\ year^{-1}$ [48]; this was scaled down for a pot diameter of 6.2 cm and applied across a split-dose at 21 and 23 days to prevent leaching. Groups LLN and SLN were provided only with water and received no additional nitrogen or micronutrients.

Harvest

Two leaves were excised from each plant for the analysis 4-8 h into the photoperiod in order to fall within a stable period of the plants' circadian rhythm. The youngest leaf from the top of plants was placed in liquid nitrogen, freeze-dried, and finely ground for hormone analysis by U-HPLC-HRMS, and the second leaf down was treated similarly for analysis by ATR-FTIR spectroscopy. Following this, the plant was de-topped and the whole pot inserted into a Scholander-type pressure chamber (Soil Moisture Equipment Corp., Santa Barbara, CA,

USA) with the stem protruding for xylem sap collection. The pressure was matched to the flow rate by increasing the pressure gradually above the balance pressure. For each trial pressure, the flow rate was calculated by weighing the sap collected for twenty seconds, until the flow rate matched that calculated by mass loss following the method previously described in [49]. This was necessary as it has been shown that ABA concentration are influenced by sap flow rate [49]. Sap was collected in Eppendorf vials, immediately frozen in liquid nitrogen and stored at −80°C for hormone determination, and ATR-FTIR spectral analysis.

Plant hormones

Plant hormones were quantified from frozen xylem sap and freeze-dried ground leaf material using UHPLC–HRMS as described previously with some modifications [50,51]. Freeze-dried ground leaf samples were prepared with several extraction steps and sonication before analysis, whilst only the filtration and centrifugation steps were necessary for the xylem sap samples. In the first extraction up to 250 mg of raw material was mixed with methanol (1.25 mL, 80%) and an internal-standards mix composed of deuterium labelled hormones ($[^2H_5]$tZ, $[_2H^5]$tZR, $[^2H_6]$iP, $[^2H_2]GA_1$, $[^2H_2]GA_3$, $[^2H_2]GA_4$, $[^2H_5]$IAA, $[^2H_6]$ABA, $[^2H_4]$SA, $[^2H_6]$JA, $[^2H_4]$ACC, Olchemim Ltd, Olomouc, Czech Republic) at a concentration of 5 μg mL^{-1} in 80% methanol. Samples were vortexed, incubated for 30 min at 4°C, and centrifuged (20000 g, 4°C, 15 min). Supernatants were passed through Chromafix C18 columns (MachereyNagel, Düren/Germany) previously pre-equilibrated with 80% methanol and filtrates were collected on ice. Extraction was repeated with 1.25 mL 80% methanol; second extracts were passed through the same columns. The combined extracts were collected and concentrated to complete dryness using the Integrated SpeedVac® Concentrator System AES1000 (Savant Instruments Inc., Holbrook/USA). The residues were resolved in 500 or 1000 μL 20% methanol, sonicated for 8 min using a ultrasonic bath, passed through 0.2-μm syringe filters (Chromafil PES-20/25) and placed in HPLC vials for analysis, and optionally

stored at –80°C. Phytohormone analyses were performed using a UHPLC–HRMS system consisting of a Thermo ACCELA pump (Thermo Scientific, Waltham/USA) coupled to a tempered HTC-PAL autosampler (CTC Analytics, Zwingen/Switzerland), and connected to a Thermo Exactive Spectrometer (Thermo Scientific) with a heated electrospray ionization (HESI) interface. Due to the high resolution of the Orbitrap, we recorded the total ion chromatogram of the samples and did not fragment the molecules. A typical chromatogram for SA is shown in Figure S2†. The analysis was performed in the negative mode $[M-H]^-$ (Table S3†), and the instrument settings included: sheath gas flow rate = 35 $ml \cdot min^{-1}$, auxiliary gas flow rate = 10 $ml \cdot min^{-1}$, spray voltage = 2.5 kV, capillary temperature = 275ºC, capillary voltage = -40 V, tube lens voltage = -110 V, skimmer voltage = -20 V. Mass spectra were obtained using the Xcalibur software version 2.2 (ThermoFisher Scientific, Waltham, MA, USA). For quantification of the plant hormones, calibration curves were constructed for each analysed component (1, 10, 50, and 100 µg l^{-1}) and corrected for 10 µg l^{-1} deuterated internal standards. Recovery percentages ranged between 92 and 95%.

ATR-FTIR spectral acquisition

Freeze-dried ground leaves and xylem sap were analysed using a Tensor 27 FTIR spectrometer with a Helios ATR attachment (Bruker Optics Ltd, Coventry, UK). The sampling area, defined by the Internal Reflection Element (IRE), which was a diamond crystal, was 250 µm x 250 µm. Spectral resolution was 8 cm^{-1} with 2 times zero-filling, giving a data-spacing of 4 cm^{-1} over the range 4000 to 400 cm^{-1}; 32 co-additions and a mirror velocity of 2.2 kHz were used for optimum signal to noise ratio. To minimise bias, ten spectra were taken for each sample. Each sample was placed on a slide with the side to be analysed facing upwards, placed on a moving platform, and then raised to ensure a consistent contact with the diamond crystal. For xylem sap samples, 30 mL of xylem sap was placed on a tin foil-covered slide and allowed to dry before analysis. For freeze-dried ground leaves a

small amount of powder was transferred to each slide using a spatula. A total of 410 spectra were taken for xylem sap and 330 spectra were taken of freeze-dried ground leaf tissue.

Data analysis

The 'mergetool' function of an in-house developed MATLAB (Mathworks, Natick, USA) toolbox called IRootLab [52,53] was used to convert all spectral information from OPUS format to suitable files (.txt). Following this, it was necessary to pre-process the acquired spectra to improve the signal-to-noise ratio. Pre-processing corrects problems associated with random or systematic artefacts during spectral acquisition and is an essential step of all spectroscopic experiments. Pre-processing and computational analysis of the data were performed using a combination of IRootLab toolbox [52,53] and the PLS Toolbox version 7.9.3 (Eigenvector Research, Inc., Manson, USA). The pre-processing steps applied to all spectra were firstly the selection of the spectral biochemical fingerprint region (1800-900 cm^{-1}), followed by Savitzky–Golay (SG) second differentiation (nine smoothing points) and vector normalisation. All data were mean centred before multivariate analysis, where multiple dependant variables are observed simultaneously to determine a pattern.

Four machine learning techniques were used in this study: an unsupervised dimensionality reduction method, two supervised classification methods and one regression. The unsupervised method principal component analysis (PCA) simplifies complex multivariate datasets, allowing them to be presented intuitively and enabling pattern recognition. Two supervised chemometric techniques, principal component analysis with linear discriminant analysis (PCA-LDA) and support vector machines (SVM), were used for the classification of groups [37,38]. PCA-LDA was also used for the determination of biomarkers. Most importantly, hormone prediction was achieved using a multivariate analysis technique called PLSR of both ATR-FTIR spectral data and real hormone data as measured by UHPLC-HRMS [39]. Regression by PLSR was performed with the same pre-processed data without vector

normalization. Multivariate analysis techniques allow multiple variables to be compared at the same time enabling spectral absorbance values across a range of wavelengths to be simultaneously correlated against concentrations of multiple hormones for numerous samples. Observing all these data at once allows patterns to be seen and enables predictions to be made. To form these models, an X-block of ATR-FTIR spectral absorbance data for plants was analysed by PLSR against a Y-block of hormone concentrations for the corresponding plants as measured using UHPLC-HRMS. Environments were analysed separately, allowing a model to be created for each of them. The PLSR models were validated by Monte-Carlo cross-validation, where 20% of the spectral data is randomly left-out for validation and the remaining 80% is used for training the model in an exhaustive process to ensure model consistency and validation reliability. In this study, Monte-Carlo cross-validation was performed with 1000 iteration cycles. The number of principal components for PCA-LDA was set at 10, to ensure more than 95% of the original data explained variance was contemplated. PLSR models were built varying the number of latent variables according to the smallest root-mean-squared error (RMSE) of cross-validation. Once made, these models can be applied to new ATR-FTIR spectral data in the absence of UHPLC-HRMS data to predict plant hormone concentrations.

Results

ATR-FTIR spectral analysis classifies plants from different environments via spectral differences

The sensitive nature of IR spectroscopy allowed indications of plant responses to environment to be observed visually as differences between spectral profiles. The pre-processed fingerprint spectra exhibit distinguishable differences between spectra of different treatment groups, for both xylem sap and freeze-dried ground samples, at 950, 1050, 1150, 1250, 1325, 1400, 1525, 1575 and 1610 cm^{-1} (Figure S3b†) and 950, 1050, 1275, 1400, 1525

and 1610 cm^{-1} (Figure S3d†), respectively. Three chemometric techniques (PCA, PCA-LDA and SVM) were used to extract further information from the spectral absorbance profiles of xylem sap (Figures 1a-d) and freeze-dried ground leaves (Figures 2a-d). The unsupervised technique, PCA, showed poor separation between treatment groups in xylem sap samples (Figure 1a). However, addition of the supervised classifier LDA created biologically meaningful separation along the linear discriminant 1 (LD1) axis. Xylem sap samples in the low nutrient categories (LLN and SLN) fall to the right of the other samples with the same lighting regine (LC, LD, LN and SC, SD and SN respectively) along the LD1 axis (Figure 1b). In leaf samples, the separation along the LD1 axis relates to light regime (Figure 2b), with 'light' to the left and 'shade' to the right. For the xylem sap samples, the left-hand side of the PCA-LDA scatter graph contains both control and drought plant samples (LC and LD) which were watered with Hoagland solution, the central portion contains clusters of nitrogen fed and low nutrient shaded plants (SN and SLN), and the right-hand side contains the light samples of the nitrogen and low nutrient categories (LN and LLN). The pattern observed in Figure 2a is distinctive due to the homogenisation introduced by the grinding process; PCA of freeze-dried ground leaves separated spectra from individual samples into clusters. PCA-LDA of freeze-dried leaf samples (Figure 2b) resulted in a separation along the axis LD1; LD to the left, LC, LN and LLN in the central portion, and all shaded groups to the right (SC, SD, SN and SLN). The stronger chemometric technique, SVM, achieved the best classification results for both sample types. Analysis of spectra from xylem sap samples using SVM achieved 99.0% accuracy, 98.2% sensitivity, and 99.8% specificity (Figures 1c-d). However, application of SVM to spectra of freeze-dried ground leaves attained even better separation with 99.8% accuracy, 99.6% sensitivity and 100.0% specificity (Figures 2c-d). For SVM model parameters, cost, gamma and number of support vectors, see Table S4†.

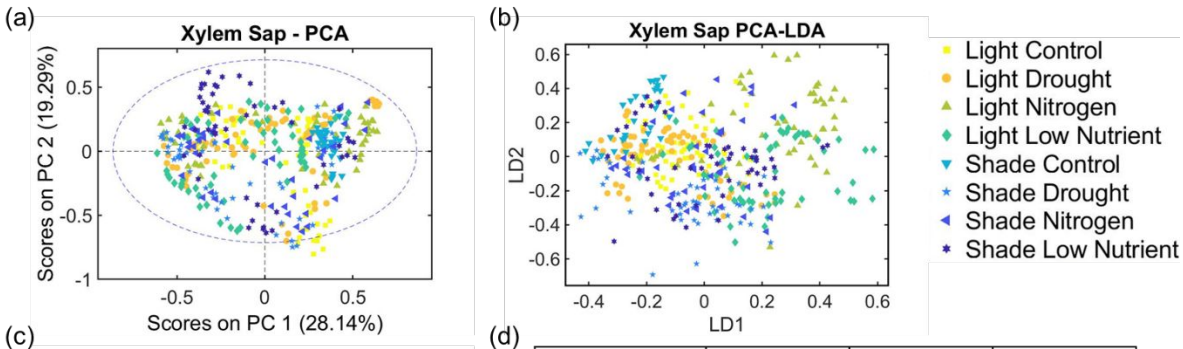

(d)

Xylem Sap - SVM	% Accuracy	% Sensitivity	% Specificity
Light Control	99.9	100	99.7
Light Drought	99.9	100	99.7
Light Nitrogen	99.6	100	99.2
Light Low Nitrogen	99.0	98.3	99.7
Shade Control	100	100	100
Shade Drought	96.0	92.0	100
Shade Nitrogen	97.4	95.0	99.7
Shade Low Nitrogen	100	100	100

Figure 1: (a) PCA scores plot showing poor separation between classes, **(b)** PCA-LDA scatter plot showing some separation by nutrient levels, **(c)** SVM sample/measured plot showing correct classification (Y-axis) of spectra from samples of different treatment categories (X-axis) and **(d)** SVM results for ATR-FTIR spectra taken of xylem sap samples showing excellent classification, grouped by treatments; Light Control (LC), Light Drought (LD), Light Nitrogen (LN), Light Low Nitrogen (LLN), Shade Control (SC), Shade Drought (SD), Shade Nitrogen (SN) and Shade Low Nitrogen (SLN).

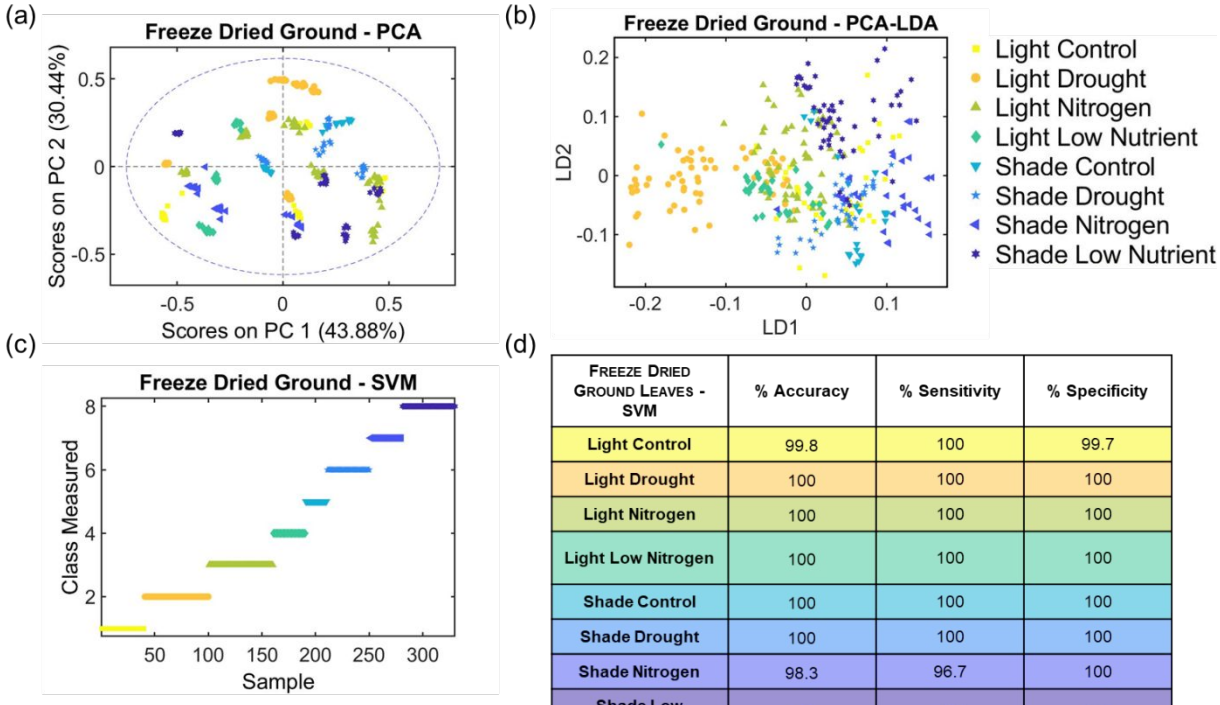

(d)

Freeze Dried Ground Leaves - SVM	% Accuracy	% Sensitivity	% Specificity
Light Control	99.8	100	99.7
Light Drought	100	100	100
Light Nitrogen	100	100	100
Light Low Nitrogen	100	100	100
Shade Control	100	100	100
Shade Drought	100	100	100
Shade Nitrogen	98.3	96.7	100
Shade Low Nitrogen	100	100	100

Figure 2: (a) PCA scores plot in which each cluster is formed from separate samples due to the homogenisation introduced by the grinding process, **(b)** PCA-LDA scatter plot showing some separation by light levels, **(c)** SVM sample/measured plot showing correct classification (Y-axis) of spectra from samples of different treatment categories (X-axis) and **(d)** SVM results for ATR-FTIR spectra taken of freeze-dried ground leaves samples showing excellent classification, grouped by treatments; Light Control (LC), Light Drought (LD), Light Nitrogen (LN), Light Low Nitrogen (LLN), Shade Control (SC), Shade Drought (SD), Shade Nitrogen (SN) and Shade Low Nitrogen (SLN).

ATR-FTIR spectral analysis identifies biomolecular differences between treatments

ATR-FTIR spectroscopy can detect changes in concentration or molecular structure of compounds. Significant biomolecular differences can be deciphered by examination of the key wavenumbers, which differentiate spectral profiles of different treatment groups from one another. These wavenumbers are called loadings (Figure S4†) and their tentative molecular assignments have been found through examination of the literature for both xylem sap and leaf sample types for biomarker information and references (see Table S5†). The peaks which differentiate treatment groups in xylem sap samples were related to a range of biomolecules such as triacylglycerol, proteins, glutamate, cellulose, tannins, starch, and RNA [54–62]. For freeze-dried ground leaves, the differences were found in much the same compounds: triacylglycerol, proteins and amino acids, pectin, polysaccharides such as starch and cellulose, and DNA [55,56,59,63–65].

UHPLC– HRMS hormone analysis indicates that hormone concentrations are impacted by applied treatments

Plants respond to their environment via signalling molecules such as hormones, to enable a plastic response. This is reflected in the concentrations of plant hormones measured by UHPLC-HRMS (ACC, tZ, iP, SA, ABA, JA, GA_1, GA_4, GA_3, tZR, and IAA) which were different between plants belonging to different treatment groups (see Figure 3a and c; Figures S5† and S6†). Figure 3a shows separation of LD and SD plants along PC1 based on xylem sap hormone concentrations accounting for 65.07% of the variance. This is primarily due to

increased ABA and tZ (see Figure 3b, PC1 loadings in blue). The separation along PC2 for xylem sap samples is due to the antagonistic relationship between JA and ABA (Figure 3b, PC2 loadings in green), which is variable within treatment categories (Figure 3a). Figure 3c also shows a separation along PC1 of droughted samples based on the hormone concentrations of freeze-dried ground leaves, accounting for 46.32% of the sample variance. High leaf ABA and low leaf ACC, JA and tZ concentrations were primary responsible for separation along axis PC1 (Figure 3d, PC1 loadings in blue). The PC2 axis of Figure 3c shows some separation by lighting treatment, however this separation was of lesser importance and only explained 38.23% of the variance. The green line in Figure 3d indicates that ABA, JA, tZ, and SA were all higher in LC and LD samples to create this separation along axis PC2, whilst ACC was lower. JA concentrations in plants with a low red: far-red ratio were lower.

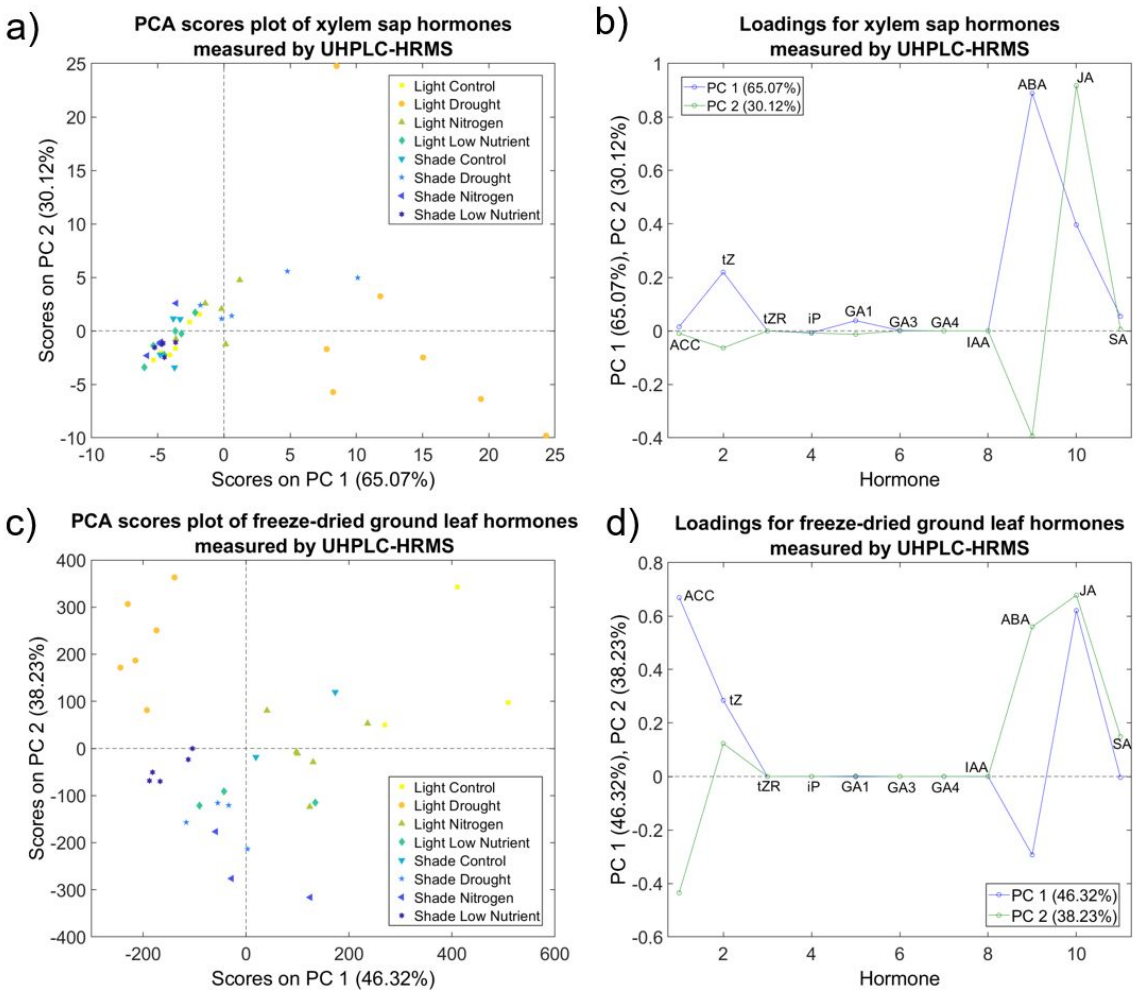

Figure 3: UHPLC-HRMS measurements of plant hormone concentrations analysed by PCA: a) xylem sap PCA scores showing separation of droughted plants along the PC1 axis, b) xylem sap loadings highlighting the importance of ABA in droughted samples, c) freeze-dried ground leaf scores showing separation by drought along PC1 and red: far red ratio along PC2, d) freeze-dried ground leaf loadings indicating that droughted plants exhibited high ABA and low ACC, JA and tZ concentrations whilst plants with a high red: far-red ratio had high ABA, JA, tZ, and SA but low ACC concentrations.

In xylem sap samples (Figure S5†), ABA concentration was highest in the drought categories; LD and SD, at ~17 and ~7 ng·ml^{-1} of sap ABA respectively, whilst the other categories ranged between ~1 and 3 ng·ml^{-1} sap. Leaf ABA concentrations (Figure S6†) were approximately quadruple in LD than those of the other categories. Shade plants had notably lower xylem SA concentrations, in the range of 0.7-1.1 ng·ml^{-1} sap compared with 1.6-4.5 ng·ml^{-1} sap for 'light' plants. Leaf tZ was 4.5-fold higher in LC plants than in those of SLN.

Leaf JA concentration was significantly higher in the light control group LC (~710 ng·g^{-1} dry weight) compared to all other groups (ranging 170-420 ng·g^{-1} dry weight), except the shade control group SC (~460 ng·g^{-1} dry weight). LC had the highest iP concentrations at 0.25 ng·g^{-1} dry weight, significantly higher compared to groups LD, LN, SD, SN (ranging 0.03-0.6 ng·g^{-1} dry weight), with the other groups falling in between.

Combined ATR-FTIR UHPLC-HRMS analysis identifies key spectral wavenumber for hormone prediction via ATR-FTIR spectroscopy

Whilst the plant hormone concentrations quantified by using UHPLC-HRMS served to confirm that the applied treatments were effective at inducing a phenotypic response, importantly the UHPLC-HRMS data enabled the generation of predictive models for hormone concentrations using ATR-FTIR spectral data by means of a multivariate analysis technique called partial least squares regression. PLSR allows simultaneous comparison of multivariate datasets, in this case, the spectral absorbance values for either freeze-dried ground leaf tissue or from xylem sap compared with the plant hormone values obtained by HPLC-HRMS. Using PLSR, the extracted plant hormone concentrations measured by UHPLC-HRMS were accurately predicted from ATR-FTIR spectral profiles of the same sample material.

Spectroscopy-based environmental metabolomics

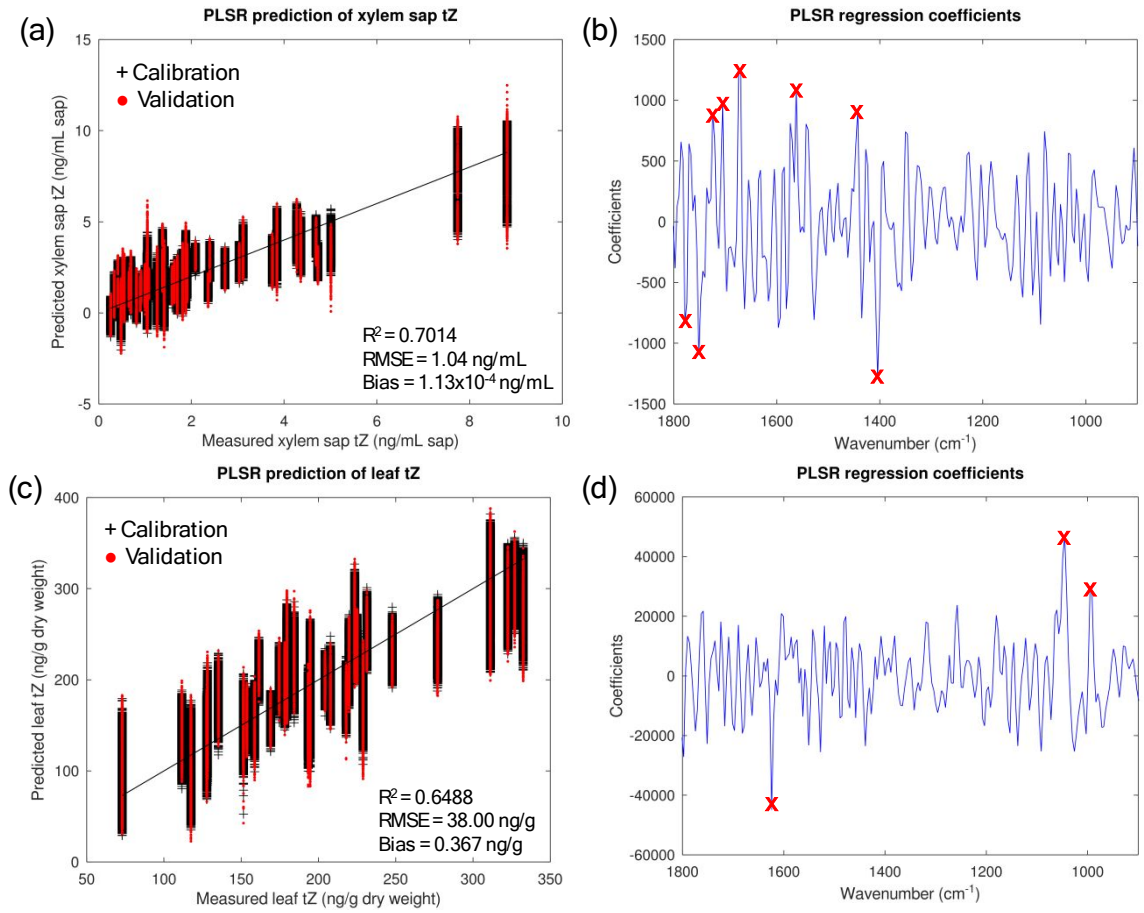

Figure 4: PLS regression and regression coefficients of *trans*-Zeatin concentrations as measured using UHPLC-HRMS against predicted values using ATR-FTIR spectra of a) xylem sap (ng mL^{-1}), and c) freeze-dried ground leaves (in ng·g^{-1} dry weight) grown under all treatment conditions. In panels a) and c), the black line shows the ideal prediction gradient of one, which would be 100% accurate. The black and red scatters points represent the calibration and validation samples during the Monte-Carlo cross-validation with 1000 iterations. The R^2, root mean square error (RMSE) and bias are reported for the validation samples of xylem sap (a) and freeze-dried ground leaves (c). These models were created using spectral data from all treatment categories for individual hormones. The model in panels a) and c) were constructed using 10 latent variables. Panels b) and d) show the regression coefficients which indicates some of the most important wavenumbers (marked with a red X) involved in making this prediction for xylem sap and freeze-dried leaves, respectively.

The graphs in Figure 4 show the PLS regressions and regression coefficients of tZ hormone concentrations as measured using UHPLC-HRMS against predicted concentrations using ATR-FTIR spectra of either xylem sap or freeze-dried ground leaves from all treatment categories as an example of the predictive models generated using this approach (see Figure S7† and S9† for of the predictive models for the other hormones). For the regressions in

Figure 4a and Figure 4c, the black lines show the ideal prediction gradient of one, which would be 100% accurate. Leaf samples achieved a more accurate prediction of R^2s= 0.649 ($[^2H_5]$tZ) to 0.848 ($[^2H_6]$ABA) compared with 0.529 ($[^2H_4]$SA) to 0.820 ($[^2H_2]GA_1$) for xylem sap samples (see Figures S7 and S9†). The PLSR models in Figures 4, S7† and S9† use hormonal data measured by UHPLC-HRMS to train them on the correlation between different hormone concentrations and the corresponding differences in ATR-FTIR spectral profiles. For each hormone, and each sample type, different spectral wavenumbers are important in making this prediction. These key wavenumbers can be identified by the PLS regression coefficients, which are presented in Figures S8† and S10† for each hormone and sample type. The regression coefficients with higher weights (either positive or negative) represent key wavenumbers, since they are more correlated with the increase or decrease of hormone concentration. These were detected mostly in the regions around 1000, 1400-1600 and 1750 cm^{-1} (ABA); 1000-1100 and 1600-1650 cm^{-1} (tZ); 1000-1100, 1300 and 1500-1700 cm^{-1} (SA); 1000-1100 cm^{-1} (JA); 1000-1000 cm^{-1} and 1600-1800 cm^{-1} (ACC) for prediction of leaf hormone concentration; and, around 1000-1100 and 1500-1800 cm^{-1} (ABA); 1400, 1600-1800 cm^{-1} (tZ); 1300-1450 and 1700-1800 cm^{-1} (SA); 1100, 1400 and 1600-1700 cm^{-1} (JA); 1000-1200 and 1700-1800 cm^{-1} (GA1) for xylem sap hormone concentration.

Combined ATR-FTIR UHPLC-HRMS analysis gives a high correlation between predicted and measured hormone concentrations

Analysis of data from each treatment separately allowed the generation of treatment-specific models. Table 1 shows the validation R^2 and root mean square error (RMSE) values for predicted against measured hormone concentrations from xylem sap, with each row being a separate treatment. The R^2 values for the predictions from xylem sap samples ranged between 0.831 (iP for light control) to 0.940 (GA1 for light nitrogen), and the RMSE values ranged from 0.0004 ng/mL sap (GA4 for light control) to 2.655 ng/mL sap (ABA for light drought)

(Table 1). Likewise, the validation R^2 and RMSE values for predicted against measured hormone concentrations from freeze-dried ground leaves are shown in Table 2. The R^2 values varied between 0.811 (ABA for shade control) to 0.957 (JA for shade low nutrient), and the RMSE values ranged from 1.692 ng/g dry weight (ABA for shade nitrogen) to 60.244 ng/g dry weight (JA for light control) (Table 2). In xylem sap samples, light nitrogen achieved the best correlations for hormones iP (R^2 = 0.934), GA1 (R^2 = 0.940) and GA3 (R^2 = 0.889); shade low nutrient for hormones ABA (R^2 = 0.933) and JA (R^2 = 0.935); light drought for hormone tZ (R^2 = 0.904); shade nitrogen for hormone IAA (R^2 = 0.892); shade drought for hormone SA (R^2 = 0.926); and, light control for GA1 (R^2 = 0.924), being the only treatment associated with GA1 hormone. In freeze-dried ground leaves, the best correlations were: shade low nutrient for hormones ACC (R^2 = 0.948) and JA (R^2 = 0.957); shade drought for hormone tZ (R^2 = 0.932); shade nitrogen for hormone ABA (R^2 = 0.950); and, light drought for hormone SA (R^2 = 0.952). These models therefore provide a valuable resource that can be saved and applied to new spectral data obtained from plants grown under similar conditions thereby allowing the hormone concentrations to be accurately predicted without the requirement for exhaustive UHPLC– HRMS analysis.

Table 1: R^2 and root-mean square error (RMSE) values for predicted against measured hormone concentrations from partial least squares regression for xylem sap ATR-FTIR spectral data against UHPLC-HRMS-measured hormone concentrations. Hormones with zero values for multiple plants were excluded from the model and are designated as NA. The treatments with best R^2 results for each hormone are shaded in gray. The number of latent variables to construct the PLSR regression models are shown in Table S6†.

Xylem Sap RMSE (ng/mL sap)	**tz**	**iP**	**GA1**	**GA3**	**GA4**	**IAA**	**ABA**	**JA**	**SA**
Light Control	0.294	0.347	0.042	NA	0.0004	0.006	0.190	0.589	0.323
Light Drought	0.741	0.008	0.116	0.034	NA	NA	2.655	2.570	0.482
Light Nitrogen	0.384	0.001	0.001	0.010	NA	NA	0.326	0.817	0.737
Light Low Nutrient	0.205	0.002	0.001	NA	NA	NA	0.189	0.708	0.222
Shade Control	0.031	0.060	0.014	0.006	NA	NA	0.295	0.671	0.138
Shade Drought	0.318	NA	0.044	0.009	NA	NA	0.939	0.870	0.043
Shade Nitrogen	0.051	0.002	0.008	0.001	NA	0.007	0.084	0.534	0.086
Shade Low Nutrient	0.088	NA	0.020	NA	NA	NA	0.112	0.143	0.086
Xylem Sap R^2	**tz**	**iP**	**GA1**	**GA3**	**GA4**	**IAA**	**ABA**	**JA**	**SA**

Light Control	0.876	0.831	0.881	NA	0.924	0.865	0.856	0.905	0.888
Light Drought	0.904	0.887	0.914	0.862	NA	NA	0.894	0.897	0.863
Light Nitrogen	0.891	0.934	0.940	0.889	NA	NA	0.902	0.886	0.884
Light Low Nutrient	0.872	0.881	0.888	NA	NA	NA	0.865	0.875	0.907
Shade Control	0.896	0.891	0.918	0.880	NA	NA	0.881	0.884	0.902
Shade Drought	0.886	NA	0.889	0.884	NA	NA	0.914	0.932	0.926
Shade Nitrogen	0.900	0.902	0.876	0.884	NA	0.892	0.862	0.928	0.867
Shade Low Nutrient	0.903	NA	0.910	NA	NA	NA	0.933	0.935	0.882

Table 2: R^2 and root-mean square error (RMSE) values for predicted against measured hormone concentrations from partial least squares regression for freeze-dried ground (FDG) leaves ATR-FTIR spectral data against UHPLC-HRMS-measured hormone concentrations. The treatments with best R^2 results for each hormone are shaded in gray. The number of latent variables to construct the PLSR regression models are shown in Table S6†.

FDG Leaves RMSE (ng/g dry weight)	**ACC**	**tz**	**ABA**	**JA**	**SA**
Light Control	52.465	18.024	6.864	60.244	11.221
Light Drought	10.090	12.066	24.915	19.672	11.330
Light Nitrogen	27.340	11.509	6.686	19.963	5.345
Light Low Nutrient	25.134	7.362	6.981	11.333	2.982
Shade Control	7.344	17.257	6.601	29.534	4.753
Shade Drought	14.084	9.137	5.466	9.035	4.121
Shade Nitrogen	32.843	9.663	1.692	5.879	2.691
Shade Low Nutrient	3.852	10.446	2.218	7.824	3.650
FDG Leaves R^2	**ACC**	**tz**	**ABA**	**JA**	**SA**
Light Control	0.904	0.873	0.916	0.901	0.900
Light Drought	0.883	0.909	0.914	0.894	0.952
Light Nitrogen	0.909	0.902	0.902	0.925	0.926
Light Low Nutrient	0.921	0.906	0.887	0.953	0.909
Shade Control	0.840	0.829	0.811	0.855	0.860
Shade Drought	0.876	0.932	0.925	0.917	0.942
Shade Nitrogen	0.892	0.863	0.950	0.954	0.907
Shade Low Nutrient	0.948	0.900	0.933	0.957	0.918

Discussion

Differences in ATR-FTIR spectral profiles are highlighted through chemometrics

Japanese knotweed and other invasive species with low genetic variation exhibit a plastic response to their environment which is thought to contribute to their invasion success [23,66,67]. This phenotypic plasticity was reflected in the present study in the differences found between spectral profiles between treatment groups. This is consistent with the results of studies in

which ATR-FTIR spectroscopy has been successful in differentiating plants' nutrient status and plants from different growing environments [68–71]. The environmentally induced phenotypic changes were successfully captured by the ATR-FTIR spectral profiles, which were visibly different (see Figure S3†). Figures 1 and 2 demonstrate the power of chemometrics to emphasise these differences. SVM was the most successful technique applied and had marginally more success in the freeze-dried ground samples, likely due to the homogenisation of the samples during the grinding process leading to more predictable results. The higher separation of spectra from freeze-dried ground leaves (Figure 2a) by PCA than that of xylem sap spectra (Figure 1a) could be due to the averaging effect of leaf growth over time, adapted to each environment, compared with the nature of the xylem-sap samples which capture a moment in time and could be influenced by compounds related to development stage. Leaf samples reflect a balance between synthesis and metabolism and the import and export of compounds, whilst xylem sap samples reflect instantaneous transport. The sample type more closely correlated to the physiological response therefore depends on the analyte of interest.

Hormone profiles reflect plant response to environment

It is well established that plant stresses such as drought, nutrient deficiency and shading can have a marked impact on the concentrations of plant hormones [1,3]. Our measurement of plant hormones with the highly specific technique, UHPLC-HRMS, from xylem sap (Figure S5†) and leaves (Figure S6†) are consistent with this. The applied treatments (LC, LD, LN, LLN, SC, SD, SN and SLN) were sufficiently different to alter the hormone profiles in the plants, reflecting adaptations to each environment [72]. Importantly, such a range of hormone concentrations was essential prerequisite to create good datasets for regression analysis.

Hormonal biomarkers identified for mid-infrared spectroscopy

The process from chemometric biomarker identification to physical biomolecular extraction is a developing area of spectroscopy with ongoing research to optimise concentration quantification [73,74], molecular definition databases [59] and new applications [35,36,69,71,75]. It was therefore crucial that predictions for expected hormone profiles from spectroscopic data were made and verified against actual hormone concentrations quantified by mass spectrometry. PLSR comparison of the ATR-FTIR spectral data with the quantitative data from UHPLC–HRMS analysis allowed the effect of each hormone on the spectral absorbances to be viewed in isolation. The regression coefficients in Figure 4 aid to point to key spectral wavenumbers used in the model creation for tZ concentration prediction. These suggest that the most important regions for prediction of hormone concentrations using ATR-FTIR spectral profiles are around 1000-1100 and 1620 cm^{-1} for leaf samples; and, around 1400-1450, 1580 and 1650-1780 cm^{-1} for xylem sap samples.

Three tentative wavenumbers used to predict ABA hormone concentration in leaf samples, 1612, 1566 and 1323 cm^{-1} are often attributed to the Amide I [57], Amide II bands of proteins (N-H bending and C-N stretching) [63] and Amide III, respectively [62]. As ABA does not contain nitrogen within its structure this suggests that ABA-associated biochemical changes in other compounds within the leaves could be acting as proxy indicators for the estimation of ABA concentration. Similarly, 1516 cm^{-1} is also tentatively associated with Amide II vibrations of proteins and appears to be one of the key indicators for prediction of tZ, JA and SA concentrations in leaves [59]. The Amide III-associated [62] peak identified at 1323 cm^{-1} was also used to tentatively predict leaf SA concentrations. Two phosphorus-associated peaks that were suggested were used for the prediction of leaf ABA concentration: 1211 cm^{-1}, which is tentatively associated with PO^{2-} asymmetric stretching (Phosphate I); and, 1065 cm^{-1} linked to C–O stretching of the phosphodiester and the ribose of bases [59]. As ABA also does not

contain phosphorus, this supports the hypothesis that compounds other than ABA contribute to a 'spectral signature' for ABA-associated biochemical changes and suggest the use of associated compounds as a proxy, would be useful to gain an overall picture of plant health in agricultural and ecological settings.

In contrast, leaf SA concentrations were predicted using two peaks which could be tentatively associated with the structure of SA: 1582 cm^{-1}, which is linked to the ring C–C stretch of phenyl; and, 1339 cm^{-1} is associated with in-plane C–O stretching vibration combined with the ring stretch of phenyl [59]. As a consequence, 1339 cm^{-1} was used for prediction of leaf ABA and SA, as well as xylem ABA, tZ and SA. Other tentative wavenumbers relating to Amides I and II (1663, 1547, 1570, 1555 cm^{-1}) also appeared important for the prediction of hormone concentrations [55,56,59,76].

When plants are under stress, signalling cascades including hormones and reactive oxygen species (ROS) induce biochemical changes [77]. As an important regulator in response to drought-induced stress, ABA induces ROS accumulation to facilitate stomatal closure [78], whilst SA, which is part of the innate immune response [79], ameliorates oxidative damage through regulation of redox signalling and the antioxidant defence system [80]. To prevent oxidative damage, excess ROS may be absorbed and quenched by phenolic compounds, which have antioxidant properties [81]. This coordinated biochemical response perhaps explains why the possible biomarker at 1512 cm^{-1}, which is tentatively associated with ν(C-C) aromatic (conjugated with C=C phenolic compounds [82] appears to allow the prediction of xylem sap ABA and SA concentrations. Another peak 1177 cm^{-1}, could be associated with the C–O stretch vibration of tannins [61], and is possibly a predictor of xylem JA concentrations.

Polysaccharides are another class of compounds commonly used for the prediction of hormone concentrations, particularly within leaf samples. The peak at 1038 cm^{-1} is tentatively associated with the polysaccharide galactan [83]; this appears to be important in the prediction of leaf SA concentrations. Leaf tZ and leaf JA concentrations appear to be predicted using a peak at 1130 cm^{-1}, which has previously been tentatively attributed to the stretching vibrations [ν(CO)] of the COC glycosidic linkage of polysaccharides [84]. Pectin is potentially associated with a peak at 1443 cm^{-1} [64]; this was hypothesised as useful in the prediction of leaf tZ, SA, JA and ACC concentrations. In addition, a possible peak at 972 cm^{-1} (specifically from the OCH_3 group of polysaccharides such as pectin) [59] has potential to be used in the prediction of leaf ABA, tZ, JA and ACC . This association with leaf JA could be linked to jasmonate-mediated accumulation of leaf-soluble sugars in response to far-red light [85]. A potential peak at 1636 cm^{-1} can be tentatively linked to C=O stretching of carbonyl group, typical of saccharide absorption [59]; this appears to be important in prediction of xylem JA and leaf SA concentrations. Leaf ABA levels appeared to be predicted using a peak at 1049 cm^{-1}, which is associated with cellulose [58]. A potential peak biomarker at 1732 cm^{-1} has been associated with both hemicellulose [83]; this appeared to be a predictor of leaf ABA concentrations. As a key hormone in the drought-induced response, it is perhaps unsurprising that ABA might be estimated using hemicellulose because the leaves of drought-treated plants are known to exhibit a higher content of hemicellulosic polysaccharides [86]. A potential peak biomarker at 1732 cm^{-1} has also been associated with lipid fatty acid esters [83], which is the more probable molecular assignment in its use for estimation of xylem JA concentrations because the fatty acid, linolenic acid, is an important precursor of JA synthesis [87]. Whilst an isolated and controlled peak assignment that could be unambiguously correlated with endpoint effect would be the ideal, in the complex cellular environment this is unlikely to be attainable. In this complex scenario, there will inevitably be a large number of differing peaks

with some more obvious than others. However, we would argue that these shed new insights into mechanism and have the potential to be further investigated.

Whilst leaf hormone concentrations appear to be strongly associated with sugar compounds, in xylem sap samples nucleic acids and bases generally appear to be more relevant indicators of hormone concentration. ABA, tZ and SA concentrations in xylem sap appear to be predicted using a possible peak at 1690 cm^{-1}, which is associated with nucleic acids due to the base carbonyl (C=O) stretching and ring breathing mode [59]. Similar to 1065 cm^{-1}, the peak at 991 cm^{-1} is also associated with C–O stretching of the phosphodiester and the ribose of bases [59]. This peak appeared to be important in xylem sap samples for the prediction of ABA, tZ, SA, and GA1 concentrations. A possible peak at 1713 cm^{-1}, associated with the C=O of the base thymine [59], was identified as important in prediction of tZ and SA concentrations in xylem sap samples. Another possible peak at 1690 cm^{-1}, linked to nucleic acids due to the base carbonyl (C=O) stretching and ring breathing mode [59], appeared to be useful in prediction of xylem sap concentrations of ABA, tZ and SA. A possible peak at 1574 cm^{-1} relating to the C=N of adenine [59], was identified as important in the prediction of xylem GA1 concentrations. Finally, a possible peak at 1531 cm^{-1}, associated previously with modified guanine [59], was used in the prediction of xylem tZ and SA. Again, these peak assignments are tentative but lend novel insights into this changing cellular environment.

ATR-FTIR spectral profiles allow prediction of hormone concentrations

The ATR-FTIR spectrum is information rich and provides an integrated holistic picture of the entire cellular biochemistry [40]. In response to the growth environment, biomolecules unrelated, related and influenced by hormonal activity will be altered, presumably in a dose-related fashion. Chemometrics provides a method to extract this chemical information from spectral absorbances, considering the ratios of different biochemical entities and potentially allowing us to find the "needle in a haystack" of individual hormones in their natural state.

PLSR models have previously been applied to the infrared and Raman spectroscopic absorbances of plant-derived samples to quantify individual components within molecular mixtures [10,11,88–90].

Here we have presented a demonstration of PLSR for the accurate prediction of plant hormone concentrations from ATR-FTIR spectral profiles. The accuracy of PLSR prediction of tZ concentrations was higher for xylem sap (Figure 4a, R^2=0.701) compared with leaf samples (Figure 4c, R^2=0.649). To improve the regression, for example, it would be necessary to narrow down the regression to specicic treatment-hormone models. For example, to create an ABA specific model, application of a wide range of drought severities would be ideal, because ABA is the main regulator of the drought stress response [78] and appears as a key hormone for separation of droughted plants in Figure 3, however this would not be the optimal calibration dataset for another hormone. The PCA loadings based on hormonal data alone (Figures 3b and 3d) show that in both leaf and xylem samples, tZ is a key loading for separation along the axis PC1 in Figures 3a and 3b. Whilst leaf samples in Figure 3b show a good distribution along PCA1, indicating a variety of leaf tZ levels, xylem samples Figure 3a show overlapping clusters. This overlap indicates similarity of xylem sap hormones concentrations across treatment categories, which explains why the xylem sap models have poorer predictive levels than those based on leaf samples.

This trend was also consistent when models were created by treatment categories, in which the hormone predictions based on xylem sap samples (Table 1) did not achieve as high a level of accuracy as those based on freeze-dried ground leaves (Table 2); the high R^2 values achieved in Table 2 indicate an excellent level of prediction from leaf samples. This effect could also be attributed to the fact that these are liquid samples that were injected directly into the HPLC-MS system without any previous extraction, and the higher variability between xylem sap samples (Figure S5†). Refinements to the technique used for collecting

xylem sap [91] and concentrating the samples prior to analysis with UHPLC-HRMS could improve the accuracy of xylem sap hormone quantification. Importantly, Tables 1 and 2 show that it is possible to identify different hormones at the same time to a high accuracy, as these models predicted all hormones in a row simultaneously.

Conclusions

In this study we present a method to predict hormone concentrations using ATR-FTIR spectroscopic measurements and chemometrics, calibrated by UHPLC-HRMS. Once made, the models generated can be applied to new ATR-FTIR spectral data in the absence of UHPLC-HRMS data to predict plant hormone concentrations. As plant hormone concentrations are a key physiological interface for modulation of plant responses in relation to examined processes, the ability to predict them rapidly and non-destructively from spectral data makes it a valuable tool for efficient physiological phenotyping. This methodology has potential for application across a range of species as key plant hormones are conserved [2,92]. ATR-FTIR spectroscopy is a rapid and non-destructive tool, which although demonstrated here using sample preparation, can also be used *in planta* [68]. Consequently, this method could be used in the field to monitor plant hormones and other key signalling molecules produced upon the perception of environmental stress. Biomolecular indications of stress can allow for intervention before the occurrence of phenotypic change, thereby reducing waste, increasing crop yield, and maintaining quality. As can be seen from the variation in R^2 values (Tables 1 and 2) however the accuracy of prediction varies between leaf and xylem sap and between different hormones and environments, suggesting the choice of tissue and growth environment is important when creating models, and would be improved through calibration data.

Authors' Contributions

CAH conceived, planned, and carried out the experiments and data analysis. CLMM provided revision and support for constructing the data analysis models. The manuscript was written by CAH, FLM and MM with contributions from all the authors. FLM provided equipment and expertise in the field of FTIR spectroscopy and chemometrics. PB provided funding for CAH's studentship and expertise in Japanese Knotweed. MM, FLM and JET supervised the project. AA and CMA conducted hormonal analysis.

Conflicts of Interest

The authors declare that there is no conflict of interest.

Acknowledgements

CAH is a member of the Centre for Global Eco-Innovation that is funded by the European Union Regional Development Fund and mediates the collaboration between Lancaster University and Phlorum Ltd. FLM received funding from NIHR Manchester Biomedical Research Centre (NIHR203308). The views expressed are those of the authors and not necessarily those of the NIHR or the Department of Health and Social Care.

References

(1) Anfang, M.; Shani, E. Transport Mechanisms of Plant Hormones. *Curr. Opin. Plant Biol.* **2021**, *63*, 102055. https://doi.org/10.1016/J.PBI.2021.102055.

(2) Blázquez, M. A.; Nelson, D. C.; Weijers, D. Evolution of Plant Hormone Response Pathways. *https://doi.org/10.1146/annurev-arplant-050718-100309* **2020**, *71*, 327–353. https://doi.org/10.1146/ANNUREV-ARPLANT-050718-100309.

(3) Davies, P. J. The Plant Hormones: Their Nature, Occurrence, and Functions. *Plant*

Horm. Biosynthesis, Signal Transduction, Action! **2010**, 1–15. https://doi.org/10.1007/978-1-4020-2686-7_1.

(4) Šimura, J.; Antoniadi, I.; Široká, J.; Tarkowská, D.; Strnad, M.; Ljung, K.; Novák, O. Plant Hormonomics: Multiple Phytohormone Profiling by Targeted Metabolomics. *Plant Physiol.* **2018**, *177* (2), 476. https://doi.org/10.1104/PP.18.00293.

(5) Porfírio, S.; Sonon, R.; Gomes da Silva, M. D. R.; Peixe, A.; Cabrita, M. J.; Azadi, P. Quantification of Free Auxins in Semi-Hardwood Plant Cuttings and Microshoots by Dispersive Liquid–Liquid Microextraction/Microwave Derivatization and GC/MS Analysis. *Anal. Methods* **2016**, *8* (31), 6089–6098. https://doi.org/10.1039/C6AY01289B.

(6) Pradko, A. G.; Litvinovskaya, R. P.; Sauchuk, A. L.; Drach, S. V.; Baranovsky, A. V.; Zhabinskii, V. N.; Mirantsova, T. V.; Khripach, V. A. A New ELISA for Quantification of Brassinosteroids in Plants. *Steroids* **2015**, *97*, 78–86. https://doi.org/10.1016/J.STEROIDS.2014.08.022.

(7) Bosco, R.; Daeseleire, E.; Van Pamel, E.; Scariot, V.; Leus, L. Development of an Ultrahigh-Performance Liquid Chromatography–Electrospray Ionization–Tandem Mass Spectrometry Method for the Simultaneous Determination of Salicylic Acid, Jasmonic Acid, and Abscisic Acid in Rose Leaves. *J. Agric. Food Chem.* **2014**, *62* (27), 6278–6284. https://doi.org/10.1021/JF5023884.

(8) Ge, L.; Peh, C. Y. C.; Yong, J. W. H.; Tan, S. N.; Hua, L.; Ong, E. S. Analyses of Gibberellins by Capillary Electrophoresis–Mass Spectrometry Combined with Solid-Phase Extraction. *J. Chromatogr. A* **2007**, *1159* (1–2), 242–249. https://doi.org/10.1016/J.CHROMA.2007.05.041.

(9) Anagnostopoulos, C. J.; Liapis, K.; Haroutounian, S.; Paspatis, E. Simultaneous

Determination of Different Classes of Plant Growth Regulator in High Water Content Agricultural Products by Liquid Chromatography Tandem Mass Spectrometry and Time of Flight Mass Spectrometry. *J. Liq. Chromatogr. Relat. Technol.* **2013**, *36* (3), 315–335. https://doi.org/10.1080/10826076.2012.657730/SUPPL_FILE/LJLC_A_657730_SUP_26001789.DOC.

(10) Naqvi, S. M. Z. A.; Zhang, Y.; Ahmed, S.; Abdulraheem, M. I.; Hu, J.; Tahir, M. N.; Raghavan, V. Applied Surface Enhanced Raman Spectroscopy in Plant Hormones Detection, Annexation of Advanced Technologies: A Review. *Talanta* **2022**, *236*, 122823. https://doi.org/10.1016/J.TALANTA.2021.122823.

(11) Lew, T. T. S.; Sarojam, R.; Jang, I.-C.; Park, B. S.; Naqvi, N. I.; Wong, M. H.; Singh, G. P.; Ram, R. J.; Shoseyov, O.; Saito, K.; Chua, N.-H.; Strano, M. S. Species-Independent Analytical Tools for next-Generation Agriculture. *Nat. Plants 2020 612* **2020**, *6* (12), 1408–1417. https://doi.org/10.1038/s41477-020-00808-7.

(12) Zhang, C.; Žukauskaitė, A.; Petřík, I.; Pěnčík, A.; Hönig, M.; Grúz, J.; Široká, J.; Novák, O.; Doležal, K. In Situ Characterisation of Phytohormones from Wounded Arabidopsis Leaves Using Desorption Electrospray Ionisation Mass Spectrometry Imaging. *Analyst* **2021**, *146* (8), 2653–2663. https://doi.org/10.1039/D0AN02118K.

(13) Karasov, T. L.; Chae, E.; Herman, J. J.; Bergelson, J. Mechanisms to Mitigate the Trade-Off between Growth and Defense. *Plant Cell* **2017**, *29* (4), 666–680. https://doi.org/10.1105/TPC.16.00931.

(14) Herman, J. J.; Sultan, S. E. Adaptive Transgenerational Plasticity in Plants: Case Studies, Mechanisms, and Implications for Natural Populations. *Front. Plant Sci.* **2011**, *2* (DEC). https://doi.org/10.3389/fpls.2011.00102.

(15) Asif, A.; Baig, M. A.; Siddiqui, M. B. Role of Jasmonates and Salicylates in Plant Allelopathy. **2021**, 115–127. https://doi.org/10.1007/978-3-030-75805-9_6.

(16) Liu, Y.; Oduor, A. M. O.; Dai, Z. C.; Gao, F. L.; Li, J.; Zhang, X.; Yu, F. H. Suppression of a Plant Hormone Gibberellin Reduces Growth of Invasive Plants More than Native Plants. *Oikos* **2021**, *130* (5), 781–789. https://doi.org/10.1111/OIK.07819.

(17) Manoharan, B.; Qi, S. S.; Dhandapani, V.; Chen, Q.; Rutherford, S.; Wan, J. S. H.; Jegadeesan, S.; Yang, H. Y.; Li, Q.; Li, J.; Dai, Z. C.; Du, D. L. Gene Expression Profiling Reveals Enhanced Defense Responses in an Invasive Weed Compared to Its Native Congener During Pathogenesis. *Int. J. Mol. Sci.* **2019**, *20* (19), 4916. https://doi.org/10.3390/IJMS20194916.

(18) Lowry, D. B.; Popovic, D.; Brennan, D. J.; Holeski, L. M. Mechanisms of a Locally Adaptive Shift in Allocation among Growth, Reproduction, and Herbivore Resistance in Mimulus Guttatus*. *Evolution (N. Y).* **2019**, *73* (6), 1168–1181. https://doi.org/10.1111/EVO.13699.

(19) Grossmann, K. Mediation of Herbicide Effects by Hormone Interactions. *J. Plant Growth Regul.* **2003**, *22* (1), 109–122. https://doi.org/10.1007/S00344-003-0020-0/FIGURES/6.

(20) Fennell, M.; Wade, M.; Bacon, K. L. Japanese Knotweed (*Fallopia Japonica*): An Analysis of Capacity to Cause Structural Damage (Compared to Other Plants) and Typical Rhizome Extension. *PeerJ* **2018**, *6*, e5246. https://doi.org/10.7717/peerj.5246.

(21) Santo, P. Assessing Diminution in Value of Residential Properties Affected by Japanese Knotweed. *J. Build. Surv. Apprais. Valuat.* **2017**, *Volume 6* (Number 3), Winter 2017-18, pp. 211-221(11).

(22) Lavoie, C. The Impact of Invasive Knotweed Species (Reynoutria Spp.) on the Environment: Review and Research Perspectives. *Biol. Invasions* **2017**, *19* (8), 2319–2337. https://doi.org/10.1007/s10530-017-1444-y.

(23) van Kleunen, M.; Bossdorf, O.; Dawson, W. The Ecology and Evolution of Alien Plants. *Annu. Rev. Ecol. Evol. Syst.* **2018**, *49* (1), 25–47. https://doi.org/10.1146/annurev-ecolsys-110617-062654.

(24) Parepa, M.; Fischer, M.; Bossdorf, O. Environmental Variability Promotes Plant Invasion. *Nat. Commun.* **2013**, *4* (1), 1–4. https://doi.org/10.1038/ncomms2632.

(25) Urcelay, C.; Austin, A. T. Exotic Plants Get a Little Help from Their Friends. *Science (New York, N.Y.)*. NLM (Medline) May 29, 2020, pp 934–936. https://doi.org/10.1126/science.abc3587.

(26) Liu, Y.; Oduor, A. M. O.; Dai, Z. C.; Gao, F. L.; Li, J.; Zhang, X.; Yu, F. H. Suppression of a Plant Hormone Gibberellin Reduces Growth of Invasive Plants More than Native Plants. *Oikos* **2021**, *130* (5), 781–789. https://doi.org/10.1111/OIK.07819.

(27) Zhang, Y.-Y.; Parepa, M.; Fischer, M.; Bossdorf, O. Epigenetics of Colonizing Species? A Study of Japanese Knotweed in Central Europe. In *Barrett SCH, Colautti RI, Dlugosch KM, Rieseberg LH (Eds) Invasion Genetics*; John Wiley & Sons, Ltd: Chichester, UK, 2016; pp 328–340. https://doi.org/10.1002/9781119072799.ch19.

(28) Richards, C. L.; Schrey, A. W.; Pigliucci, M. Invasion of Diverse Habitats by Few Japanese Knotweed Genotypes Is Correlated with Epigenetic Differentiation. *Ecol. Lett.* **2012**, *15* (9), 1016–1025. https://doi.org/10.1111/j.1461-0248.2012.01824.x.

(29) Rouifed, S.; Byczek, C.; Laffray, D.; Piola, F. Invasive Knotweeds Are Highly Tolerant to Salt Stress. *Environ. Manage.* **2012**, *50*, 1027–1034.

https://doi.org/10.1007/s00267-012-9934-2.

(30) Michalet, S.; Rouifed, S.; Pellassa-Simon, T.; Fusade-Boyer, M.; Meiffren, G.; Nazaret, S.; Piola, F. Tolerance of Japanese Knotweed s.l. to Soil Artificial Polymetallic Pollution: Early Metabolic Responses and Performance during Vegetative Multiplication. *Environ. Sci. Pollut. Res.* **2017**, *24* (26), 20897–20907. https://doi.org/10.1007/s11356-017-9716-8.

(31) Sołtysiak, J. Heavy Metals Tolerance in an Invasive Weed (Fallopia Japonica) under Different Levels of Soils Contamination. *J. Ecol. Eng.* **2020**, *21* (7), 81–91. https://doi.org/10.12911/22998993/125447.

(32) Holm, A. K.; Elameen, A.; Oliver, B. W.; Brandsæter, L. O.; Fløistad, I. S.; Brurberg, M. B. Low Genetic Variation of Invasive Fallopia Spp. in Their Northernmost European Distribution Range. *Ecol. Evol.* **2018**, *8* (1), 755–764. https://doi.org/10.1002/ece3.3703.

(33) Bailey, J. P.; Conolly, A. P. Prize-Winners to Pariahs -A History of Japanese Knotweed s.l. (Polygonaceae) in the British Isles. *Watsonia* **2000**, *23*, 93–110.

(34) Hollingsworth, M. L.; Bailey, J. P. Evidence for Massive Clonal Growth in the Invasive Weed Fallopia Japonica (Japanese Knotweed). *Bot. J. Linn. Soc.* **2000**, *133*, 463–472. https://doi.org/10.1006/bojl.2000.0359.

(35) Skolik, P.; Morais, C. L. M.; Martin, F. L.; McAinsh, M. R. Determination of Developmental and Ripening Stages of Whole Tomato Fruit Using Portable Infrared Spectroscopy and Chemometrics. *BMC Plant Biol.* **2019**, *19* (1), 236. https://doi.org/10.1186/s12870-019-1852-5.

(36) Skolik, P.; McAinsh, M. R.; Martin, F. L. ATR-FTIR Spectroscopy Non-Destructively

Detects Damage-Induced Sour Rot Infection in Whole Tomato Fruit. *Planta* **2019**, *249* (3), 925–939. https://doi.org/10.1007/s00425-018-3060-1.

(37) Morais, C. L. M.; Lima, K. M. G. Principal Component Analysis with Linear and Quadratic Discriminant Analysis for Identification of Cancer Samples Based on Mass Spectrometry. *Artic. J. Braz. Chem. Soc* **2018**, *29* (3), 472–481. https://doi.org/10.21577/0103-5053.20170159.

(38) Morais, C. L. M.; Costa, F. S. L.; Lima, K. M. G. Variable Selection with a Support Vector Machine for Discriminating: Cryptococcus Fungal Species Based on ATR-FTIR Spectroscopy. *Anal. Methods* **2017**, *9* (20), 2964–2970. https://doi.org/10.1039/c7ay00428a.

(39) Mehmood, T.; Liland, K. H.; Snipen, L.; Sæbø, S. A Review of Variable Selection Methods in Partial Least Squares Regression. *Chemom. Intell. Lab. Syst.* **2012**, *118*, 62–69. https://doi.org/10.1016/J.CHEMOLAB.2012.07.010.

(40) Morais, C. L. M.; Lima, K. M. G.; Singh, M.; Martin, F. L. Tutorial: Multivariate Classification for Vibrational Spectroscopy in Biological Samples. *Nature Protocols*. Nature Research July 1, 2020, pp 2143–2162. https://doi.org/10.1038/s41596-020-0322-8.

(41) Met Office. UK Regional Climates. *https://www.metoffice.gov.uk/research/climate/maps-and-data/regional-climates/index* **2019**.

(42) Bailey, J. The Japanese Knotweed Invasion Viewed as a Vast Unintentional Hybridisation Experiment. *Heredity (Edinb).* **2013**. https://doi.org/10.1038/hdy.2012.98.

(43) Smith, H. Light Quality, Photoperception, and Plant Strategy. *Annu. Rev. Plant Physiol.* **1982**, *33* (1), 481–518.

(44) Larsen, D. H.; Woltering, E. J.; Nicole, C. C. S.; Marcelis, L. F. M. Response of Basil Growth and Morphology to Light Intensity and Spectrum in a Vertical Farm. *Front. Plant Sci.* **2020**, *11*, 1893. https://doi.org/10.3389/FPLS.2020.597906/BIBTEX.

(45) Pennisi, G.; Pistillo, A.; Orsini, F.; Cellini, A.; Spinelli, F.; Nicola, S.; Fernandez, J. A.; Crepaldi, A.; Gianquinto, G.; Marcelis, L. F. M. Optimal Light Intensity for Sustainable Water and Energy Use in Indoor Cultivation of Lettuce and Basil under Red and Blue LEDs. *Sci. Hortic. (Amsterdam).* **2020**, *272*, 109508. https://doi.org/10.1016/J.SCIENTA.2020.109508.

(46) Zou, T.; Huang, C.; Wu, P.; Ge, L.; Xu, Y. Optimization of Artificial Light for Spinach Growth in Plant Factory Based on Orthogonal Test. *Plants 2020, Vol. 9, Page 490* **2020**, *9* (4), 490. https://doi.org/10.3390/PLANTS9040490.

(47) Park, Y.; Runkle, E. S. Spectral Effects of Light-Emitting Diodes on Plant Growth, Visual Color Quality, and Photosynthetic Photon Efficacy: White versus Blue plus Red Radiation. *PLoS One* **2018**, *13* (8). https://doi.org/10.1371/JOURNAL.PONE.0202386.

(48) Monaghan, R. M.; Paton, R. J.; Smith, L. C.; Drewry, J. J.; Littlejohn, R. P. The Impacts of Nitrogen Fertilisation and Increased Stocking Rate on Pasture Yield, Soil Physical Condition and Nutrient Losses in Drainage from a Cattle-Grazed Pasture. *New Zeal. J. Agric. Res.* **2005**, *48* (2), 227–240. https://doi.org/10.1080/00288233.2005.9513652.

(49) Dodd, I. C.; Egea, G.; Davies, W. J. Abscisic Acid Signalling When Soil Moisture Is Heterogeneous: Decreased Photoperiod Sap Flow from Drying Roots Limits Abscisic

Acid Export to the Shoots. *Plant. Cell Environ.* **2008**, *31* (9), 1263–1274. https://doi.org/10.1111/J.1365-3040.2008.01831.X.

(50) Albacete, A.; Ghanem, M. E.; Martínez-Andújar, C.; Acosta, M.; Sánchez-Bravo, J.; Martínez, V.; Lutts, S.; Dodd, I. C.; Pérez-Alfocea, F. Hormonal Changes in Relation to Biomass Partitioning and Shoot Growth Impairment in Salinized Tomato (Solanum Lycopersicum L.) Plants. *J. Exp. Bot.* **2008**, *59* (15), 4119–4131. https://doi.org/10.1093/JXB/ERN251.

(51) Groãÿkinsky, D. K.; Albacete, A.; Jammer, A.; Krbez, P.; Van der Graaff, E.; Pfeifhofer, H.; Roitsch, T. A Rapid Phytohormone and Phytoalexin Screening Method for Physiological Phenotyping. *Mol. Plant* **2014**, *7*, 1053–1056. https://doi.org/10.1093/mp/ssu015.

(52) Martin, F. L.; Kelly, J. G.; Llabjani, V.; Martin-Hirsch, P. L.; Patel, I. I.; Trevisan, J.; Fullwood, N. J.; Walsh, M. J. Distinguishing Cell Types or Populations Based on the Computational Analysis of Their Infrared Spectra. *Nat. Protoc.* **2010**, *5* (11), 1748–1760. https://doi.org/10.1038/nprot.2010.133.

(53) Trevisan, J.; Angelov, P. P.; Scott, A. D.; Carmichael, P. L.; Martin, F. L. IRootLab: A Free and Open-Source MATLAB Toolbox for Vibrational Biospectroscopy Data Analysis. *Bioinformatics* **2013**, *29* (8), 1095–1097. https://doi.org/10.1093/bioinformatics/btt084.

(54) Nozahic, V.; Amziane, S. Influence of Sunflower Aggregates Surface Treatments on Physical Properties and Adhesion with a Mineral Binder. *Compos. Part A Appl. Sci. Manuf.* **2012**, *43* (11), 1837–1849. https://doi.org/10.1016/j.compositesa.2012.07.011.

(55) Belfer, S.; Purinson, Y.; Kedem, O. Surface Modification of Commercial Polyamide Reverse Osmosis Membranes by Radical Grafting: An ATR-FTIR Study. *Acta Polym.*

1998, *49* (10–11), 574–582. https://doi.org/10.1002/(sici)1521-4044(199810)49:10/11<574::aid-apol574>3.0.co;2-0.

(56) Shivu, B.; Seshadri, S.; Li, J.; Oberg, K. A.; Uversky, V. N.; Fink, A. L. Distinct β-Sheet Structure in Protein Aggregates Determined by ATR−FTIR Spectroscopy. **2013**. https://doi.org/10.1021/bi400625v.

(57) Jin, N.; Semple, K. T.; Jiang, L.; Luo, C.; Zhang, D.; Martin, F. L. Spectrochemical Analyses of Growth Phase-Related Bacterial Responses to Low (Environmentally-Relevant) Concentrations of Tetracycline and Nanoparticulate Silver. *Analyst* **2018**, *143* (3), 768–776. https://doi.org/10.1039/c7an01800b.

(58) Moskal, P.; Wesełucha-Birczyńska, A.; Łabanowska, M.; Filek, M. Adaxial and Abaxial Pattern of Urtica Dioica Leaves Analyzed by 2DCOS ATR-FTIR as a Function of Their Growth Time and Impact of Environmental Pollution. *Vib. Spectrosc.* **2019**, *104*, 102948. https://doi.org/10.1016/j.vibspec.2019.102948.

(59) Talari, A. C. S.; Martinez, M. A. G.; Movasaghi, Z.; Rehman, S.; Rehman, I. U. Advances in Fourier Transform Infrared (FTIR) Spectroscopy of Biological Tissues. *Appl. Spectrosc. Rev.* **2017**, *52* (5), 456–506. https://doi.org/10.1080/05704928.2016.1230863.

(60) Gorzsas, A. ATR-FTIR Microspectroscopy Brings a Novel Insight Into the Study of Cell Wall Chemistry at the Cellular Level. In *Proceedings of IPSC 2019-2nd International Plant Spectroscopy Conference*; Frontiers Media SA, 2020.

(61) Falcão, L.; Araújo, M. E. M. Tannins Characterization in Historic Leathers by Complementary Analytical Techniques ATR-FTIR, UV-Vis and Chemical Tests. *J. Cult. Herit.* **2013**, *14* (6), 499–508. https://doi.org/10.1016/J.CULHER.2012.11.003.

(62) Morais, C. L. M.; Costa, F. S. L.; Lima, K. M. G. Variable Selection with a Support Vector Machine for Discriminating Cryptococcus Fungal Species Based on ATR-FTIR Spectroscopy. *Anal. Methods* **2017**, *9* (20), 2964–2970. https://doi.org/10.1039/C7AY00428A.

(63) Rana, R.; Herz, K.; Bruelheide, H.; Dietz, S.; Haider, S.; Jandt, U.; Pena, R. Leaf Attenuated Total Reflection Fourier Transform Infrared (ATR-FTIR) Biochemical Profile of Grassland Plant Species Related to Land-Use Intensity. *Ecol. Indic.* **2018**, *84*, 803–810. https://doi.org/10.1016/j.ecolind.2017.09.047.

(64) Sharma, S.; Uttam, K. N. Early Stage Detection of Stress Due to Copper on Maize (Zea Mays L.) by Laser-Induced Fluorescence and Infrared Spectroscopy. *J. Appl. Spectrosc.* **2018**, *85* (4), 771–780. https://doi.org/10.1007/s10812-018-0717-2.

(65) Ajitha, B.; Ashok Kumar Reddy, Y.; Shameer, S.; Rajesh, K. M.; Suneetha, Y.; Sreedhara Reddy, P. Lantana Camara Leaf Extract Mediated Silver Nanoparticles: Antibacterial, Green Catalyst. *J. Photochem. Photobiol. B Biol.* **2015**, *149*, 84–92. https://doi.org/10.1016/j.jphotobiol.2015.05.020.

(66) Geng, Y.; van Klinken, R. D.; Sosa, A.; Li, B.; Chen, J.; Xu, C.-Y. The Relative Importance of Genetic Diversity and Phenotypic Plasticity in Determining Invasion Success of a Clonal Weed in the USA and China. *Front. Plant Sci.* **2016**, *7*, 216. https://doi.org/10.3389/fpls.2016.00213.

(67) Richards, C. L.; Bossdorf, O.; Muth, N. Z.; Gurevitch, J.; Pigliucci, M. Jack of All Trades, Master of Some? On the Role of Phenotypic Plasticity in Plant Invasions. *Ecol. Lett.* **2006**, *9* (8), 981–993. https://doi.org/10.1111/j.1461-0248.2006.00950.x.

(68) Butler, H. J.; McAinsh, M. R.; Adams, S.; Martin, F. L. Application of Vibrational Spectroscopy Techniques to Non-Destructively Monitor Plant Health and

Development. *Anal. Methods* **2015**, *7* (10), 4059–4070. https://doi.org/10.1039/C5AY00377F.

(69) Holden, C. A.; Morais, C. L. M.; Taylor, J. E.; Martin, F. L.; Beckett, P.; McAinsh, M. Regional Differences in Clonal Japanese Knotweed Revealed by Chemometrics-Linked Attenuated Total Reflection Fourier-Transform Infrared Spectroscopy. *BMC Plant Biol. 2021 211* **2021**, *21* (1), 1–20. https://doi.org/10.1186/S12870-021-03293-Y.

(70) Traoré, M.; Kaal, J.; Martínez Cortizas, A. Differentiation between Pine Woods According to Species and Growing Location Using FTIR-ATR. *Wood Sci. Technol.* **2018**, *52* (2), 487–504. https://doi.org/10.1007/s00226-017-0967-9.

(71) Holden, C. A.; Bailey, J. P.; Taylor, J. E.; Martin, F.; Beckett, P.; McAinsh, M. Know Your Enemy: Application of ATR-FTIR Spectroscopy to Invasive Species Control. *PLoS One* **2022**, *17* (1), e0261742. https://doi.org/10.1371/JOURNAL.PONE.0261742.

(72) Wolters, H.; Jürgens, G. Survival of the Flexible: Hormonal Growth Control and Adaptation in Plant Development. *Nat. Rev. Genet.* **2009**, *10* (5), 305–317. https://doi.org/10.1038/NRG2558.

(73) Spalding, K.; Bonnier, F.; Bruno, C.; Blasco, H.; Board, R.; Benz-de Bretagne, I.; Byrne, H. J.; Butler, H. J.; Chourpa, I.; Radhakrishnan, P.; Baker, M. J. Enabling Quantification of Protein Concentration in Human Serum Biopsies Using Attenuated Total Reflectance – Fourier Transform Infrared (ATR-FTIR) Spectroscopy. *Vib. Spectrosc.* **2018**, *99*, 50–58. https://doi.org/10.1016/j.vibspec.2018.08.019.

(74) Wagner, H.; Liu, Z.; Langner, U.; Stehfest, K.; Wilhelm, C. The Use of FTIR Spectroscopy to Assess Quantitative Changes in the Biochemical Composition of

Microalgae. *J. Biophotonics* **2010**, *3* (8–9), 557–566. https://doi.org/10.1002/jbio.201000019.

(75) Butler, H. J.; Martin, F. L.; Roberts, M. R.; Adams, S.; McAinsh, M. R. Observation of Nutrient Uptake at the Adaxial Surface of Leaves of Tomato (*Solanum Lycopersicum*) Using Raman Spectroscopy. *Anal. Lett.* **2020**, *53* (4), 536–562. https://doi.org/10.1080/00032719.2019.1658199.

(76) Strong, R.; Martin, F. L.; Jones, K. C.; Shore, R. F.; Halsall, C. J. Subtle Effects of Environmental Stress Observed in the Early Life Stages of the Common Frog, Rana Temporaria. *Sci. Rep.* **2017**, *7* (1), 1–13. https://doi.org/10.1038/srep44438.

(77) Heap, B.; Holden, C.; Taylor, J.; McAinsh, M. <scp>ROS</Scp> Crosstalk in Signalling Pathways. In *eLS*; Wiley, 2020; pp 1–9. https://doi.org/10.1002/9780470015902.a0025271.

(78) Bharath, P.; Gahir, S.; Raghavendra, A. S. Abscisic Acid-Induced Stomatal Closure: An Important Component of Plant Defense Against Abiotic and Biotic Stress. *Front. Plant Sci.* **2021**, *12*, 324. https://doi.org/10.3389/FPLS.2021.615114/BIBTEX.

(79) Maruri-López, I.; Aviles-Baltazar, N. Y.; Buchala, A.; Serrano, M. Intra and Extracellular Journey of the Phytohormone Salicylic Acid. *Front. Plant Sci.* **2019**, *0*, 423. https://doi.org/10.3389/FPLS.2019.00423.

(80) Saleem, M.; Fariduddin, Q.; Castroverde, C. D. M. Salicylic Acid: A Key Regulator of Redox Signalling and Plant Immunity. *Plant Physiol. Biochem.* **2021**, *168*, 381–397. https://doi.org/10.1016/J.PLAPHY.2021.10.011.

(81) Zheng, W.; Wang, S. Y. Antioxidant Activity and Phenolic Compounds in Selected Herbs. *J. Agric. Food Chem.* **2001**, *49* (11), 5165–5170.

https://doi.org/10.1021/JF010697N.

(82) Heredia-Guerrero, J. A.; Benítez, J. J.; Domínguez, E.; Bayer, I. S.; Cingolani, R.; Athanassiou, A.; Heredia, A. Infrared and Raman Spectroscopic Features of Plant Cuticles: A Review. *Front. Plant Sci.* **2014**, *5*, 305. https://doi.org/10.3389/fpls.2014.00305.

(83) Ord, J.; Butler, H. J.; McAinsh, M. R.; Martin, F. L. Spectrochemical Analysis of Sycamore (Acer Pseudoplatanus) Leaves for Environmental Health Monitoring. *Analyst* **2016**, *141* (10), 2896–2903. https://doi.org/10.1039/C6AN00392C.

(84) Liu, X.; Renard, C. M. G. C.; Bureau, S.; Le Bourvellec, C. Revisiting the Contribution of ATR-FTIR Spectroscopy to Characterize Plant Cell Wall Polysaccharides. *Carbohydr. Polym.* **2021**, *262*, 117935. https://doi.org/10.1016/J.CARBPOL.2021.117935.

(85) Courbier, S.; Grevink, S.; Sluijs, E.; Bonhomme, P.-O.; Kajala, K.; Wees, S. C. M. Van; Pierik, R. Far-Red Light Promotes Botrytis Cinerea Disease Development in Tomato Leaves via Jasmonate-Dependent Modulation of Soluble Sugars. *Plant. Cell Environ.* **2020**, *43* (11), 2769–2781. https://doi.org/10.1111/PCE.13870.

(86) van der Weijde, T.; Huxley, L. M.; Hawkins, S.; Sembiring, E. H.; Farrar, K.; Dolstra, O.; Visser, R. G. F.; Trindade, L. M. Impact of Drought Stress on Growth and Quality of Miscanthus for Biofuel Production. *GCB Bioenergy* **2017**, *9* (4), 770–782. https://doi.org/10.1111/GCBB.12382.

(87) Gfeller, A.; Dubugnon, L.; Liechti, R.; Farmer, E. E. Jasmonate Biochemical Pathway. *Sci. Signal.* **2010**, *3* (109). https://doi.org/10.1126/SCISIGNAL.3109CM3/ASSET/57BCEEBB-B6E4-4299-8646-8E4F84042400/ASSETS/GRAPHIC/3109CM3-F3.JPEG.

(88) Zhu, J.; Agyekum, A. A.; Kutsanedzie, F. Y. H.; Li, H.; Chen, Q.; Ouyang, Q.; Jiang, H. Qualitative and Quantitative Analysis of Chlorpyrifos Residues in Tea by Surface-Enhanced Raman Spectroscopy (SERS) Combined with Chemometric Models. *LWT* **2018**, *97*, 760–769. https://doi.org/10.1016/J.LWT.2018.07.055.

(89) Romera-Fernández, M.; Berrueta, L. A.; Garmón-Lobato, S.; Gallo, B.; Vicente, F.; Moreda, J. M. Feasibility Study of FT-MIR Spectroscopy and PLS-R for the Fast Determination of Anthocyanins in Wine. *Talanta* **2012**, *88*, 303–310. https://doi.org/10.1016/J.TALANTA.2011.10.045.

(90) Bensemmane, N.; Bouzidi, N.; Daghbouche, Y.; Garrigues, S.; de la Guardia, M.; El Hattab, M. Quantification of Phenolic Acids by Partial Least Squares Fourier-Transform Infrared (PLS-FTIR) in Extracts of Medicinal Plants. *Phytochem. Anal.* **2021**, *32* (2), 206–221. https://doi.org/10.1002/PCA.2974.

(91) Netting, A. G.; Theobald, J. C.; Dodd, I. C. Xylem Sap Collection and Extraction Methodologies to Determine in Vivo Concentrations of ABA and Its Bound Forms by Gas Chromatography-Mass Spectrometry (GC-MS). *Plant Methods* **2012**, *8* (1), 1–14. https://doi.org/10.1186/1746-4811-8-11/FIGURES/8.

(92) Wang, C.; Liu, Y.; Li, S.-S.; Han, G.-Z. Insights into the Origin and Evolution of the Plant Hormone Signaling Machinery. *Plant Physiol.* **2015**, *167* (3), 872–886. https://doi.org/10.1104/PP.114.247403.

Footnotes

† Electronic supplementary information (ESI):

- **Table S1:** Lighting conditions within each Snijder cabinet.

- **Figure S1:** Spectra from a) 'Light' (LC, LD, LN, LLN) b) 'Shade' (SC, SD, SN, SLN) cabinets, providing red: far-red ratios of 5.6 and 0.4 respectively.
- **Table S2:** Reagents used for Hoagland's solution.
- **Figure S2:** Chromatogram and mass spectra for the hormone salicylic acid
- **Table S3:** Hormone descriptions and molecular ion masses
- **Figure S3: (a)** Raw and **(b)** pre-processed class means spectra in the fingerprint region from xylem sap, **(c)** Raw and **(d)** pre-processed (Savitzky–Golay 2nd differentiation, n=9, and vector normalisation) class means spectra in the fingerprint region from freeze-dried ground leaves.
- **Table S4:** SVM parameters for classification.
- **Figure S4:** Loadings from spectra of a) xylem sap and b) freeze-dried ground leaf samples
- **Table S5:** PCA-loadings and biomarkers: key wavenumbers and compounds, which differentiate spectral profiles of plants from different growth conditions for both xylem sap and freeze-dried ground sample types.
- **Figure S5:** Hormone profiles from xylem sap in ng·ml^{-1} sap for a) 1-amino-cyclopropanecarboxylic acid (ACC), b) trans-Zeatin (tZ), c) isopentyl-adenine (iP), d) salicylic acid (SA), e) abscisic acid (ABA), f) jasmonic acid (JA), g) gibberellin A1 (GA_1), gibberellin A4 (GA_4), gibberellic acid (GA_3), *trans*-zeatin riboside (tZR), and indole-3-acetic acid (IAA).
- **Figure S6:** Hormone profiles from freeze-dried ground leaves ng·g^{-1} dry weight for a) 1-amino-cyclopropanecarboxylic acid (ACC), b) trans-Zeatin (tZ), c) isopentyl-adenine (iP), d) salicylic acid (SA), e) abscisic acid (ABA), f) jasmonic acid (JA), g) gibberellin A1 (GA_1), gibberellin A4 (GA_4), gibberellic acid (GA_3), *trans*-zeatin riboside (tZR), and indole-3-acetic acid (IAA).

- **Figure S7:** PLS regression graphs for prediction of plant hormones from xylem sap. Validation was performed by Monte-Carlo cross-validation with 20% of samples left-out for validation during 1000 iterations. All models were built using 10 latent variables.
- **Figure S8:** PLSR regression coefficients for prediction of plant hormones from xylem sap.
- **Figure S9:** PLS regression graphs for prediction of plant hormones from freeze-dried ground leaves. Validation was performed by Monte-Carlo cross-validation with 20% of samples left-out for validation during 1000 iterations. All models were built using 10 latent variables.
- **Figure S10:** PLSR regression coefficients for prediction of plant hormones from freeze-dried ground leaves.
- **Table S6:** Number of latent variables (LVs) used to build the PLSR models between different types of treatment and hormone levels for xylem sap and freeze-dried ground (FDG) leaves. Higher number of LVs represents higher model complexity.
- **Data S1:** Hormone concentrations measured by ultra-high-performance liquid chromatography-high-resolution mass spectrometry and spectral absorbances measured by attenuated total reflection Fourier-transform infrared spectroscopy for freeze-dried ground leaf and xylem sap samples.

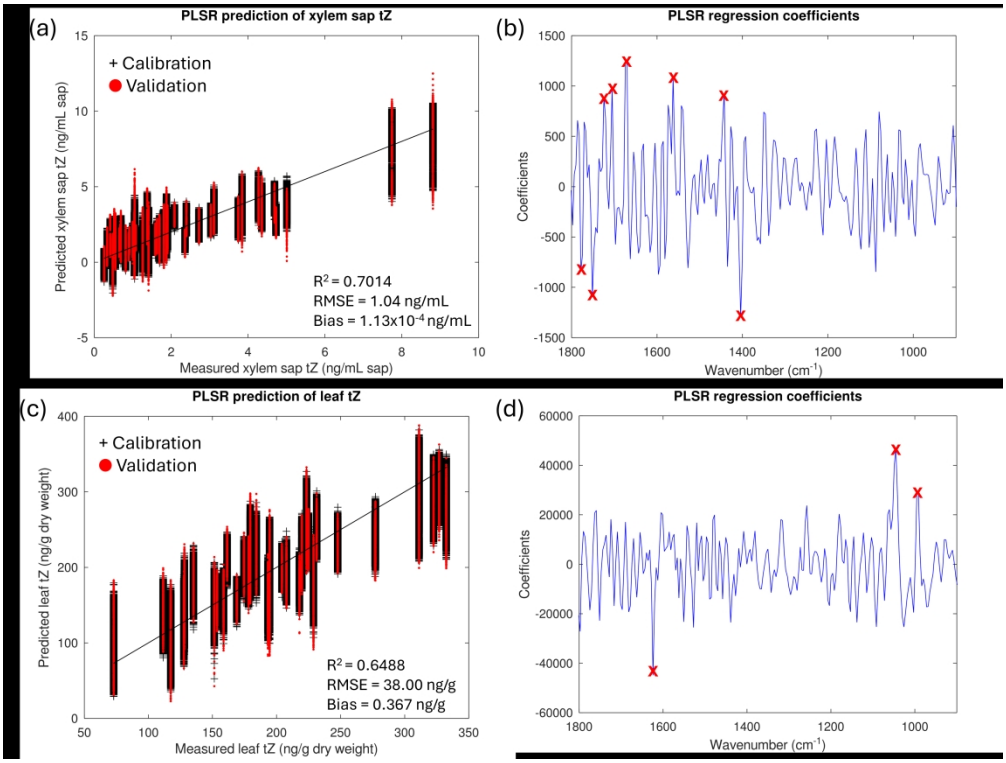

Figure 4: PLS regression and regression coefficients of trans-Zeatin concentrations as measured using UHPLC-HRMS against predicted values using ATR-FTIR spectra of a) xylem sap (ng mL-1), and c) freeze-dried ground leaves (in ng·g-1 dry weight) grown under all treatment conditions. In panels a) and c), the black line shows the ideal prediction gradient of one, which would be 100% accurate. The black and red scatters points represent the calibration and validation samples during the Monte-Carlo cross-validation with 1000 iterations. The R2, root mean square error (RMSE) and bias are reported for the validation samples of xylem sap (a) and freeze-dried ground leaves (c). These models were created using spectral data from all treatment categories for individual hormones. The model in panels a) and c) were constructed using 10 latent variables. Panels b) and d) show the regression coefficients which indicates some of the most important wavenumbers (marked with a red X) involved in making this prediction for xylem sap and freeze-dried leaves, respectively.

765x576mm (130 x 130 DPI)

Attenuated total reflection Fourier-transform infrared spectroscopy for the prediction of hormone concentrations in plants

Claire A Holden[1], Martin McAinsh[1], Jane E Taylor[1], Paul Beckett[2], Alfonso Albacete[3,4], Cristina Martínez-Andújar[4], Camilo L. M. Morais[5,6], Francis L Martin[7,8]*

[1] Lancaster Environment Centre, Lancaster University, UK

[2] Phlorum Ltd, UK

[3] Institute for Agro-Environmental Research and Development of Murcia (IMIDA), Department of Plant Production and Agrotechnology, C/ Mayor s/n, E-30150 La Alberca, Murcia, Spain

[4] CEBAS-CSIC. Department of Plant Nutrition. Campus Universitario de Espinardo, E-30100 Murcia, Spain

[5] Center for Education, Science and Technology of the Inhamuns Region, State University of Ceará, Tauá 63660-000, Brazil

[6] Graduate Program in Chemistry, Institute of Chemistry, Federal University of Rio Grande do Norte, Natal 59072-970, Brazil

[7] Department of Cellular Pathology, Blackpool Teaching Hospitals NHS Foundation Trust, Whinney Heys Road, Blackpool FY3 8NR, UK

[8] Biocel UK Ltd., Hull HU10 6TS, UK

***Corresponding author:** Francis L Martin; Email: francis.martin2@nhs.net

Spectroscopy-based environmental metabolomics

ToC graphic

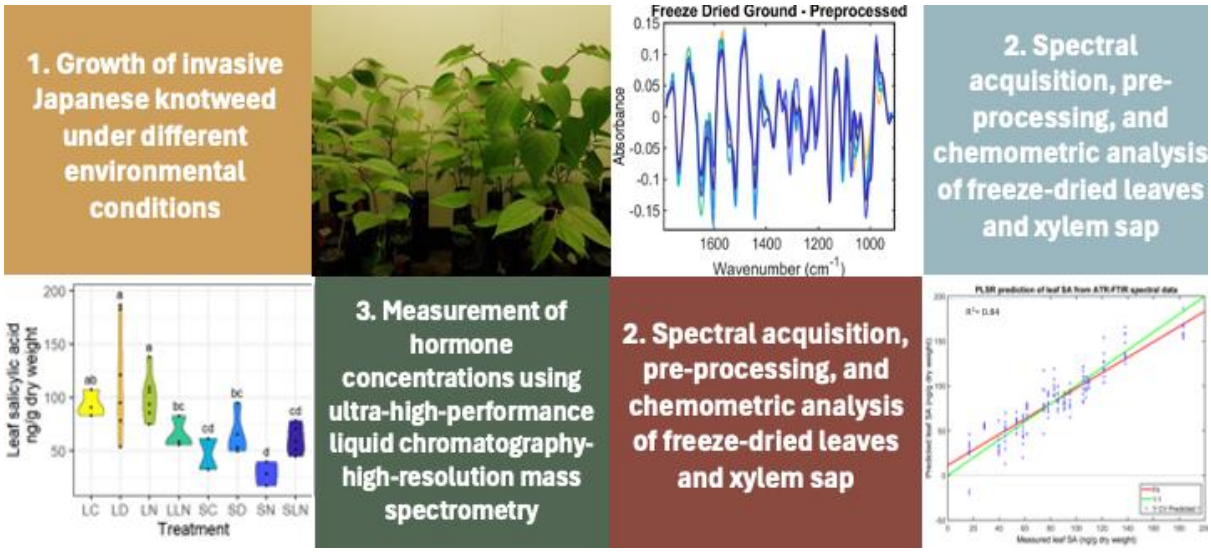

Analysis with ATR-FTIR spectroscopy combined with chemometrics methods facilitates determination of hormone concentrations in Japanese knotweed samples under different environmental conditions.

Abstract

Plant hormones are important in the control of physiological and developmental processes including seed germination, senescence, flowering, stomatal aperture, and ultimately the overall growth and yield of plants. Many currently available methods to quantify such growth regulators quickly and accurately require extensive sample purification using complex analytic techniques. Herein we used ultra-performance liquid chromatography-high-resolution mass spectrometry (UHPLC-HRMS) to create and validate the prediction of hormone concentrations made using attenuated total reflection Fourier-transform infrared (ATR-FTIR) spectral profiles of both freeze-dried ground leaf tissue and extracted xylem sap of Japanese knotweed (*Reynoutria japonica*) plants grown under different environmental conditions. In addition to these predictions made with partial least squares regression, further analysis of spectral data was performed using chemometric techniques, including principal component analysis, linear discriminant analysis, and support vector machines (SVM). Plants grown in different environments had sufficiently different biochemical profiles, including plant hormonal compounds, to allow successful differentiation by ATR-FTIR spectroscopy coupled with SVM. ATR-FTIR spectral biomarkers highlighted a range of biomolecules responsible for the differing spectral signatures between growth environments, such as triacylglycerol, proteins and amino acids, tannins, pectin, polysaccharides such as starch and cellulose, DNA and RNA. Using partial least squares regression, we show the potential for accurate prediction of plant hormone concentrations from ATR-FTIR spectral profiles, calibrated with hormonal data quantified by UHPLC-HRMS. The application of ATR-FTIR spectroscopy and chemometrics offers accurate prediction of hormone concentrations in plant samples, with advantages over existing approaches.

Introduction

As sessile organisms, plants rely on signalling molecules such as plant hormones to enable them to react appropriately to their environment; they contribute to a plastic adaptive response, regulating plant growth and stress tolerance [1], and plants grown under different environmental conditions show significant differences in hormone profiles [2,3]. Plant hormones include: ethylene, auxin, gibberellins (GAs), cytokinins (CKs), abscisic acid (ABA), salicylic acid (SA), strigolactones (SLs), brassinosteroids (BRs) and jasmonic acid (JA) [1,3]. Plant hormone identification is challenging due to their low concentrations, ranging stabilities and similar core structures, including isomers with the same MS fragmentation patterns (e.g. cis- and trans-zeatin, topolin isomers, brassinolide and 24-epibrassinolide [24-epiBL], and castasterone and 24-epicastasterone; Šimura *et al.*, 2018). Current methods for plant hormone analysis include: gas chromatography-mass spectrometry (GC-MS), capillary electrophoresis-mass spectroscopy (CE-MS) [5], enzyme-linked immune sorbent assay (ELISA) [6], ultra-performance liquid chromatography-mass spectrometry (UPLC-MS) [7], high performance liquid chromatography-mass spectrometry (HPLC-MS) [8] and liquid chromatography-ultraviolet detection (LC-UV) [9]. Liquid chromatography is a versatile method that allows the separation of compounds of a wide range of polarity, but these classical chromatographic techniques require destruction of the plant and lengthy sample preparation. More recently the research focus has shifted towards the development of non-destructive spectroscopic techniques for plant hormone detection, such as Raman spectroscopy [10,11] and desorption electrospray ionisation mass spectrometry imaging (DESI-MSI)[12].

Plant hormones control a range of complex physiological and developmental processes including seed germination, senescence, flowering, and stomatal control, and affect overall plant growth and crop yield [1]. Antagonistic hormonal crosstalk also regulates numerous

factors influencing the success of invasive alien species (IAS), for example, the trade-off between growth and defence [13], adaptive transgenerational plasticity [14], and the biosynthesis of allelopathic chemicals [15]. The importance of hormonal regulation in plant invasions has been demonstrated in the differential biomass allocation [16] and defence responses [17] of invasive and native plants, and in locally adaptive chromosomal inversion in invasive plants [18]. Additionally, many herbicides used for the control of IAS are plant hormone analogues or interfere with hormonal signalling and synthesis pathways [19]. IAS have significant negative socio-economic [20,21] and environmental [22] impacts and therefore it is critical to gain an increased understanding of the factors, including the role of plant hormones, that enable the invasiveness and superior growth performance of these species [23–26].

Japanese knotweed (*Reynoutria japonica*) is an IAS found across a broad geographic range, colonising diverse habitats including riparian wetlands, urban transport courses, and coastal areas [27,28]. It is very tolerant to abiotic stress, occupying extreme environments such as salt marshes [29] and metal-polluted soil [30,31]. Although its habitats are diverse, Japanese knotweed exhibits minimal genetic variation in Central Europe [27], Norway [32] and the USA [28], and exists as a female clone in the United Kingdom from a single introduction [33,34]. The ecological adaptability of Japanese knotweed as an invasive weed renders this species an ideal model for investigating the contribution of plant hormones to IAS invasiveness through a concatenated approach combining ultra-performance liquid chromatography-high resolution mass spectrometry (UHPLC-HRMS) and attenuated total reflection Fourier-transform infrared (ATR-FTIR) spectral data.

In this study we used UHPLC-HRMS to quantitatively measure the concentrations of a set of plant hormones at nanogram per millilitre concentrations: the active CKs *trans*-Zeatin (t-Z), *trans*-zeatin riboside (tZR) and isopentyl-adenine (iP), the active GAs gibberellin A1 (GA_1), gibberellin A4 (GA_4), gibberellin A3 (GA_3), the active auxin indole-3-acetic acid (IAA),

ABA, JA, SA, and the ethylene precursor 1-amino-cyclopropane-1-carboxylic acid (ACC); and compared these measured concentrations to those predicted from ATR-FTIR spectral profiles of both xylem sap and freeze-dried ground leaves. ATR-FTIR spectroscopy employs infrared (IR) light to alter the molecular vibrations of a sample, providing information on the compounds within. It is a rapid analytical technique well-suited to environmental monitoring with the advantages of a high degree of specificity and sensitivity, minimal sample preparation, and portable enough for use in the field. It can be used non-destructively on whole plant tissues, even *in planta* [35,36]. We used chemometric algorithms to allow further information to be gained from the absorbance profiles, such as molecular biomarkers associated with the plants' environments. Chemometric techniques used included principal component analysis (PCA), PCA in combination with linear discriminant analysis (LDA), support vector machines (SVMs), and partial least squares regression (PLSR) [37–39]. These highlighted a range of biomolecules responsible for the differing IR spectral signatures between growth environments, such as triacylglycerol, proteins and amino acids, tannins, pectin, polysaccharides such as starch and cellulose, deoxyribonucleic acid (DNA) and ribonucleic acid (RNA) [40]. PLSR comparison of the ATR-FTIR spectral data with the quantitative data from UHPLC– HRMS analysis allowed the effect of each hormone on the spectral absorbances to be viewed in isolation. Key wavenumbers within the mid-infrared fingerprint region were identified for prediction of plant hormone concentrations using ATR-FTIR spectroscopy; predominantly in the region of 1200-1000 cm^{-1} for leaf samples and 1600-1500 cm^{-1} for xylem sap samples. In leaf samples these often related to polysaccharide molecules, whilst in xylem compounds these key wavenumbers were more commonly associated with nucleic acids and bases. Predictive models were built to consider the concentrations of each hormone in turn and also to detect concentrations of several different hormones at once.

Materials and Methods

Plant growth

Japanese knotweed readily reproduces asexually from small fragments of an underground storage organ called a rhizome, which has a woody root-like structure. Rhizomes were collected from a site on the River Wyre, Google map reference 53.94977780, -2.75541670, with landowner permission from Lancashire County Council. Ninety fragments of rhizome (10-50 g, volume 2-58 cm^3) were planted in fertilized organic loam (John Innes No. 1, J. Arthur Bowers, UK) in cylindrical pots designed to tightly fit in a Scholander-type pressure chamber (Soil Moisture Equipment Corp., Santa Barbara, CA, USA) measuring 6.5 cm in diameter and 23 cm in length with a volume of 763.2 cm^3, and featured a stainless-steel mesh (0.7 mm aperture) at the base to assist drainage. Pots were placed in one of two climate-controlled cabinets (Microclima 1750, Snijders Scientific BV, Netherlands) at 80% humidity, 16 h of photoperiod, and 19/11°C day/night temperature where the treatments were applied and plants were grown for a total of fifty days before harvesting. The long photoperiod and temperature range were selected to simulate an average British Summer in the areas where Japanese knotweed usually colonises, using a comparison of temperature maps from the Met Office [41] and a distribution map of Japanese knotweed in the British Isles [42].

Treatments

Rhizome fragments were divided into eight treatment groups to give an even split of rhizome masses in each group. The treatments applied were: Light Control ‘LC’, Light Drought ‘LD’, Light Nitrogen ‘LN’, Light Low Nutrient ‘LLN’, Shade Control ‘SC’, Shade Drought ‘SD’, Shade Nitrogen ‘SN’ and Shade Low Nutrient ‘SLN’. Four groups were placed in each of two growth cabinets. In both cabinets, the light emitted from the two high-pressure sodium lamps (SON-T 400 W, Philips Lighting, Eindhoven, The Netherlands) was reduced using a LEE 209 filter (LEE Filters Worldwide, Andover, Hampshire, UK). In one cabinet, a matrix

of far-red LEDs (EPILEDS, 740-745 nm) distributed in five rows 30 cm apart was used to decrease the red: far-red ratio (R:FR) to simulate shading. Wavelengths emitted were measured using an UPRtek (Taiwan) PG100N light spectrometer. The resultant combined light conditions (see Table S1†) resulted in a 'light' treatment with a R:FR of 5.6 and a 'shade' treatment with a R:FR of 0.4 (see Figure S1† for the spectral profile). Plants were shuffled weekly within each cabinet to minimise positional effects from the LED matrix pattern. The R:FR of natural sunlight during the day is approximately 1.15 [43] and the R:FR of 0.4 in the shade treatment was chosen to replicate that found within vegetative canopies such as sugar beet, deciduous woodland, coniferous woodland and tropical rainforest [43]. In both cases, the photosynthetic photon flux density (PPFD) was between 124.7 and 189.8 $\mu mol \cdot m^{-2} \cdot s^{-1}$ which is typical of growth cabinet studies [44–47].

Plants were provided with water (75 mL/pot / 48 h), apart from LD and SD in which water was withheld for 7 days prior to harvest. Once a week, four groups (LC, LD, SC, SD) were watered with 75 mL Hoagland solution to provide both nitrogen and micronutrients, see Table S2† for details. LN and SN were fed with the commonly used agricultural dose of 50 $kg\ ha^{-1}\ year^{-1}$ [48]; this was scaled down for a pot diameter of 6.2 cm and applied across a split-dose at 21 and 23 days to prevent leaching. Groups LLN and SLN were provided only with water and received no additional nitrogen or micronutrients.

Harvest

Two leaves were excised from each plant for the analysis 4-8 h into the photoperiod in order to fall within a stable period of the plants' circadian rhythm. The youngest leaf from the top of plants was placed in liquid nitrogen, freeze-dried, and finely ground for hormone analysis by U-HPLC-HRMS, and the second leaf down was treated similarly for analysis by ATR-FTIR spectroscopy. Following this, the plant was de-topped and the whole pot inserted into a Scholander-type pressure chamber (Soil Moisture Equipment Corp., Santa Barbara, CA,

USA) with the stem protruding for xylem sap collection. The pressure was matched to the flow rate by increasing the pressure gradually above the balance pressure. For each trial pressure, the flow rate was calculated by weighing the sap collected for twenty seconds, until the flow rate matched that calculated by mass loss following the method previously described in [49]. This was necessary as it has been shown that ABA concentration are influenced by sap flow rate [49]. Sap was collected in Eppendorf vials, immediately frozen in liquid nitrogen and stored at −80°C for hormone determination, and ATR-FTIR spectral analysis.

Plant hormones

Plant hormones were quantified from frozen xylem sap and freeze-dried ground leaf material using UHPLC–HRMS as described previously with some modifications [50,51]. Freeze-dried ground leaf samples were prepared with several extraction steps and sonication before analysis, whilst only the filtration and centrifugation steps were necessary for the xylem sap samples. In the first extraction up to 250 mg of raw material was mixed with methanol (1.25 mL, 80%) and an internal-standards mix composed of deuterium labelled hormones ([$^2H_5$]tZ, [$_2H^5$]tZR, [$^2H_6$]iP, [$^2H_2$]GA_1, [$^2H_2$]GA_3, [$^2H_2$]GA_4, [$^2H_5$]IAA, [$^2H_6$]ABA, [$^2H_4$]SA, [$^2H_6$]JA, [$^2H_4$]ACC, Olchemim Ltd, Olomouc, Czech Republic) at a concentration of 5 μg mL^{-1} in 80% methanol. Samples were vortexed, incubated for 30 min at 4°C, and centrifuged (20000 g, 4°C, 15 min). Supernatants were passed through Chromafix C18 columns (MachereyNagel, Düren/Germany) previously pre-equilibrated with 80% methanol and filtrates were collected on ice. Extraction was repeated with 1.25 mL 80% methanol; second extracts were passed through the same columns. The combined extracts were collected and concentrated to complete dryness using the Integrated SpeedVac® Concentrator System AES1000 (Savant Instruments Inc., Holbrook/USA). The residues were resolved in 500 or 1000 μL 20% methanol, sonicated for 8 min using a ultrasonic bath, passed through 0.2-μm syringe filters (Chromafil PES-20/25) and placed in HPLC vials for analysis, and optionally

stored at –80°C. Phytohormone analyses were performed using a UHPLC–HRMS system consisting of a Thermo ACCELA pump (Thermo Scientific, Waltham/USA) coupled to a tempered HTC-PAL autosampler (CTC Analytics, Zwingen/Switzerland), and connected to a Thermo Exactive Spectrometer (Thermo Scientific) with a heated electrospray ionization (HESI) interface. Due to the high resolution of the Orbitrap, we recorded the total ion chromatogram of the samples and did not fragment the molecules. A typical chromatogram for SA is shown in Figure S2†. The analysis was performed in the negative mode $[M-H]^-$ (Table S3†), and the instrument settings included: sheath gas flow rate = 35 $ml \cdot min^{-1}$, auxiliary gas flow rate = 10 $ml \cdot min^{-1}$, spray voltage = 2.5 kV, capillary temperature = 275ºC, capillary voltage = -40 V, tube lens voltage = -110 V, skimmer voltage = -20 V. Mass spectra were obtained using the Xcalibur software version 2.2 (ThermoFisher Scientific, Waltham, MA, USA). For quantification of the plant hormones, calibration curves were constructed for each analysed component (1, 10, 50, and 100 $\mu g\ l^{-1}$) and corrected for 10 $\mu g\ l^{-1}$ deuterated internal standards. Recovery percentages ranged between 92 and 95%.

ATR-FTIR spectral acquisition

Freeze-dried ground leaves and xylem sap were analysed using a Tensor 27 FTIR spectrometer with a Helios ATR attachment (Bruker Optics Ltd, Coventry, UK). The sampling area, defined by the Internal Reflection Element (IRE), which was a diamond crystal, was 250 µm x 250 µm. Spectral resolution was 8 cm^{-1} with 2 times zero-filling, giving a data-spacing of 4 cm^{-1} over the range 4000 to 400 cm^{-1}; 32 co-additions and a mirror velocity of 2.2 kHz were used for optimum signal to noise ratio. To minimise bias, ten spectra were taken for each sample. Each sample was placed on a slide with the side to be analysed facing upwards, placed on a moving platform, and then raised to ensure a consistent contact with the diamond crystal. For xylem sap samples, 30 mL of xylem sap was placed on a tin foil-covered slide and allowed to dry before analysis. For freeze-dried ground leaves a

small amount of powder was transferred to each slide using a spatula. A total of 410 spectra were taken for xylem sap and 330 spectra were taken of freeze-dried ground leaf tissue.

Data analysis

The 'mergetool' function of an in-house developed MATLAB (Mathworks, Natick, USA) toolbox called IRootLab [52,53] was used to convert all spectral information from OPUS format to suitable files (.txt). Following this, it was necessary to pre-process the acquired spectra to improve the signal-to-noise ratio. Pre-processing corrects problems associated with random or systematic artefacts during spectral acquisition and is an essential step of all spectroscopic experiments. Pre-processing and computational analysis of the data were performed using a combination of IRootLab toolbox [52,53] and the PLS Toolbox version 7.9.3 (Eigenvector Research, Inc., Manson, USA). The pre-processing steps applied to all spectra were firstly the selection of the spectral biochemical fingerprint region (1800-900 cm^{-1}), followed by Savitzky–Golay (SG) second differentiation (nine smoothing points) and vector normalisation. All data were mean centred before multivariate analysis, where multiple dependant variables are observed simultaneously to determine a pattern.

Four machine learning techniques were used in this study: an unsupervised dimensionality reduction method, two supervised classification methods and one regression. The unsupervised method principal component analysis (PCA) simplifies complex multivariate datasets, allowing them to be presented intuitively and enabling pattern recognition. Two supervised chemometric techniques, principal component analysis with linear discriminant analysis (PCA-LDA) and support vector machines (SVM), were used for the classification of groups [37,38]. PCA-LDA was also used for the determination of biomarkers. Most importantly, hormone prediction was achieved using a multivariate analysis technique called PLSR of both ATR-FTIR spectral data and real hormone data as measured by UHPLC-HRMS [39]. Regression by PLSR was performed with the same pre-processed data without vector

normalization. Multivariate analysis techniques allow multiple variables to be compared at the same time enabling spectral absorbance values across a range of wavelengths to be simultaneously correlated against concentrations of multiple hormones for numerous samples. Observing all these data at once allows patterns to be seen and enables predictions to be made. To form these models, an X-block of ATR-FTIR spectral absorbance data for plants was analysed by PLSR against a Y-block of hormone concentrations for the corresponding plants as measured using UHPLC-HRMS. Environments were analysed separately, allowing a model to be created for each of them. The PLSR models were validated by Monte-Carlo cross-validation, where 20% of the spectral data is randomly left-out for validation and the remaining 80% is used for training the model in an exhaustive process to ensure model consistency and validation reliability. In this study, Monte-Carlo cross-validation was performed with 1000 iteration cycles. The number of principal components for PCA-LDA was set at 10, to ensure more than 95% of the original data explained variance was contemplated. PLSR models were built varying the number of latent variables according to the smallest root-mean-squared error (RMSE) of cross-validation. Once made, these models can be applied to new ATR-FTIR spectral data in the absence of UHPLC-HRMS data to predict plant hormone concentrations.

Results

ATR-FTIR spectral analysis classifies plants from different environments via spectral differences

The sensitive nature of IR spectroscopy allowed indications of plant responses to environment to be observed visually as differences between spectral profiles. The pre-processed fingerprint spectra exhibit distinguishable differences between spectra of different treatment groups, for both xylem sap and freeze-dried ground samples, at 950, 1050, 1150, 1250, 1325, 1400, 1525, 1575 and 1610 cm^{-1} (Figure S3b†) and 950, 1050, 1275, 1400, 1525

and 1610 cm^{-1} (Figure S3d†), respectively. Three chemometric techniques (PCA, PCA-LDA and SVM) were used to extract further information from the spectral absorbance profiles of xylem sap (Figures 1a-d) and freeze-dried ground leaves (Figures 2a-d). The unsupervised technique, PCA, showed poor separation between treatment groups in xylem sap samples (Figure 1a). However, addition of the supervised classifier LDA created biologically meaningful separation along the linear discriminant 1 (LD1) axis. Xylem sap samples in the low nutrient categories (LLN and SLN) fall to the right of the other samples with the same lighting regine (LC, LD, LN and SC, SD and SN respectively) along the LD1 axis (Figure 1b). In leaf samples, the separation along the LD1 axis relates to light regime (Figure 2b), with 'light' to the left and 'shade' to the right. For the xylem sap samples, the left-hand side of the PCA-LDA scatter graph contains both control and drought plant samples (LC and LD) which were watered with Hoagland solution, the central portion contains clusters of nitrogen fed and low nutrient shaded plants (SN and SLN), and the right-hand side contains the light samples of the nitrogen and low nutrient categories (LN and LLN). The pattern observed in Figure 2a is distinctive due to the homogenisation introduced by the grinding process; PCA of freeze-dried ground leaves separated spectra from individual samples into clusters. PCA-LDA of freeze-dried leaf samples (Figure 2b) resulted in a separation along the axis LD1; LD to the left, LC, LN and LLN in the central portion, and all shaded groups to the right (SC, SD, SN and SLN). The stronger chemometric technique, SVM, achieved the best classification results for both sample types. Analysis of spectra from xylem sap samples using SVM achieved 99.0% accuracy, 98.2% sensitivity, and 99.8% specificity (Figures 1c-d). However, application of SVM to spectra of freeze-dried ground leaves attained even better separation with 99.8% accuracy, 99.6% sensitivity and 100.0% specificity (Figures 2c-d). For SVM model parameters, cost, gamma and number of support vectors, see Table S4†.

Spectroscopy-based environmental metabolomics

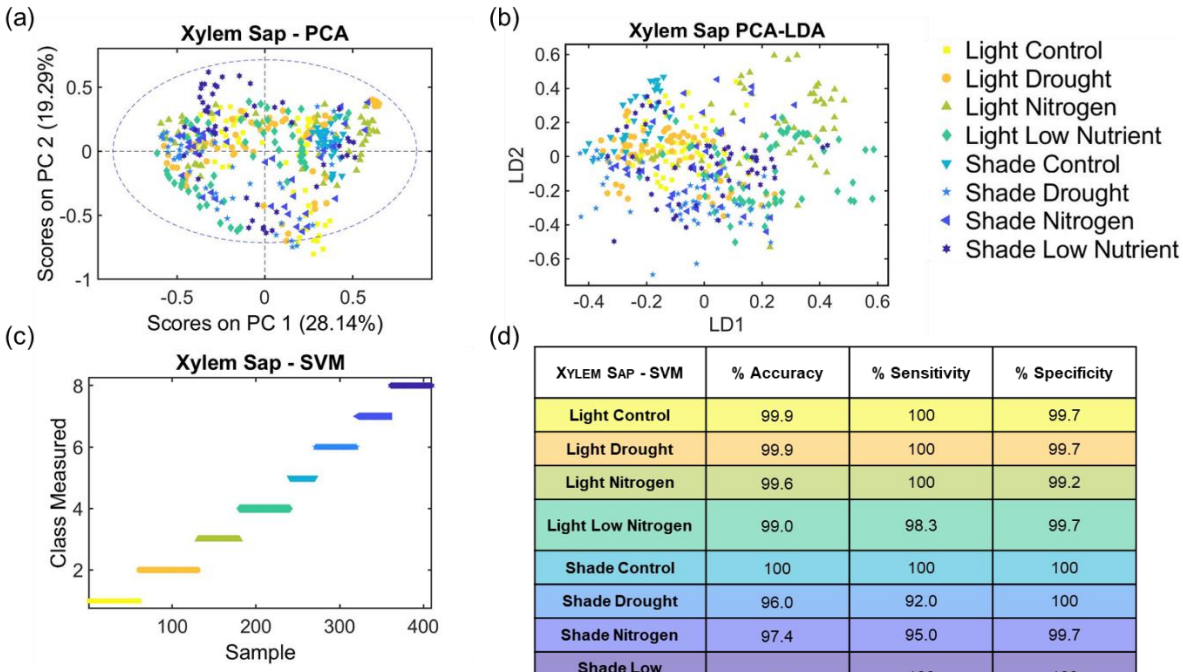

Xylem Sap - SVM	% Accuracy	% Sensitivity	% Specificity
Light Control	99.9	100	99.7
Light Drought	99.9	100	99.7
Light Nitrogen	99.6	100	99.2
Light Low Nitrogen	99.0	98.3	99.7
Shade Control	100	100	100
Shade Drought	96.0	92.0	100
Shade Nitrogen	97.4	95.0	99.7
Shade Low Nitrogen	100	100	100

Figure 1: (a) PCA scores plot showing poor separation between classes, **(b)** PCA-LDA scatter plot showing some separation by nutrient levels, **(c)** SVM sample/measured plot showing correct classification (Y-axis) of spectra from samples of different treatment categories (X-axis) and **(d)** SVM results for ATR-FTIR spectra taken of xylem sap samples showing excellent classification, grouped by treatments; Light Control (LC), Light Drought (LD), Light Nitrogen (LN), Light Low Nitrogen (LLN), Shade Control (SC), Shade Drought (SD), Shade Nitrogen (SN) and Shade Low Nitrogen (SLN).

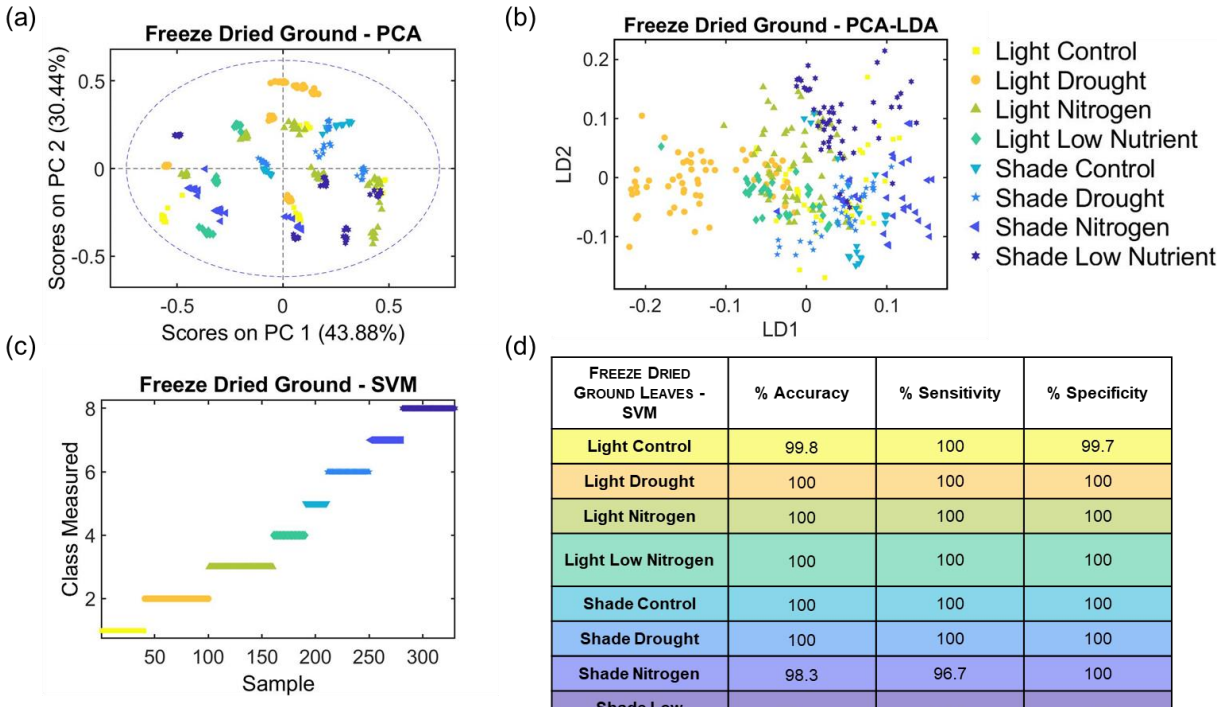

Freeze Dried Ground Leaves - SVM	% Accuracy	% Sensitivity	% Specificity
Light Control	99.8	100	99.7
Light Drought	100	100	100
Light Nitrogen	100	100	100
Light Low Nitrogen	100	100	100
Shade Control	100	100	100
Shade Drought	100	100	100
Shade Nitrogen	98.3	96.7	100
Shade Low Nitrogen	100	100	100

Figure 2: (a) PCA scores plot in which each cluster is formed from separate samples due to the homogenisation introduced by the grinding process, **(b)** PCA-LDA scatter plot showing some separation by light levels, **(c)** SVM sample/measured plot showing correct classification (Y-axis) of spectra from samples of different treatment categories (X-axis) and **(d)** SVM results for ATR-FTIR spectra taken of freeze-dried ground leaves samples showing excellent classification, grouped by treatments; Light Control (LC), Light Drought (LD), Light Nitrogen (LN), Light Low Nitrogen (LLN), Shade Control (SC), Shade Drought (SD), Shade Nitrogen (SN) and Shade Low Nitrogen (SLN).

ATR-FTIR spectral analysis identifies biomolecular differences between treatments

ATR-FTIR spectroscopy can detect changes in concentration or molecular structure of compounds. Significant biomolecular differences can be deciphered by examination of the key wavenumbers, which differentiate spectral profiles of different treatment groups from one another. These wavenumbers are called loadings (Figure S4†) and their tentative molecular assignments have been found through examination of the literature for both xylem sap and leaf sample types for biomarker information and references (see Table S5†). The peaks which differentiate treatment groups in xylem sap samples were related to a range of biomolecules such as triacylglycerol, proteins, glutamate, cellulose, tannins, starch, and RNA [54–62]. For freeze-dried ground leaves, the differences were found in much the same compounds: triacylglycerol, proteins and amino acids, pectin, polysaccharides such as starch and cellulose, and DNA [55,56,59,63–65].

UHPLC– HRMS hormone analysis indicates that hormone concentrations are impacted by applied treatments

Plants respond to their environment via signalling molecules such as hormones, to enable a plastic response. This is reflected in the concentrations of plant hormones measured by UHPLC-HRMS (ACC, tZ, iP, SA, ABA, JA, GA_1, GA_4, GA_3, tZR, and IAA) which were different between plants belonging to different treatment groups (see Figure 3a and c; Figures S5† and S6†). Figure 3a shows separation of LD and SD plants along PC1 based on xylem sap hormone concentrations accounting for 65.07% of the variance. This is primarily due to

increased ABA and tZ (see Figure 3b, PC1 loadings in blue). The separation along PC2 for xylem sap samples is due to the antagonistic relationship between JA and ABA (Figure 3b, PC2 loadings in green), which is variable within treatment categories (Figure 3a). Figure 3c also shows a separation along PC1 of droughted samples based on the hormone concentrations of freeze-dried ground leaves, accounting for 46.32% of the sample variance. High leaf ABA and low leaf ACC, JA and tZ concentrations were primary responsible for separation along axis PC1 (Figure 3d, PC1 loadings in blue). The PC2 axis of Figure 3c shows some separation by lighting treatment, however this separation was of lesser importance and only explained 38.23% of the variance. The green line in Figure 3d indicates that ABA, JA, tZ, and SA were all higher in LC and LD samples to create this separation along axis PC2, whilst ACC was lower. JA concentrations in plants with a low red: far-red ratio were lower.

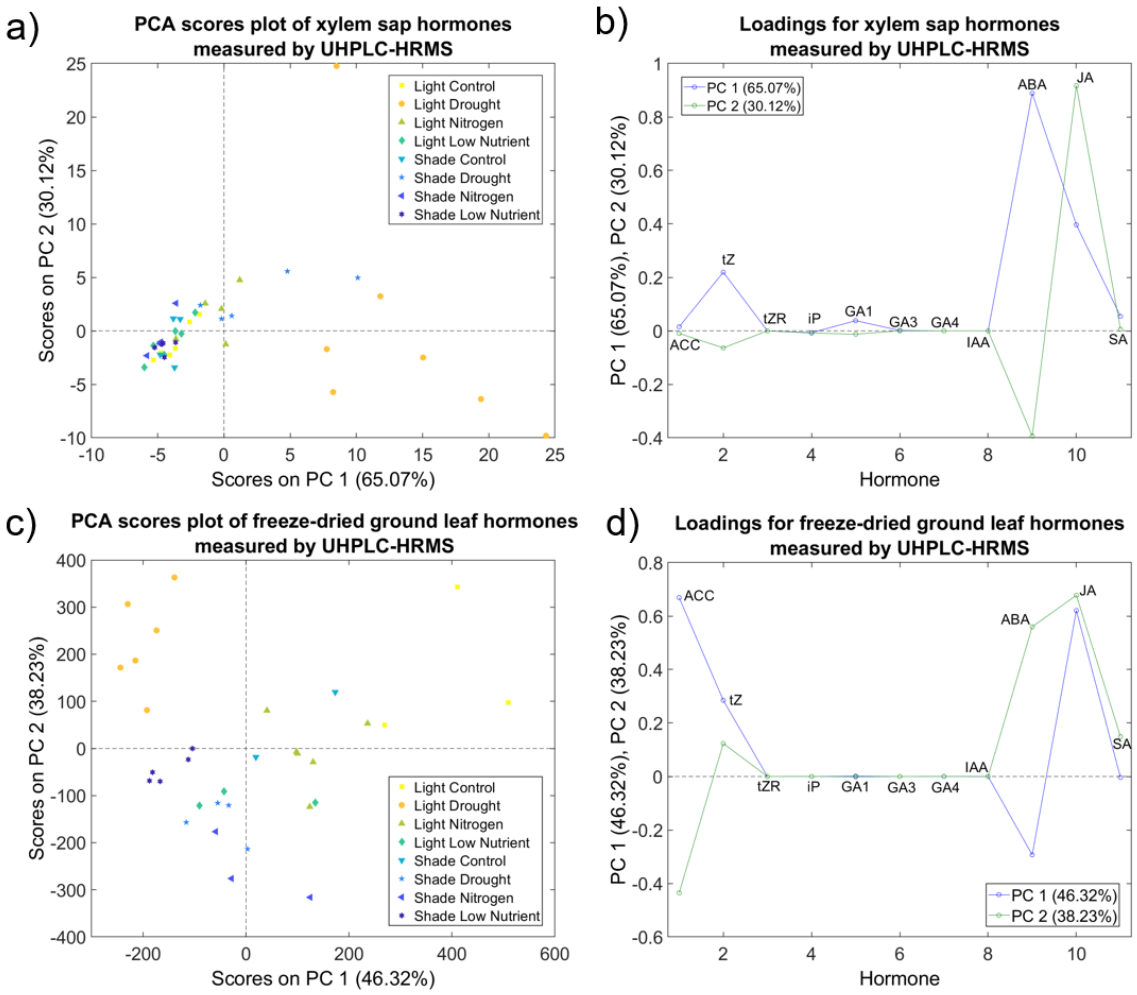

Figure 3: UHPLC-HRMS measurements of plant hormone concentrations analysed by PCA: a) xylem sap PCA scores showing separation of droughted plants along the PC1 axis, b) xylem sap loadings highlighting the importance of ABA in droughted samples, c) freeze-dried ground leaf scores showing separation by drought along PC1 and red: far red ratio along PC2, d) freeze-dried ground leaf loadings indicating that droughted plants exhibited high ABA and low ACC, JA and tZ concentrations whilst plants with a high red: far-red ratio had high ABA, JA, tZ, and SA but low ACC concentrations.

In xylem sap samples (Figure S5†), ABA concentration was highest in the drought categories; LD and SD, at ~17 and ~7 ng·ml^{-1} of sap ABA respectively, whilst the other categories ranged between ~1 and 3 ng·ml^{-1} sap. Leaf ABA concentrations (Figure S6†) were approximately quadruple in LD than those of the other categories. Shade plants had notably lower xylem SA concentrations, in the range of 0.7-1.1 ng·ml^{-1} sap compared with 1.6-4.5 ng·ml^{-1} sap for 'light' plants. Leaf tZ was 4.5-fold higher in LC plants than in those of SLN.

Leaf JA concentration was significantly higher in the light control group LC (~710 $ng \cdot g^{-1}$ dry weight) compared to all other groups (ranging 170-420 $ng \cdot g^{-1}$ dry weight), except the shade control group SC (~460 $ng \cdot g^{-1}$ dry weight). LC had the highest iP concentrations at 0.25 $ng \cdot g^{-1}$ dry weight, significantly higher compared to groups LD, LN, SD, SN (ranging 0.03-0.6 $ng \cdot g^{-1}$ dry weight), with the other groups falling in between.

Combined ATR-FTIR UHPLC-HRMS analysis identifies key spectral wavenumber for hormone prediction via ATR-FTIR spectroscopy

Whilst the plant hormone concentrations quantified by using UHPLC-HRMS served to confirm that the applied treatments were effective at inducing a phenotypic response, importantly the UHPLC-HRMS data enabled the generation of predictive models for hormone concentrations using ATR-FTIR spectral data by means of a multivariate analysis technique called partial least squares regression. PLSR allows simultaneous comparison of multivariate datasets, in this case, the spectral absorbance values for either freeze-dried ground leaf tissue or from xylem sap compared with the plant hormone values obtained by HPLC-HRMS. Using PLSR, the extracted plant hormone concentrations measured by UHPLC-HRMS were accurately predicted from ATR-FTIR spectral profiles of the same sample material.

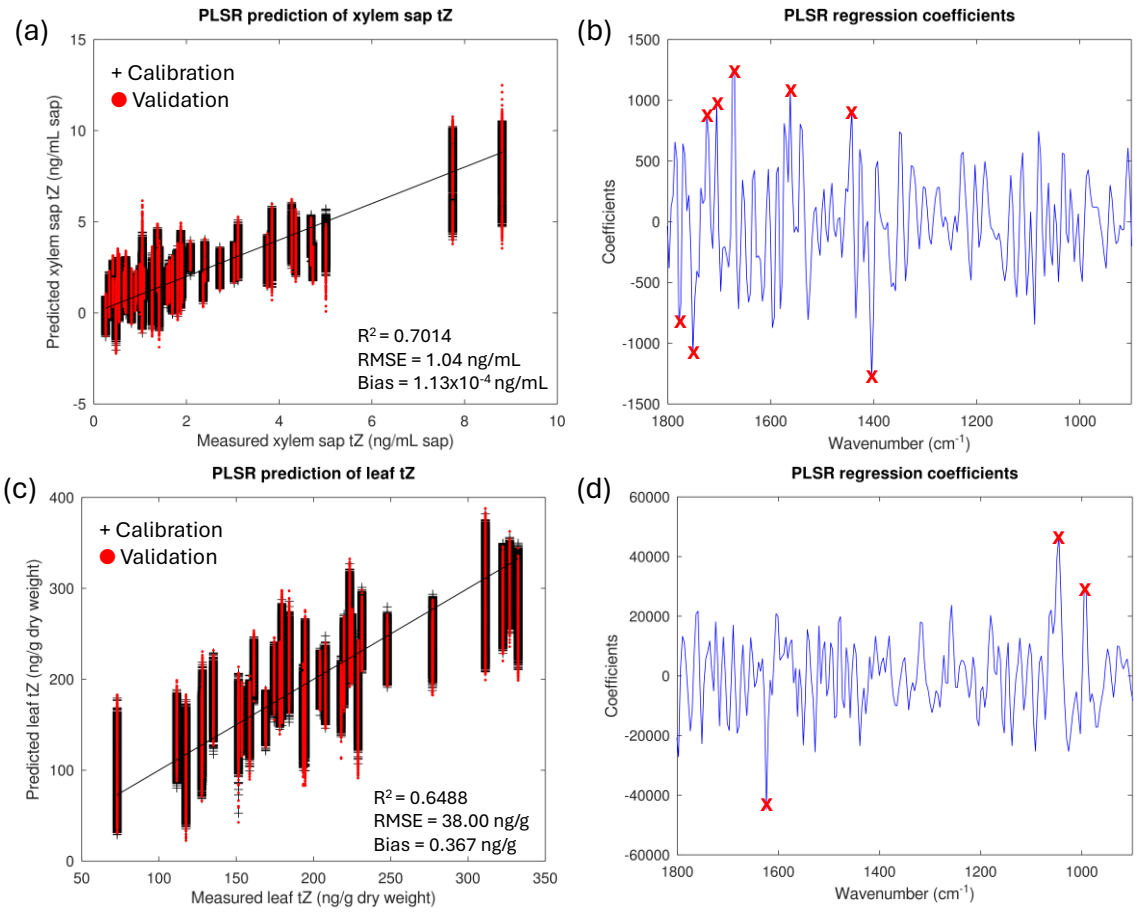

Figure 4: PLS regression and regression coefficients of *trans*-Zeatin concentrations as measured using UHPLC-HRMS against predicted values using ATR-FTIR spectra of a) xylem sap (ng mL^{-1}), and c) freeze-dried ground leaves (in ng·g^{-1} dry weight) grown under all treatment conditions. In panels a) and c), the black line shows the ideal prediction gradient of one, which would be 100% accurate. The black and red scatters points represent the calibration and validation samples during the Monte-Carlo cross-validation with 1000 iterations. The R^2, root mean square error (RMSE) and bias are reported for the validation samples of xylem sap (a) and freeze-dried ground leaves (c). These models were created using spectral data from all treatment categories for individual hormones. The model in panels a) and c) were constructed using 10 latent variables. Panels b) and d) show the regression coefficients which indicates some of the most important wavenumbers (marked with a red X) involved in making this prediction for xylem sap and freeze-dried leaves, respectively.

The graphs in Figure 4 show the PLS regressions and regression coefficients of tZ hormone concentrations as measured using UHPLC-HRMS against predicted concentrations using ATR-FTIR spectra of either xylem sap or freeze-dried ground leaves from all treatment categories as an example of the predictive models generated using this approach (see Figure S7† and S9† for of the predictive models for the other hormones). For the regressions in

Figure 4a and Figure 4c, the black lines show the ideal prediction gradient of one, which would be 100% accurate. Leaf samples achieved a more accurate prediction of R^2s= 0.649 ($[^2H_5]$tZ) to 0.848 ($[^2H_6]$ABA) compared with 0.529 ($[^2H_4]$SA) to 0.820 ($[^2H_2]GA_1$) for xylem sap samples (see Figures S7 and S9†). The PLSR models in Figures 4, S7† and S9† use hormonal data measured by UHPLC-HRMS to train them on the correlation between different hormone concentrations and the corresponding differences in ATR-FTIR spectral profiles. For each hormone, and each sample type, different spectral wavenumbers are important in making this prediction. These key wavenumbers can be identified by the PLS regression coefficients, which are presented in Figures S8† and S10† for each hormone and sample type. The regression coefficients with higher weights (either positive or negative) represent key wavenumbers, since they are more correlated with the increase or decrease of hormone concentration. These were detected mostly in the regions around 1000, 1400-1600 and 1750 cm^{-1} (ABA); 1000-1100 and 1600-1650 cm^{-1} (tZ); 1000-1100, 1300 and 1500-1700 cm^{-1} (SA); 1000-1100 cm^{-1} (JA); 1000-1000 cm^{-1} and 1600-1800 cm^{-1} (ACC) for prediction of leaf hormone concentration; and, around 1000-1100 and 1500-1800 cm^{-1} (ABA); 1400, 1600-1800 cm^{-1} (tZ); 1300-1450 and 1700-1800 cm^{-1} (SA); 1100, 1400 and 1600-1700 cm^{-1} (JA); 1000-1200 and 1700-1800 cm^{-1} (GA1) for xylem sap hormone concentration.

Combined ATR-FTIR UHPLC-HRMS analysis gives a high correlation between predicted and measured hormone concentrations

Analysis of data from each treatment separately allowed the generation of treatment-specific models. Table 1 shows the validation R^2 and root mean square error (RMSE) values for predicted against measured hormone concentrations from xylem sap, with each row being a separate treatment. The R^2 values for the predictions from xylem sap samples ranged between 0.831 (iP for light control) to 0.940 (GA1 for light nitrogen), and the RMSE values ranged from 0.0004 ng/mL sap (GA4 for light control) to 2.655 ng/mL sap (ABA for light drought)

(Table 1). Likewise, the validation R^2 and RMSE values for predicted against measured hormone concentrations from freeze-dried ground leaves are shown in Table 2. The R^2 values varied between 0.811 (ABA for shade control) to 0.957 (JA for shade low nutrient), and the RMSE values ranged from 1.692 ng/g dry weight (ABA for shade nitrogen) to 60.244 ng/g dry weight (JA for light control) (Table 2). In xylem sap samples, light nitrogen achieved the best correlations for hormones iP (R^2 = 0.934), GA1 (R^2 = 0.940) and GA3 (R^2 = 0.889); shade low nutrient for hormones ABA (R^2 = 0.933) and JA (R^2 = 0.935); light drought for hormone tZ (R^2 = 0.904); shade nitrogen for hormone IAA (R^2 = 0.892); shade drought for hormone SA (R^2 = 0.926); and, light control for GA1 (R^2 = 0.924), being the only treatment associated with GA1 hormone. In freeze-dried ground leaves, the best correlations were: shade low nutrient for hormones ACC (R^2 = 0.948) and JA (R^2 = 0.957); shade drought for hormone tZ (R^2 = 0.932); shade nitrogen for hormone ABA (R^2 = 0.950); and, light drought for hormone SA (R^2 = 0.952). These models therefore provide a valuable resource that can be saved and applied to new spectral data obtained from plants grown under similar conditions thereby allowing the hormone concentrations to be accurately predicted without the requirement for exhaustive UHPLC– HRMS analysis.

Table 1: R^2 and root-mean square error (RMSE) values for predicted against measured hormone concentrations from partial least squares regression for xylem sap ATR-FTIR spectral data against UHPLC-HRMS-measured hormone concentrations. Hormones with zero values for multiple plants were excluded from the model and are designated as NA. The treatments with best R^2 results for each hormone are shaded in gray. The number of latent variables to construct the PLSR regression models are shown in Table S6†.

Xylem Sap RMSE (ng/mL sap)	**tz**	**iP**	**GA1**	**GA3**	**GA4**	**IAA**	**ABA**	**JA**	**SA**
Light Control	0.294	0.347	0.042	NA	0.0004	0.006	0.190	0.589	0.323
Light Drought	0.741	0.008	0.116	0.034	NA	NA	2.655	2.570	0.482
Light Nitrogen	0.384	0.001	0.001	0.010	NA	NA	0.326	0.817	0.737
Light Low Nutrient	0.205	0.002	0.001	NA	NA	NA	0.189	0.708	0.222
Shade Control	0.031	0.060	0.014	0.006	NA	NA	0.295	0.671	0.138
Shade Drought	0.318	NA	0.044	0.009	NA	NA	0.939	0.870	0.043
Shade Nitrogen	0.051	0.002	0.008	0.001	NA	0.007	0.084	0.534	0.086
Shade Low Nutrient	0.088	NA	0.020	NA	NA	NA	0.112	0.143	0.086
Xylem Sap R^2	**tz**	**iP**	**GA1**	**GA3**	**GA4**	**IAA**	**ABA**	**JA**	**SA**

Light Control	0.876	0.831	0.881	NA	0.924	0.865	0.856	0.905	0.888
Light Drought	0.904	0.887	0.914	0.862	NA	NA	0.894	0.897	0.863
Light Nitrogen	0.891	0.934	0.940	0.889	NA	NA	0.902	0.886	0.884
Light Low Nutrient	0.872	0.881	0.888	NA	NA	NA	0.865	0.875	0.907
Shade Control	0.896	0.891	0.918	0.880	NA	NA	0.881	0.884	0.902
Shade Drought	0.886	NA	0.889	0.884	NA	NA	0.914	0.932	0.926
Shade Nitrogen	0.900	0.902	0.876	0.884	NA	0.892	0.862	0.928	0.867
Shade Low Nutrient	0.903	NA	0.910	NA	NA	NA	0.933	0.935	0.882

Table 2: R^2 and root-mean square error (RMSE) values for predicted against measured hormone concentrations from partial least squares regression for freeze-dried ground (FDG) leaves ATR-FTIR spectral data against UHPLC-HRMS-measured hormone concentrations. The treatments with best R^2 results for each hormone are shaded in gray. The number of latent variables to construct the PLSR regression models are shown in Table S6†.

FDG Leaves RMSE (ng/g dry weight)	**ACC**	**tz**	**ABA**	**JA**	**SA**
Light Control	52.465	18.024	6.864	60.244	11.221
Light Drought	10.090	12.066	24.915	19.672	11.330
Light Nitrogen	27.340	11.509	6.686	19.963	5.345
Light Low Nutrient	25.134	7.362	6.981	11.333	2.982
Shade Control	7.344	17.257	6.601	29.534	4.753
Shade Drought	14.084	9.137	5.466	9.035	4.121
Shade Nitrogen	32.843	9.663	1.692	5.879	2.691
Shade Low Nutrient	3.852	10.446	2.218	7.824	3.650
FDG Leaves R^2	**ACC**	**tz**	**ABA**	**JA**	**SA**
Light Control	0.904	0.873	0.916	0.901	0.900
Light Drought	0.883	0.909	0.914	0.894	0.952
Light Nitrogen	0.909	0.902	0.902	0.925	0.926
Light Low Nutrient	0.921	0.906	0.887	0.953	0.909
Shade Control	0.840	0.829	0.811	0.855	0.860
Shade Drought	0.876	0.932	0.925	0.917	0.942
Shade Nitrogen	0.892	0.863	0.950	0.954	0.907
Shade Low Nutrient	0.948	0.900	0.933	0.957	0.918

Discussion

Differences in ATR-FTIR spectral profiles are highlighted through chemometrics

Japanese knotweed and other invasive species with low genetic variation exhibit a plastic response to their environment which is thought to contribute to their invasion success [23,66,67]. This phenotypic plasticity was reflected in the present study in the differences found between spectral profiles between treatment groups. This is consistent with the results of studies in

which ATR-FTIR spectroscopy has been successful in differentiating plants' nutrient status and plants from different growing environments [68–71]. The environmentally induced phenotypic changes were successfully captured by the ATR-FTIR spectral profiles, which were visibly different (see Figure S3†). Figures 1 and 2 demonstrate the power of chemometrics to emphasise these differences. SVM was the most successful technique applied and had marginally more success in the freeze-dried ground samples, likely due to the homogenisation of the samples during the grinding process leading to more predictable results. The higher separation of spectra from freeze-dried ground leaves (Figure 2a) by PCA than that of xylem sap spectra (Figure 1a) could be due to the averaging effect of leaf growth over time, adapted to each environment, compared with the nature of the xylem-sap samples which capture a moment in time and could be influenced by compounds related to development stage. Leaf samples reflect a balance between synthesis and metabolism and the import and export of compounds, whilst xylem sap samples reflect instantaneous transport. The sample type more closely correlated to the physiological response therefore depends on the analyte of interest.

Hormone profiles reflect plant response to environment

It is well established that plant stresses such as drought, nutrient deficiency and shading can have a marked impact on the concentrations of plant hormones [1,3]. Our measurement of plant hormones with the highly specific technique, UHPLC-HRMS, from xylem sap (Figure S5†) and leaves (Figure S6†) are consistent with this. The applied treatments (LC, LD, LN, LLN, SC, SD, SN and SLN) were sufficiently different to alter the hormone profiles in the plants, reflecting adaptations to each environment [72]. Importantly, such a range of hormone concentrations was essential prerequisite to create good datasets for regression analysis.

Hormonal biomarkers identified for mid-infrared spectroscopy

The process from chemometric biomarker identification to physical biomolecular extraction is a developing area of spectroscopy with ongoing research to optimise concentration quantification [73,74], molecular definition databases [59] and new applications [35,36,69,71,75]. It was therefore crucial that predictions for expected hormone profiles from spectroscopic data were made and verified against actual hormone concentrations quantified by mass spectrometry. PLSR comparison of the ATR-FTIR spectral data with the quantitative data from UHPLC–HRMS analysis allowed the effect of each hormone on the spectral absorbances to be viewed in isolation. The regression coefficients in Figure 4 aid to point to key spectral wavenumbers used in the model creation for tZ concentration prediction. These suggest that the most important regions for prediction of hormone concentrations using ATR-FTIR spectral profiles are around 1000-1100 and 1620 cm^{-1} for leaf samples; and, around 1400-1450, 1580 and 1650-1780 cm^{-1} for xylem sap samples.

Three tentative wavenumbers used to predict ABA hormone concentration in leaf samples, 1612, 1566 and 1323 cm^{-1} are often attributed to the Amide I [57], Amide II bands of proteins (N-H bending and C-N stretching) [63] and Amide III, respectively [62]. As ABA does not contain nitrogen within its structure this suggests that ABA-associated biochemical changes in other compounds within the leaves could be acting as proxy indicators for the estimation of ABA concentration. Similarly, 1516 cm^{-1} is also tentatively associated with Amide II vibrations of proteins and appears to be one of the key indicators for prediction of tZ, JA and SA concentrations in leaves [59]. The Amide III-associated [62] peak identified at 1323 cm^{-1} was also used to tentatively predict leaf SA concentrations. Two phosphorus-associated peaks that were suggested were used for the prediction of leaf ABA concentration: 1211 cm^{-1}, which is tentatively associated with PO^{2-} asymmetric stretching (Phosphate I); and, 1065 cm^{-1} linked to C–O stretching of the phosphodiester and the ribose of bases [59]. As ABA also does not

contain phosphorus, this supports the hypothesis that compounds other than ABA contribute to a 'spectral signature' for ABA-associated biochemical changes and suggest the use of associated compounds as a proxy, would be useful to gain an overall picture of plant health in agricultural and ecological settings.

In contrast, leaf SA concentrations were predicted using two peaks which could be tentatively associated with the structure of SA: 1582 cm^{-1}, which is linked to the ring C–C stretch of phenyl; and, 1339 cm^{-1} is associated with in-plane C–O stretching vibration combined with the ring stretch of phenyl [59]. As a consequence, 1339 cm^{-1} was used for prediction of leaf ABA and SA, as well as xylem ABA, tZ and SA. Other tentative wavenumbers relating to Amides I and II (1663, 1547, 1570, 1555 cm^{-1}) also appeared important for the prediction of hormone concentrations [55,56,59,76].

When plants are under stress, signalling cascades including hormones and reactive oxygen species (ROS) induce biochemical changes [77]. As an important regulator in response to drought-induced stress, ABA induces ROS accumulation to facilitate stomatal closure [78], whilst SA, which is part of the innate immune response [79], ameliorates oxidative damage through regulation of redox signalling and the antioxidant defence system [80]. To prevent oxidative damage, excess ROS may be absorbed and quenched by phenolic compounds, which have antioxidant properties [81]. This coordinated biochemical response perhaps explains why the possible biomarker at 1512 cm^{-1}, which is tentatively associated with ν(C-C) aromatic (conjugated with C=C phenolic compounds [82] appears to allow the prediction of xylem sap ABA and SA concentrations. Another peak 1177 cm^{-1}, could be associated with the C–O stretch vibration of tannins [61], and is possibly a predictor of xylem JA concentrations.

Polysaccharides are another class of compounds commonly used for the prediction of hormone concentrations, particularly within leaf samples. The peak at 1038 cm^{-1} is tentatively associated with the polysaccharide galactan [83]; this appears to be important in the prediction of leaf SA concentrations. Leaf tZ and leaf JA concentrations appear to be predicted using a peak at 1130 cm^{-1}, which has previously been tentatively attributed to the stretching vibrations [ν(CO)] of the COC glycosidic linkage of polysaccharides [84]. Pectin is potentially associated with a peak at 1443 cm^{-1} [64]; this was hypothesised as useful in the prediction of leaf tZ, SA, JA and ACC concentrations. In addition, a possible peak at 972 cm^{-1} (specifically from the OCH_3 group of polysaccharides such as pectin) [59] has potential to be used in the prediction of leaf ABA, tZ, JA and ACC . This association with leaf JA could be linked to jasmonate-mediated accumulation of leaf-soluble sugars in response to far-red light [85]. A potential peak at 1636 cm^{-1} can be tentatively linked to C=O stretching of carbonyl group, typical of saccharide absorption [59]; this appears to be important in prediction of xylem JA and leaf SA concentrations. Leaf ABA levels appeared to be predicted using a peak at 1049 cm^{-1}, which is associated with cellulose [58]. A potential peak biomarker at 1732 cm^{-1} has been associated with both hemicellulose [83]; this appeared to be a predictor of leaf ABA concentrations. As a key hormone in the drought-induced response, it is perhaps unsurprising that ABA might be estimated using hemicellulose because the leaves of drought-treated plants are known to exhibit a higher content of hemicellulosic polysaccharides [86]. A potential peak biomarker at 1732 cm^{-1} has also been associated with lipid fatty acid esters [83], which is the more probable molecular assignment in its use for estimation of xylem JA concentrations because the fatty acid, linolenic acid, is an important precursor of JA synthesis [87]. Whilst an isolated and controlled peak assignment that could be unambiguously correlated with endpoint effect would be the ideal, in the complex cellular environment this is unlikely to be attainable. In this complex scenario, there will inevitably be a large number of differing peaks

with some more obvious than others. However, we would argue that these shed new insights into mechanism and have the potential to be further investigated.

Whilst leaf hormone concentrations appear to be strongly associated with sugar compounds, in xylem sap samples nucleic acids and bases generally appear to be more relevant indicators of hormone concentration. ABA, tZ and SA concentrations in xylem sap appear to be predicted using a possible peak at 1690 cm^{-1}, which is associated with nucleic acids due to the base carbonyl (C=O) stretching and ring breathing mode [59]. Similar to 1065 cm^{-1}, the peak at 991 cm^{-1} is also associated with C–O stretching of the phosphodiester and the ribose of bases [59]. This peak appeared to be important in xylem sap samples for the prediction of ABA, tZ, SA, and GA1 concentrations. A possible peak at 1713 cm^{-1}, associated with the C=O of the base thymine [59], was identified as important in prediction of tZ and SA concentrations in xylem sap samples. Another possible peak at 1690 cm^{-1}, linked to nucleic acids due to the base carbonyl (C=O) stretching and ring breathing mode [59], appeared to be useful in prediction of xylem sap concentrations of ABA, tZ and SA. A possible peak at 1574 cm^{-1} relating to the C=N of adenine [59], was identified as important in the prediction of xylem GA1 concentrations. Finally, a possible peak at 1531 cm^{-1}, associated previously with modified guanine [59], was used in the prediction of xylem tZ and SA. Again, these peak assignments are tentative but lend novel insights into this changing cellular environment.

ATR-FTIR spectral profiles allow prediction of hormone concentrations

The ATR-FTIR spectrum is information rich and provides an integrated holistic picture of the entire cellular biochemistry [40]. In response to the growth environment, biomolecules unrelated, related and influenced by hormonal activity will be altered, presumably in a dose-related fashion. Chemometrics provides a method to extract this chemical information from spectral absorbances, considering the ratios of different biochemical entities and potentially allowing us to find the "needle in a haystack" of individual hormones in their natural state.

PLSR models have previously been applied to the infrared and Raman spectroscopic absorbances of plant-derived samples to quantify individual components within molecular mixtures [10,11,88–90].

Here we have presented a demonstration of PLSR for the accurate prediction of plant hormone concentrations from ATR-FTIR spectral profiles. The accuracy of PLSR prediction of tZ concentrations was higher for xylem sap (Figure 4a, R^2=0.701) compared with leaf samples (Figure 4c, R^2=0.649). To improve the regression, for example, it would be necessary to narrow down the regression to specicic treatment-hormone models. For example, to create an ABA specific model, application of a wide range of drought severities would be ideal, because ABA is the main regulator of the drought stress response [78] and appears as a key hormone for separation of droughted plants in Figure 3, however this would not be the optimal calibration dataset for another hormone. The PCA loadings based on hormonal data alone (Figures 3b and 3d) show that in both leaf and xylem samples, tZ is a key loading for separation along the axis PC1 in Figures 3a and 3b. Whilst leaf samples in Figure 3b show a good distribution along PCA1, indicating a variety of leaf tZ levels, xylem samples Figure 3a show overlapping clusters. This overlap indicates similarity of xylem sap hormones concentrations across treatment categories, which explains why the xylem sap models have poorer predictive levels than those based on leaf samples.

This trend was also consistent when models were created by treatment categories, in which the hormone predictions based on xylem sap samples (Table 1) did not achieve as high a level of accuracy as those based on freeze-dried ground leaves (Table 2); the high R^2 values achieved in Table 2 indicate an excellent level of prediction from leaf samples. This effect could also be attributed to the fact that these are liquid samples that were injected directly into the HPLC-MS system without any previous extraction, and the higher variability between xylem sap samples (Figure S5†). Refinements to the technique used for collecting

xylem sap [91] and concentrating the samples prior to analysis with UHPLC-HRMS could improve the accuracy of xylem sap hormone quantification. Importantly, Tables 1 and 2 show that it is possible to identify different hormones at the same time to a high accuracy, as these models predicted all hormones in a row simultaneously.

Conclusions

In this study we present a method to predict hormone concentrations using ATR-FTIR spectroscopic measurements and chemometrics, calibrated by UHPLC-HRMS. Once made, the models generated can be applied to new ATR-FTIR spectral data in the absence of UHPLC-HRMS data to predict plant hormone concentrations. As plant hormone concentrations are a key physiological interface for modulation of plant responses in relation to examined processes, the ability to predict them rapidly and non-destructively from spectral data makes it a valuable tool for efficient physiological phenotyping. This methodology has potential for application across a range of species as key plant hormones are conserved [2,92]. ATR-FTIR spectroscopy is a rapid and non-destructive tool, which although demonstrated here using sample preparation, can also be used *in planta* [68]. Consequently, this method could be used in the field to monitor plant hormones and other key signalling molecules produced upon the perception of environmental stress. Biomolecular indications of stress can allow for intervention before the occurrence of phenotypic change, thereby reducing waste, increasing crop yield, and maintaining quality. As can be seen from the variation in R^2 values (Tables 1 and 2) however the accuracy of prediction varies between leaf and xylem sap and between different hormones and environments, suggesting the choice of tissue and growth environment is important when creating models, and would be improved through calibration data.

Authors' Contributions

CAH conceived, planned, and carried out the experiments and data analysis. CLMM provided revision and support for constructing the data analysis models. The manuscript was written by CAH, FLM and MM with contributions from all the authors. FLM provided equipment and expertise in the field of FTIR spectroscopy and chemometrics. PB provided funding for CAH's studentship and expertise in Japanese Knotweed. MM, FLM and JET supervised the project. AA and CMA conducted hormonal analysis.

Conflicts of Interest

The authors declare that there is no conflict of interest.

Acknowledgements

CAH is a member of the Centre for Global Eco-Innovation that is funded by the European Union Regional Development Fund and mediates the collaboration between Lancaster University and Phlorum Ltd. FLM received funding from NIHR Manchester Biomedical Research Centre (NIHR203308). The views expressed are those of the authors and not necessarily those of the NIHR or the Department of Health and Social Care.

References

(1) Anfang, M.; Shani, E. Transport Mechanisms of Plant Hormones. *Curr. Opin. Plant Biol.* **2021**, *63*, 102055. https://doi.org/10.1016/J.PBI.2021.102055.

(2) Blázquez, M. A.; Nelson, D. C.; Weijers, D. Evolution of Plant Hormone Response Pathways. *https://doi.org/10.1146/annurev-arplant-050718-100309* **2020**, *71*, 327–353. https://doi.org/10.1146/ANNUREV-ARPLANT-050718-100309.

(3) Davies, P. J. The Plant Hormones: Their Nature, Occurrence, and Functions. *Plant*

Horm. Biosynthesis, Signal Transduction, Action! **2010**, 1–15. https://doi.org/10.1007/978-1-4020-2686-7_1.

(4) Šimura, J.; Antoniadi, I.; Široká, J.; Tarkowská, D.; Strnad, M.; Ljung, K.; Novák, O. Plant Hormonomics: Multiple Phytohormone Profiling by Targeted Metabolomics. *Plant Physiol.* **2018**, *177* (2), 476. https://doi.org/10.1104/PP.18.00293.

(5) Porfírio, S.; Sonon, R.; Gomes da Silva, M. D. R.; Peixe, A.; Cabrita, M. J.; Azadi, P. Quantification of Free Auxins in Semi-Hardwood Plant Cuttings and Microshoots by Dispersive Liquid–Liquid Microextraction/Microwave Derivatization and GC/MS Analysis. *Anal. Methods* **2016**, *8* (31), 6089–6098. https://doi.org/10.1039/C6AY01289B.

(6) Pradko, A. G.; Litvinovskaya, R. P.; Sauchuk, A. L.; Drach, S. V.; Baranovsky, A. V.; Zhabinskii, V. N.; Mirantsova, T. V.; Khripach, V. A. A New ELISA for Quantification of Brassinosteroids in Plants. *Steroids* **2015**, *97*, 78–86. https://doi.org/10.1016/J.STEROIDS.2014.08.022.

(7) Bosco, R.; Daeseleire, E.; Van Pamel, E.; Scariot, V.; Leus, L. Development of an Ultrahigh-Performance Liquid Chromatography–Electrospray Ionization–Tandem Mass Spectrometry Method for the Simultaneous Determination of Salicylic Acid, Jasmonic Acid, and Abscisic Acid in Rose Leaves. *J. Agric. Food Chem.* **2014**, *62* (27), 6278–6284. https://doi.org/10.1021/JF5023884.

(8) Ge, L.; Peh, C. Y. C.; Yong, J. W. H.; Tan, S. N.; Hua, L.; Ong, E. S. Analyses of Gibberellins by Capillary Electrophoresis–Mass Spectrometry Combined with Solid-Phase Extraction. *J. Chromatogr. A* **2007**, *1159* (1–2), 242–249. https://doi.org/10.1016/J.CHROMA.2007.05.041.

(9) Anagnostopoulos, C. J.; Liapis, K.; Haroutounian, S.; Paspatis, E. Simultaneous

Determination of Different Classes of Plant Growth Regulator in High Water Content Agricultural Products by Liquid Chromatography Tandem Mass Spectrometry and Time of Flight Mass Spectrometry. *J. Liq. Chromatogr. Relat. Technol.* **2013**, *36* (3), 315–335. https://doi.org/10.1080/10826076.2012.657730/SUPPL_FILE/LJLC_A_657730_SUP_26001789.DOC.

(10) Naqvi, S. M. Z. A.; Zhang, Y.; Ahmed, S.; Abdulraheem, M. I.; Hu, J.; Tahir, M. N.; Raghavan, V. Applied Surface Enhanced Raman Spectroscopy in Plant Hormones Detection, Annexation of Advanced Technologies: A Review. *Talanta* **2022**, *236*, 122823. https://doi.org/10.1016/J.TALANTA.2021.122823.

(11) Lew, T. T. S.; Sarojam, R.; Jang, I.-C.; Park, B. S.; Naqvi, N. I.; Wong, M. H.; Singh, G. P.; Ram, R. J.; Shoseyov, O.; Saito, K.; Chua, N.-H.; Strano, M. S. Species-Independent Analytical Tools for next-Generation Agriculture. *Nat. Plants 2020 612* **2020**, *6* (12), 1408–1417. https://doi.org/10.1038/s41477-020-00808-7.

(12) Zhang, C.; Žukauskaitė, A.; Petřík, I.; Pěnčík, A.; Hönig, M.; Grúz, J.; Široká, J.; Novák, O.; Doležal, K. In Situ Characterisation of Phytohormones from Wounded Arabidopsis Leaves Using Desorption Electrospray Ionisation Mass Spectrometry Imaging. *Analyst* **2021**, *146* (8), 2653–2663. https://doi.org/10.1039/D0AN02118K.

(13) Karasov, T. L.; Chae, E.; Herman, J. J.; Bergelson, J. Mechanisms to Mitigate the Trade-Off between Growth and Defense. *Plant Cell* **2017**, *29* (4), 666–680. https://doi.org/10.1105/TPC.16.00931.

(14) Herman, J. J.; Sultan, S. E. Adaptive Transgenerational Plasticity in Plants: Case Studies, Mechanisms, and Implications for Natural Populations. *Front. Plant Sci.* **2011**, *2* (DEC). https://doi.org/10.3389/fpls.2011.00102.

(15) Asif, A.; Baig, M. A.; Siddiqui, M. B. Role of Jasmonates and Salicylates in Plant Allelopathy. **2021**, 115–127. https://doi.org/10.1007/978-3-030-75805-9_6.

(16) Liu, Y.; Oduor, A. M. O.; Dai, Z. C.; Gao, F. L.; Li, J.; Zhang, X.; Yu, F. H. Suppression of a Plant Hormone Gibberellin Reduces Growth of Invasive Plants More than Native Plants. *Oikos* **2021**, *130* (5), 781–789. https://doi.org/10.1111/OIK.07819.

(17) Manoharan, B.; Qi, S. S.; Dhandapani, V.; Chen, Q.; Rutherford, S.; Wan, J. S. H.; Jegadeesan, S.; Yang, H. Y.; Li, Q.; Li, J.; Dai, Z. C.; Du, D. L. Gene Expression Profiling Reveals Enhanced Defense Responses in an Invasive Weed Compared to Its Native Congener During Pathogenesis. *Int. J. Mol. Sci.* **2019**, *20* (19), 4916. https://doi.org/10.3390/IJMS20194916.

(18) Lowry, D. B.; Popovic, D.; Brennan, D. J.; Holeski, L. M. Mechanisms of a Locally Adaptive Shift in Allocation among Growth, Reproduction, and Herbivore Resistance in Mimulus Guttatus*. *Evolution (N. Y).* **2019**, *73* (6), 1168–1181. https://doi.org/10.1111/EVO.13699.

(19) Grossmann, K. Mediation of Herbicide Effects by Hormone Interactions. *J. Plant Growth Regul.* **2003**, *22* (1), 109–122. https://doi.org/10.1007/S00344-003-0020-0/FIGURES/6.

(20) Fennell, M.; Wade, M.; Bacon, K. L. Japanese Knotweed (*Fallopia Japonica*): An Analysis of Capacity to Cause Structural Damage (Compared to Other Plants) and Typical Rhizome Extension. *PeerJ* **2018**, *6*, e5246. https://doi.org/10.7717/peerj.5246.

(21) Santo, P. Assessing Diminution in Value of Residential Properties Affected by Japanese Knotweed. *J. Build. Surv. Apprais. Valuat.* **2017**, *Volume 6* (Number 3), Winter 2017-18, pp. 211-221(11).

(22) Lavoie, C. The Impact of Invasive Knotweed Species (Reynoutria Spp.) on the Environment: Review and Research Perspectives. *Biol. Invasions* **2017**, *19* (8), 2319–2337. https://doi.org/10.1007/s10530-017-1444-y.

(23) van Kleunen, M.; Bossdorf, O.; Dawson, W. The Ecology and Evolution of Alien Plants. *Annu. Rev. Ecol. Evol. Syst.* **2018**, *49* (1), 25–47. https://doi.org/10.1146/annurev-ecolsys-110617-062654.

(24) Parepa, M.; Fischer, M.; Bossdorf, O. Environmental Variability Promotes Plant Invasion. *Nat. Commun.* **2013**, *4* (1), 1–4. https://doi.org/10.1038/ncomms2632.

(25) Urcelay, C.; Austin, A. T. Exotic Plants Get a Little Help from Their Friends. *Science (New York, N.Y.)*. NLM (Medline) May 29, 2020, pp 934–936. https://doi.org/10.1126/science.abc3587.

(26) Liu, Y.; Oduor, A. M. O.; Dai, Z. C.; Gao, F. L.; Li, J.; Zhang, X.; Yu, F. H. Suppression of a Plant Hormone Gibberellin Reduces Growth of Invasive Plants More than Native Plants. *Oikos* **2021**, *130* (5), 781–789. https://doi.org/10.1111/OIK.07819.

(27) Zhang, Y.-Y.; Parepa, M.; Fischer, M.; Bossdorf, O. Epigenetics of Colonizing Species? A Study of Japanese Knotweed in Central Europe. In *Barrett SCH, Colautti RI, Dlugosch KM, Rieseberg LH (Eds) Invasion Genetics*; John Wiley & Sons, Ltd: Chichester, UK, 2016; pp 328–340. https://doi.org/10.1002/9781119072799.ch19.

(28) Richards, C. L.; Schrey, A. W.; Pigliucci, M. Invasion of Diverse Habitats by Few Japanese Knotweed Genotypes Is Correlated with Epigenetic Differentiation. *Ecol. Lett.* **2012**, *15* (9), 1016–1025. https://doi.org/10.1111/j.1461-0248.2012.01824.x.

(29) Rouifed, S.; Byczek, C.; Laffray, D.; Piola, F. Invasive Knotweeds Are Highly Tolerant to Salt Stress. *Environ. Manage.* **2012**, *50*, 1027–1034.

https://doi.org/10.1007/s00267-012-9934-2.

(30) Michalet, S.; Rouifed, S.; Pellassa-Simon, T.; Fusade-Boyer, M.; Meiffren, G.; Nazaret, S.; Piola, F. Tolerance of Japanese Knotweed s.l. to Soil Artificial Polymetallic Pollution: Early Metabolic Responses and Performance during Vegetative Multiplication. *Environ. Sci. Pollut. Res.* **2017**, *24* (26), 20897–20907. https://doi.org/10.1007/s11356-017-9716-8.

(31) Sołtysiak, J. Heavy Metals Tolerance in an Invasive Weed (Fallopia Japonica) under Different Levels of Soils Contamination. *J. Ecol. Eng.* **2020**, *21* (7), 81–91. https://doi.org/10.12911/22998993/125447.

(32) Holm, A. K.; Elameen, A.; Oliver, B. W.; Brandsæter, L. O.; Fløistad, I. S.; Brurberg, M. B. Low Genetic Variation of Invasive Fallopia Spp. in Their Northernmost European Distribution Range. *Ecol. Evol.* **2018**, *8* (1), 755–764. https://doi.org/10.1002/ece3.3703.

(33) Bailey, J. P.; Conolly, A. P. Prize-Winners to Pariahs -A History of Japanese Knotweed s.l. (Polygonaceae) in the British Isles. *Watsonia* **2000**, *23*, 93–110.

(34) Hollingsworth, M. L.; Bailey, J. P. Evidence for Massive Clonal Growth in the Invasive Weed Fallopia Japonica (Japanese Knotweed). *Bot. J. Linn. Soc.* **2000**, *133*, 463–472. https://doi.org/10.1006/bojl.2000.0359.

(35) Skolik, P.; Morais, C. L. M.; Martin, F. L.; McAinsh, M. R. Determination of Developmental and Ripening Stages of Whole Tomato Fruit Using Portable Infrared Spectroscopy and Chemometrics. *BMC Plant Biol.* **2019**, *19* (1), 236. https://doi.org/10.1186/s12870-019-1852-5.

(36) Skolik, P.; McAinsh, M. R.; Martin, F. L. ATR-FTIR Spectroscopy Non-Destructively

Detects Damage-Induced Sour Rot Infection in Whole Tomato Fruit. *Planta* **2019**, *249* (3), 925–939. https://doi.org/10.1007/s00425-018-3060-1.

(37) Morais, C. L. M.; Lima, K. M. G. Principal Component Analysis with Linear and Quadratic Discriminant Analysis for Identification of Cancer Samples Based on Mass Spectrometry. *Artic. J. Braz. Chem. Soc* **2018**, *29* (3), 472–481. https://doi.org/10.21577/0103-5053.20170159.

(38) Morais, C. L. M.; Costa, F. S. L.; Lima, K. M. G. Variable Selection with a Support Vector Machine for Discriminating: Cryptococcus Fungal Species Based on ATR-FTIR Spectroscopy. *Anal. Methods* **2017**, *9* (20), 2964–2970. https://doi.org/10.1039/c7ay00428a.

(39) Mehmood, T.; Liland, K. H.; Snipen, L.; Sæbø, S. A Review of Variable Selection Methods in Partial Least Squares Regression. *Chemom. Intell. Lab. Syst.* **2012**, *118*, 62–69. https://doi.org/10.1016/J.CHEMOLAB.2012.07.010.

(40) Morais, C. L. M.; Lima, K. M. G.; Singh, M.; Martin, F. L. Tutorial: Multivariate Classification for Vibrational Spectroscopy in Biological Samples. *Nature Protocols*. Nature Research July 1, 2020, pp 2143–2162. https://doi.org/10.1038/s41596-020-0322-8.

(41) Met Office. UK Regional Climates. *https://www.metoffice.gov.uk/research/climate/maps-and-data/regional-climates/index* **2019**.

(42) Bailey, J. The Japanese Knotweed Invasion Viewed as a Vast Unintentional Hybridisation Experiment. *Heredity (Edinb).* **2013**. https://doi.org/10.1038/hdy.2012.98.

(43) Smith, H. Light Quality, Photoperception, and Plant Strategy. *Annu. Rev. Plant Physiol.* **1982**, *33* (1), 481–518.

(44) Larsen, D. H.; Woltering, E. J.; Nicole, C. C. S.; Marcelis, L. F. M. Response of Basil Growth and Morphology to Light Intensity and Spectrum in a Vertical Farm. *Front. Plant Sci.* **2020**, *11*, 1893. https://doi.org/10.3389/FPLS.2020.597906/BIBTEX.

(45) Pennisi, G.; Pistillo, A.; Orsini, F.; Cellini, A.; Spinelli, F.; Nicola, S.; Fernandez, J. A.; Crepaldi, A.; Gianquinto, G.; Marcelis, L. F. M. Optimal Light Intensity for Sustainable Water and Energy Use in Indoor Cultivation of Lettuce and Basil under Red and Blue LEDs. *Sci. Hortic. (Amsterdam).* **2020**, *272*, 109508. https://doi.org/10.1016/J.SCIENTA.2020.109508.

(46) Zou, T.; Huang, C.; Wu, P.; Ge, L.; Xu, Y. Optimization of Artificial Light for Spinach Growth in Plant Factory Based on Orthogonal Test. *Plants 2020, Vol. 9, Page 490* **2020**, *9* (4), 490. https://doi.org/10.3390/PLANTS9040490.

(47) Park, Y.; Runkle, E. S. Spectral Effects of Light-Emitting Diodes on Plant Growth, Visual Color Quality, and Photosynthetic Photon Efficacy: White versus Blue plus Red Radiation. *PLoS One* **2018**, *13* (8). https://doi.org/10.1371/JOURNAL.PONE.0202386.

(48) Monaghan, R. M.; Paton, R. J.; Smith, L. C.; Drewry, J. J.; Littlejohn, R. P. The Impacts of Nitrogen Fertilisation and Increased Stocking Rate on Pasture Yield, Soil Physical Condition and Nutrient Losses in Drainage from a Cattle-Grazed Pasture. *New Zeal. J. Agric. Res.* **2005**, *48* (2), 227–240. https://doi.org/10.1080/00288233.2005.9513652.

(49) Dodd, I. C.; Egea, G.; Davies, W. J. Abscisic Acid Signalling When Soil Moisture Is Heterogeneous: Decreased Photoperiod Sap Flow from Drying Roots Limits Abscisic

Acid Export to the Shoots. *Plant. Cell Environ.* **2008**, *31* (9), 1263–1274. https://doi.org/10.1111/J.1365-3040.2008.01831.X.

(50) Albacete, A.; Ghanem, M. E.; Martínez-Andújar, C.; Acosta, M.; Sánchez-Bravo, J.; Martínez, V.; Lutts, S.; Dodd, I. C.; Pérez-Alfocea, F. Hormonal Changes in Relation to Biomass Partitioning and Shoot Growth Impairment in Salinized Tomato (Solanum Lycopersicum L.) Plants. *J. Exp. Bot.* **2008**, *59* (15), 4119–4131. https://doi.org/10.1093/JXB/ERN251.

(51) Groãÿkinsky, D. K.; Albacete, A.; Jammer, A.; Krbez, P.; Van der Graaff, E.; Pfeifhofer, H.; Roitsch, T. A Rapid Phytohormone and Phytoalexin Screening Method for Physiological Phenotyping. *Mol. Plant* **2014**, *7*, 1053–1056. https://doi.org/10.1093/mp/ssu015.

(52) Martin, F. L.; Kelly, J. G.; Llabjani, V.; Martin-Hirsch, P. L.; Patel, I. I.; Trevisan, J.; Fullwood, N. J.; Walsh, M. J. Distinguishing Cell Types or Populations Based on the Computational Analysis of Their Infrared Spectra. *Nat. Protoc.* **2010**, *5* (11), 1748–1760. https://doi.org/10.1038/nprot.2010.133.

(53) Trevisan, J.; Angelov, P. P.; Scott, A. D.; Carmichael, P. L.; Martin, F. L. IRootLab: A Free and Open-Source MATLAB Toolbox for Vibrational Biospectroscopy Data Analysis. *Bioinformatics* **2013**, *29* (8), 1095–1097. https://doi.org/10.1093/bioinformatics/btt084.

(54) Nozahic, V.; Amziane, S. Influence of Sunflower Aggregates Surface Treatments on Physical Properties and Adhesion with a Mineral Binder. *Compos. Part A Appl. Sci. Manuf.* **2012**, *43* (11), 1837–1849. https://doi.org/10.1016/j.compositesa.2012.07.011.

(55) Belfer, S.; Purinson, Y.; Kedem, O. Surface Modification of Commercial Polyamide Reverse Osmosis Membranes by Radical Grafting: An ATR-FTIR Study. *Acta Polym.*

1998, *49* (10–11), 574–582. https://doi.org/10.1002/(sici)1521-4044(199810)49:10/11<574::aid-apol574>3.0.co;2-0.

(56) Shivu, B.; Seshadri, S.; Li, J.; Oberg, K. A.; Uversky, V. N.; Fink, A. L. Distinct β-Sheet Structure in Protein Aggregates Determined by ATR−FTIR Spectroscopy. **2013**. https://doi.org/10.1021/bi400625v.

(57) Jin, N.; Semple, K. T.; Jiang, L.; Luo, C.; Zhang, D.; Martin, F. L. Spectrochemical Analyses of Growth Phase-Related Bacterial Responses to Low (Environmentally-Relevant) Concentrations of Tetracycline and Nanoparticulate Silver. *Analyst* **2018**, *143* (3), 768–776. https://doi.org/10.1039/c7an01800b.

(58) Moskal, P.; Wesełucha-Birczyńska, A.; Łabanowska, M.; Filek, M. Adaxial and Abaxial Pattern of Urtica Dioica Leaves Analyzed by 2DCOS ATR-FTIR as a Function of Their Growth Time and Impact of Environmental Pollution. *Vib. Spectrosc.* **2019**, *104*, 102948. https://doi.org/10.1016/j.vibspec.2019.102948.

(59) Talari, A. C. S.; Martinez, M. A. G.; Movasaghi, Z.; Rehman, S.; Rehman, I. U. Advances in Fourier Transform Infrared (FTIR) Spectroscopy of Biological Tissues. *Appl. Spectrosc. Rev.* **2017**, *52* (5), 456–506. https://doi.org/10.1080/05704928.2016.1230863.

(60) Gorzsas, A. ATR-FTIR Microspectroscopy Brings a Novel Insight Into the Study of Cell Wall Chemistry at the Cellular Level. In *Proceedings of IPSC 2019-2nd International Plant Spectroscopy Conference*; Frontiers Media SA, 2020.

(61) Falcão, L.; Araújo, M. E. M. Tannins Characterization in Historic Leathers by Complementary Analytical Techniques ATR-FTIR, UV-Vis and Chemical Tests. *J. Cult. Herit.* **2013**, *14* (6), 499–508. https://doi.org/10.1016/J.CULHER.2012.11.003.

(62) Morais, C. L. M.; Costa, F. S. L.; Lima, K. M. G. Variable Selection with a Support Vector Machine for Discriminating Cryptococcus Fungal Species Based on ATR-FTIR Spectroscopy. *Anal. Methods* **2017**, *9* (20), 2964–2970. https://doi.org/10.1039/C7AY00428A.

(63) Rana, R.; Herz, K.; Bruelheide, H.; Dietz, S.; Haider, S.; Jandt, U.; Pena, R. Leaf Attenuated Total Reflection Fourier Transform Infrared (ATR-FTIR) Biochemical Profile of Grassland Plant Species Related to Land-Use Intensity. *Ecol. Indic.* **2018**, *84*, 803–810. https://doi.org/10.1016/j.ecolind.2017.09.047.

(64) Sharma, S.; Uttam, K. N. Early Stage Detection of Stress Due to Copper on Maize (Zea Mays L.) by Laser-Induced Fluorescence and Infrared Spectroscopy. *J. Appl. Spectrosc.* **2018**, *85* (4), 771–780. https://doi.org/10.1007/s10812-018-0717-2.

(65) Ajitha, B.; Ashok Kumar Reddy, Y.; Shameer, S.; Rajesh, K. M.; Suneetha, Y.; Sreedhara Reddy, P. Lantana Camara Leaf Extract Mediated Silver Nanoparticles: Antibacterial, Green Catalyst. *J. Photochem. Photobiol. B Biol.* **2015**, *149*, 84–92. https://doi.org/10.1016/j.jphotobiol.2015.05.020.

(66) Geng, Y.; van Klinken, R. D.; Sosa, A.; Li, B.; Chen, J.; Xu, C.-Y. The Relative Importance of Genetic Diversity and Phenotypic Plasticity in Determining Invasion Success of a Clonal Weed in the USA and China. *Front. Plant Sci.* **2016**, *7*, 216. https://doi.org/10.3389/fpls.2016.00213.

(67) Richards, C. L.; Bossdorf, O.; Muth, N. Z.; Gurevitch, J.; Pigliucci, M. Jack of All Trades, Master of Some? On the Role of Phenotypic Plasticity in Plant Invasions. *Ecol. Lett.* **2006**, *9* (8), 981–993. https://doi.org/10.1111/j.1461-0248.2006.00950.x.

(68) Butler, H. J.; McAinsh, M. R.; Adams, S.; Martin, F. L. Application of Vibrational Spectroscopy Techniques to Non-Destructively Monitor Plant Health and

Development. *Anal. Methods* **2015**, *7* (10), 4059–4070. https://doi.org/10.1039/C5AY00377F.

(69) Holden, C. A.; Morais, C. L. M.; Taylor, J. E.; Martin, F. L.; Beckett, P.; McAinsh, M. Regional Differences in Clonal Japanese Knotweed Revealed by Chemometrics-Linked Attenuated Total Reflection Fourier-Transform Infrared Spectroscopy. *BMC Plant Biol. 2021 211* **2021**, *21* (1), 1–20. https://doi.org/10.1186/S12870-021-03293-Y.

(70) Traoré, M.; Kaal, J.; Martínez Cortizas, A. Differentiation between Pine Woods According to Species and Growing Location Using FTIR-ATR. *Wood Sci. Technol.* **2018**, *52* (2), 487–504. https://doi.org/10.1007/s00226-017-0967-9.

(71) Holden, C. A.; Bailey, J. P.; Taylor, J. E.; Martin, F.; Beckett, P.; McAinsh, M. Know Your Enemy: Application of ATR-FTIR Spectroscopy to Invasive Species Control. *PLoS One* **2022**, *17* (1), e0261742. https://doi.org/10.1371/JOURNAL.PONE.0261742.

(72) Wolters, H.; Jürgens, G. Survival of the Flexible: Hormonal Growth Control and Adaptation in Plant Development. *Nat. Rev. Genet.* **2009**, *10* (5), 305–317. https://doi.org/10.1038/NRG2558.

(73) Spalding, K.; Bonnier, F.; Bruno, C.; Blasco, H.; Board, R.; Benz-de Bretagne, I.; Byrne, H. J.; Butler, H. J.; Chourpa, I.; Radhakrishnan, P.; Baker, M. J. Enabling Quantification of Protein Concentration in Human Serum Biopsies Using Attenuated Total Reflectance – Fourier Transform Infrared (ATR-FTIR) Spectroscopy. *Vib. Spectrosc.* **2018**, *99*, 50–58. https://doi.org/10.1016/j.vibspec.2018.08.019.

(74) Wagner, H.; Liu, Z.; Langner, U.; Stehfest, K.; Wilhelm, C. The Use of FTIR Spectroscopy to Assess Quantitative Changes in the Biochemical Composition of

Microalgae. *J. Biophotonics* **2010**, *3* (8–9), 557–566. https://doi.org/10.1002/jbio.201000019.

(75) Butler, H. J.; Martin, F. L.; Roberts, M. R.; Adams, S.; McAinsh, M. R. Observation of Nutrient Uptake at the Adaxial Surface of Leaves of Tomato (*Solanum Lycopersicum*) Using Raman Spectroscopy. *Anal. Lett.* **2020**, *53* (4), 536–562. https://doi.org/10.1080/00032719.2019.1658199.

(76) Strong, R.; Martin, F. L.; Jones, K. C.; Shore, R. F.; Halsall, C. J. Subtle Effects of Environmental Stress Observed in the Early Life Stages of the Common Frog, Rana Temporaria. *Sci. Rep.* **2017**, *7* (1), 1–13. https://doi.org/10.1038/srep44438.

(77) Heap, B.; Holden, C.; Taylor, J.; McAinsh, M. <scp>ROS</Scp> Crosstalk in Signalling Pathways. In *eLS*; Wiley, 2020; pp 1–9. https://doi.org/10.1002/9780470015902.a0025271.

(78) Bharath, P.; Gahir, S.; Raghavendra, A. S. Abscisic Acid-Induced Stomatal Closure: An Important Component of Plant Defense Against Abiotic and Biotic Stress. *Front. Plant Sci.* **2021**, *12*, 324. https://doi.org/10.3389/FPLS.2021.615114/BIBTEX.

(79) Maruri-López, I.; Aviles-Baltazar, N. Y.; Buchala, A.; Serrano, M. Intra and Extracellular Journey of the Phytohormone Salicylic Acid. *Front. Plant Sci.* **2019**, *0*, 423. https://doi.org/10.3389/FPLS.2019.00423.

(80) Saleem, M.; Fariduddin, Q.; Castroverde, C. D. M. Salicylic Acid: A Key Regulator of Redox Signalling and Plant Immunity. *Plant Physiol. Biochem.* **2021**, *168*, 381–397. https://doi.org/10.1016/J.PLAPHY.2021.10.011.

(81) Zheng, W.; Wang, S. Y. Antioxidant Activity and Phenolic Compounds in Selected Herbs. *J. Agric. Food Chem.* **2001**, *49* (11), 5165–5170.

https://doi.org/10.1021/JF010697N.

(82) Heredia-Guerrero, J. A.; Benítez, J. J.; Domínguez, E.; Bayer, I. S.; Cingolani, R.; Athanassiou, A.; Heredia, A. Infrared and Raman Spectroscopic Features of Plant Cuticles: A Review. *Front. Plant Sci.* **2014**, *5*, 305. https://doi.org/10.3389/fpls.2014.00305.

(83) Ord, J.; Butler, H. J.; McAinsh, M. R.; Martin, F. L. Spectrochemical Analysis of Sycamore (Acer Pseudoplatanus) Leaves for Environmental Health Monitoring. *Analyst* **2016**, *141* (10), 2896–2903. https://doi.org/10.1039/C6AN00392C.

(84) Liu, X.; Renard, C. M. G. C.; Bureau, S.; Le Bourvellec, C. Revisiting the Contribution of ATR-FTIR Spectroscopy to Characterize Plant Cell Wall Polysaccharides. *Carbohydr. Polym.* **2021**, *262*, 117935. https://doi.org/10.1016/J.CARBPOL.2021.117935.

(85) Courbier, S.; Grevink, S.; Sluijs, E.; Bonhomme, P.-O.; Kajala, K.; Wees, S. C. M. Van; Pierik, R. Far-Red Light Promotes Botrytis Cinerea Disease Development in Tomato Leaves via Jasmonate-Dependent Modulation of Soluble Sugars. *Plant. Cell Environ.* **2020**, *43* (11), 2769–2781. https://doi.org/10.1111/PCE.13870.

(86) van der Weijde, T.; Huxley, L. M.; Hawkins, S.; Sembiring, E. H.; Farrar, K.; Dolstra, O.; Visser, R. G. F.; Trindade, L. M. Impact of Drought Stress on Growth and Quality of Miscanthus for Biofuel Production. *GCB Bioenergy* **2017**, *9* (4), 770–782. https://doi.org/10.1111/GCBB.12382.

(87) Gfeller, A.; Dubugnon, L.; Liechti, R.; Farmer, E. E. Jasmonate Biochemical Pathway. *Sci. Signal.* **2010**, *3* (109). https://doi.org/10.1126/SCISIGNAL.3109CM3/ASSET/57BCEEBB-B6E4-4299-8646-8E4F84042400/ASSETS/GRAPHIC/3109CM3-F3.JPEG.

(88) Zhu, J.; Agyekum, A. A.; Kutsanedzie, F. Y. H.; Li, H.; Chen, Q.; Ouyang, Q.; Jiang, H. Qualitative and Quantitative Analysis of Chlorpyrifos Residues in Tea by Surface-Enhanced Raman Spectroscopy (SERS) Combined with Chemometric Models. *LWT* **2018**, *97*, 760–769. https://doi.org/10.1016/J.LWT.2018.07.055.

(89) Romera-Fernández, M.; Berrueta, L. A.; Garmón-Lobato, S.; Gallo, B.; Vicente, F.; Moreda, J. M. Feasibility Study of FT-MIR Spectroscopy and PLS-R for the Fast Determination of Anthocyanins in Wine. *Talanta* **2012**, *88*, 303–310. https://doi.org/10.1016/J.TALANTA.2011.10.045.

(90) Bensemmane, N.; Bouzidi, N.; Daghbouche, Y.; Garrigues, S.; de la Guardia, M.; El Hattab, M. Quantification of Phenolic Acids by Partial Least Squares Fourier-Transform Infrared (PLS-FTIR) in Extracts of Medicinal Plants. *Phytochem. Anal.* **2021**, *32* (2), 206–221. https://doi.org/10.1002/PCA.2974.

(91) Netting, A. G.; Theobald, J. C.; Dodd, I. C. Xylem Sap Collection and Extraction Methodologies to Determine in Vivo Concentrations of ABA and Its Bound Forms by Gas Chromatography-Mass Spectrometry (GC-MS). *Plant Methods* **2012**, *8* (1), 1–14. https://doi.org/10.1186/1746-4811-8-11/FIGURES/8.

(92) Wang, C.; Liu, Y.; Li, S.-S.; Han, G.-Z. Insights into the Origin and Evolution of the Plant Hormone Signaling Machinery. *Plant Physiol.* **2015**, *167* (3), 872–886. https://doi.org/10.1104/PP.114.247403.

Footnotes

† Electronic supplementary information (ESI):

- **Table S1:** Lighting conditions within each Snijder cabinet.

- **Figure S1:** Spectra from a) 'Light' (LC, LD, LN, LLN) b) 'Shade' (SC, SD, SN, SLN) cabinets, providing red: far-red ratios of 5.6 and 0.4 respectively.
- **Table S2:** Reagents used for Hoagland's solution.
- **Figure S2:** Chromatogram and mass spectra for the hormone salicylic acid
- **Table S3:** Hormone descriptions and molecular ion masses
- **Figure S3: (a)** Raw and **(b)** pre-processed class means spectra in the fingerprint region from xylem sap, **(c)** Raw and **(d)** pre-processed (Savitzky–Golay 2nd differentiation, n=9, and vector normalisation) class means spectra in the fingerprint region from freeze-dried ground leaves.
- **Table S4:** SVM parameters for classification.
- **Figure S4:** Loadings from spectra of a) xylem sap and b) freeze-dried ground leaf samples
- **Table S5:** PCA-loadings and biomarkers: key wavenumbers and compounds, which differentiate spectral profiles of plants from different growth conditions for both xylem sap and freeze-dried ground sample types.
- **Figure S5:** Hormone profiles from xylem sap in ng·ml^{-1} sap for a) 1-amino-cyclopropanecarboxylic acid (ACC), b) trans-Zeatin (tZ), c) isopentyl-adenine (iP), d) salicylic acid (SA), e) abscisic acid (ABA), f) jasmonic acid (JA), g) gibberellin A1 (GA_1), gibberellin A4 (GA_4), gibberellic acid (GA_3), *trans*-zeatin riboside (tZR), and indole-3-acetic acid (IAA).
- **Figure S6:** Hormone profiles from freeze-dried ground leaves ng·g^{-1} dry weight for a) 1-amino-cyclopropanecarboxylic acid (ACC), b) trans-Zeatin (tZ), c) isopentyl-adenine (iP), d) salicylic acid (SA), e) abscisic acid (ABA), f) jasmonic acid (JA), g) gibberellin A1 (GA_1), gibberellin A4 (GA_4), gibberellic acid (GA_3), *trans*-zeatin riboside (tZR), and indole-3-acetic acid (IAA).

- **Figure S7:** PLS regression graphs for prediction of plant hormones from xylem sap. Validation was performed by Monte-Carlo cross-validation with 20% of samples left-out for validation during 1000 iterations. All models were built using 10 latent variables.
- **Figure S8:** PLSR regression coefficients for prediction of plant hormones from xylem sap.
- **Figure S9:** PLS regression graphs for prediction of plant hormones from freeze-dried ground leaves. Validation was performed by Monte-Carlo cross-validation with 20% of samples left-out for validation during 1000 iterations. All models were built using 10 latent variables.
- **Figure S10:** PLSR regression coefficients for prediction of plant hormones from freeze-dried ground leaves.
- **Table S6:** Number of latent variables (LVs) used to build the PLSR models between different types of treatment and hormone levels for xylem sap and freeze-dried ground (FDG) leaves. Higher number of LVs represents higher model complexity.
- **Data S1:** Hormone concentrations measured by ultra-high-performance liquid chromatography-high-resolution mass spectrometry and spectral absorbances measured by attenuated total reflection Fourier-transform infrared spectroscopy for freeze-dried ground leaf and xylem sap samples.